Nonreciprocal Vibration Transmission in Nonlinear Mechanical Systems: Energy-Preserving, Phase-Preserving and Unilateral Transmission

Ali Kogani

A Thesis

In the Department of Mechanical, Industrial and Aerospace Engineering

Presented in Partial Fulfillment of the Requirements

For the Degree of

Doctor of Philosophy (Mechanical Engineering) at

Concordia University

Montreal, Quebec, Canada

May 2025

© Ali Kogani, 2025

CONCORDIA UNIVERSITY SCHOOL OF GRADUATE STUDIES

T	his	is	to	certify	that	the	thesis
---	-----	----	----	---------	------	-----	--------

		Chair
Dr. Yuho	ong Yan	
——————————————————————————————————————	nias Legrand	External Examiner
DI. Mati	nas Degrand	
Dr. Emre	e Erkmen	Arm's Length Examiner
		Examiner
Dr. Ram	in Sedaghati	
Dr. Mojt	aba Kheiri	Examiner
		Thesis Supervisor
Dr. Behr	ooz Yousefzadeh	
Approved by		
	Dr. Ramin Sedaghati, Graduate	Program Director
May 5, 2025		
	Dr. Mourad Debbabi Dean, Gina Cody School of Engir	neering and Computer Science

Abstract

Nonreciprocal Vibration Transmission in Nonlinear Mechanical Systems: Energy-Preserving, Phase-Preserving and Unilateral Transmission

Ali Kogani, Ph.D. Concordia University, 2025

Reciprocity, a fundamental property of linear, time-invariant systems, implies that wave transmission characteristics between two points in a material or structure remain unchanged upon interchanging the locations of the source and receiver. Thus, reciprocal systems cannot have direction-dependent transmission properties. One way to overcome this limitation is to utilize nonlinearity.

There has been a surge of interest in the past two decades in nonlinear nonreciprocity in the context of phononic crystals, metamaterials and lattice materials. This thesis contributes to this body of knowledge by providing a detailed account of three nonreciprocal transmission regimes: energy-preserving, phase-preserving and unilateral transmission. This computational investigation is focused exclusively on the steady-state response of spatially periodic systems to external harmonic excitation.

The most salient indicator of nonreciprocity is the ability of a system to support unidirectional transmission. This occurs when there is a large difference between the energies transmitted in opposite directions. This energy bias is accompanied by a difference in the phase of the transmitted vibrations. The role of the phase bias in nonreciprocity has primarily been overlooked in the literature. To highlight the role of phase, we consider two limiting cases. We demonstrate the existence of response regimes in which the energy bias is zero and nonreciprocity is solely caused by the phase bias. Moreover, we show that energy bias alone, without any contribution from phase, can still lead to nonreciprocity, but only at very finely tuned system parameters. We provide methodologies for systematically realizing response regimes of energy-preserving and phase-preserving nonreciprocity.

Furthermore, we investigate unilateral transmission, a phenomenon in which transmitted vibrations remain purely in tension or compression. We investigate unilateral transmission in a system with different effective elasticity in compression and tension. We show that breaking the mirror symmetry of the system in either the elastic or inertial properties enables unilateral transmission to occur near the primary resonances.

This dissertation advances the understanding of nonlinear nonreciprocity in vibration systems, with a focus on three response regimes that are characterized by distinct dynamic features. These findings provide new insights into the design of nonlinear waveguides and mechanical systems with tunable nonreciprocal properties.

Acknowledgments

First and foremost, I would like to express my deepest gratitude to my dear supervisor, Dr. Behrooz Yousefzadeh. I could not have wished for a better mentor throughout my PhD. Your constant support, thoughtful guidance, and flexibility have made every challenge easier to navigate. You have a rare ability to make even the most intricate problems feel engaging and rewarding, and through your mentorship, I have learned to approach them with the same enthusiasm. I am truly grateful for everything you have taught me, and it has been an absolute privilege to work under your guidance.

To my parents, whose unwavering love and selfless sacrifices have shaped my journey. From the moment I decided to leave my country to pursue my PhD, they have stood by me with endless encouragement, enduring the distance with patience and resilience. Their belief in me has been my greatest motivation, and I hope this work serves as a small token of my gratitude for all they have given me.

To my lovely wife, who has been my anchor, my closest friend, and my greatest source of strength. Your love, patience, and encouragement have made this journey not only easier but also more meaningful. I am deeply grateful for your presence in my life and for standing beside me through every high and low.

I acknowledge financial support from the Natural Sciences and Engineering Research Council of Canada through the Discovery Grant program.

Co-Authorship

To comply with the manuscript-based format outlined in the *Thesis Preparation Guide* provided by the Thesis Office of the School of Graduate Studies, this thesis has been prepared in alignment with the specified regulations. Co-authored works are presented in Chapters 2, 3, and 4 with the abstracts of these manuscripts excluded from the chapters. The contributions of each co-author are detailed below.

Chapter 2 is based on the manuscript "Nonreciprocal phase shifts in a nonlinear periodic waveguide", which has been published by *Nonlinear Dynamics*. Contributions of the Authors:

Ali Kogani: Conceptualization, all the mathematical modeling, result acquisition, validation, analysis, and manuscript preparation, including drafting and writing.

Behrooz Yousefzadeh: Conceptualization, manuscript review and editing, supervision, and funding acquisition.

Chapter 3 is based on the manuscript "Phase-preserving nonreciprocal dynamics in coupled nonlinear oscillators", which has been submitted to *The Journal of the Acoustic Society of America*. Contributions of the Authors:

Ali Kogani: Conceptualization, all the mathematical modeling, result acquisition, validation, analysis, and manuscript preparation, including drafting and writing.

Behrooz Yousefzadeh: Conceptualization, manuscript review and editing, supervision, and funding acquisition.

Chapter 4 is based on the manuscript "Unilateral vibration transmission in mechanical systems with bilinear coupling", which has been submitted to *Nonlinear Dynamics*. Contributions of the Authors:

Ali Kogani: Conceptualization, all the mathematical modeling, result acquisition, validation, analysis, and manuscript preparation, including drafting and writing.

Behrooz Yousefzadeh: Conceptualization, manuscript review and editing, supervision, and funding acquisition.

Contents

Li	st of	Figure	s	X
1	Intr	oductio	on	1
	1.1	Recipro	ocity	1
1.2 Nonreciprocity		Nonrec	iprocity	3
		1.2.1	Active media	4
		1.2.2	Passive media	5
	1.3	Bilinea	r stiffness	8
		1.3.1	Amplitude-independent bilinear force	8
		1.3.2	Amplitude-dependent bilinear force	9
	1.4	Nonrec	ciprocity in periodic structures	10
	1.5	Gaps in	n the literature	11
		1.5.1	Influence of phase	11
		1.5.2	Unilateral Transmission	12
	1.6	Thesis	Objectives	12
		1.6.1	Phase nonreciprocity	12
		1.6.2	Phase-preserving nonreciprocity	13
		1.6.3	Unilateral transmission	13
	1.7	Thesis	Outline	14
2	Non	recipro	ocal phase shifts in a nonlinear periodic waveguide	16
	2.1	Introdu	action	16
	2.2	Proble	m Setup	18
		2.2.1	Governing equations	19
		2.2.2	Methodology	20
		2.2.3	Response norms	21
	2.3	Freque	ncy Response Curves	22
	2.4		Nonreciprocity	26
			Influence of asymmetry (mass ratio, μ)	26
		2.4.2	Influence of the forcing amplitude (P)	26
		2.4.3	Influence of damping (ζ_g)	29
	2.5	Restori	ing reciprocity using two symmetry-breaking parameters	32
	2.6	Conclu	sions	33
	App	endices		34

		2A	Appendix A: Non-dimensional Equations of Motion	34
3	Pha	se-pre	serving nonreciprocal dynamics in coupled nonlinear oscillators	36
	3.1	Introd	luction	36
	3.2	Proble	em Setup	38
	3.3	Contro	olling the Transmitted Phase and Energy	40
		3.3.1	Phase Nonreciprocity	40
		3.3.2	Restoring Reciprocity	42
	3.4	Phase	-Preserving Nonreciprocity	42
		3.4.1	Influence of the forcing amplitude	42
		3.4.2	Influence of the linear stiffness ratio	44
	3.5	Conclu	usions	46
	App	endices		49
		3A	Non-dimensional Equations of Motion	49
		3B	Extraction of the Phase of the First Harmonic	49
4	Uni	lateral	vibration transmission in mechanical systems with bilinear	
	cou	pling		51
	4.1	Introd	luction	51
	4.2	Proble	em setup	53
		4.2.1	Governing equations	53
		4.2.2	Solution methodology	54
	4.3	Biline	arly coupled oscillators	56
		4.3.1	Unilateral transmission in a symmetric system	56
		4.3.2	Unilateral transmission in an asymmetric system	58
		4.3.3	Influence of the bilinear ratio	60
		4.3.4	Nonreciprocal Unilateral Transmission	60
	4.4	Period	lic Structure with Bilinearly Coupled Units	63
		4.4.1	Influence of the number of units	63
		4.4.2	Influence of damping	66
	4.5	Concl	usions	69
	App	endices	5	70
		4A	Non-dimensional Equations of Motion	70
		4B	Amplitude independency of bilinear systems without offset	70
5	Cor	clusio	ns and Recommendations	7 2
	5.1	Concl	usions	72
	5.2	Future	e work	73

References 86

List of Figures

Fig. 1.1	2DoF system used to explain the Betti's reciprocity theorem	2
Fig. 1.2	(a) Schematic of a waveguide under two wave transmission configurations.	
	(b) Time-domain response of two configurations	3
Fig. 1.3	[17] Nonreciprocity induced by kinetic media. (a) Doppler-based nonrecip-	
	rocal acoustic waveguide with unidirectional fluid flow. (b) Response of the	
	acoustic gyrator system in opposite directions. Cylindrical cavity connected	
	to three waveguides with (c) stationary air and (d) rotating airflow	5
Fig. 1.4	(a) Schematic representation of the two-degree-of-freedom (2DoF) system	
	with grounded cubic nonlinear stiffness. Frequency response curve of (b)	
	the symmetric system, $M_2 = M_1$ and (c) the asymmetric system, $M_2 = 2M_1$.	7
Fig. 1.5	(a) Restoring force of a bilinear spring. (b) Schematic representation of	
	the the SDoF vibration system with bilinear stiffness. Frequency response	
	curve of (c) the AC value, and (d) the DC value	9
Fig. 1.6	Frequency response curve of the single-degree-of-freedom (SDoF) system	
	with bilinear stiffness $\beta = 5$ and an offset $s = 0.6$. (a) AC value and (b)	
	DC value	10
Fig. 2.1	Schematic of the finite periodic structure. The red dashed box shows the	
O	unit cell, which consists of two linear oscillators coupled with a linear stiff-	
	ness and grounded by a nonlinear spring and a linear damping	19
Fig. 2.2	Output norms (Eq. 2.4) at $P = 0.15$ for the system with mirror symmetry	
O		
	$(\mu=1)$	23
Fig. 2.3	$(\mu = 1)$	23
Fig. 2.3	Frequency response curves at $P = 0.15$ for the system with broken mirror	23
Fig. 2.3		2324
Fig. 2.3 Fig. 2.4	Frequency response curves at $P=0.15$ for the system with broken mirror symmetry, $\mu=2$. The grey circles show points at which $N^F=N^B$. The black dots indicate unstable regions in the response	
Ū	Frequency response curves at $P=0.15$ for the system with broken mirror symmetry, $\mu=2$. The grey circles show points at which $N^F=N^B$. The black dots indicate unstable regions in the response	
Ū	Frequency response curves at $P=0.15$ for the system with broken mirror symmetry, $\mu=2$. The grey circles show points at which $N^F=N^B$. The black dots indicate unstable regions in the response	
Ū	Frequency response curves at $P=0.15$ for the system with broken mirror symmetry, $\mu=2$. The grey circles show points at which $N^F=N^B$. The black dots indicate unstable regions in the response Nonreciprocal dynamics for $P=0.15$ and $\mu=2$. (a) The reciprocity norm, R , with the markers indicating $N^F=N^B$. Diamonds denote phase nonreciprocity ($N^F=N^B$, $\phi^F\neq\phi^B$) and circles denote frequencies at	
Ū	Frequency response curves at $P=0.15$ for the system with broken mirror symmetry, $\mu=2$. The grey circles show points at which $N^F=N^B$. The black dots indicate unstable regions in the response	
Ū	Frequency response curves at $P=0.15$ for the system with broken mirror symmetry, $\mu=2$. The grey circles show points at which $N^F=N^B$. The black dots indicate unstable regions in the response Nonreciprocal dynamics for $P=0.15$ and $\mu=2$. (a) The reciprocity norm, R , with the markers indicating $N^F=N^B$. Diamonds denote phase nonreciprocity $(N^F=N^B, \phi^F \neq \phi^B)$ and circles denote frequencies at which the response of the system is almost reciprocal $(N^F=N^B, \phi^F \approx \phi^B)$. (b) The time-domain response at the red circle, $\omega_f=1.025$. (c) The time-	
Ū	Frequency response curves at $P=0.15$ for the system with broken mirror symmetry, $\mu=2$. The grey circles show points at which $N^F=N^B$. The black dots indicate unstable regions in the response Nonreciprocal dynamics for $P=0.15$ and $\mu=2$. (a) The reciprocity norm, R , with the markers indicating $N^F=N^B$. Diamonds denote phase nonreciprocity ($N^F=N^B$, $\phi^F\neq\phi^B$) and circles denote frequencies at which the response of the system is almost reciprocal ($N^F=N^B$, $\phi^F\approx\phi^B$).	
Ū	Frequency response curves at $P=0.15$ for the system with broken mirror symmetry, $\mu=2$. The grey circles show points at which $N^F=N^B$. The black dots indicate unstable regions in the response Nonreciprocal dynamics for $P=0.15$ and $\mu=2$. (a) The reciprocity norm, R , with the markers indicating $N^F=N^B$. Diamonds denote phase nonreciprocity $(N^F=N^B, \phi^F \neq \phi^B)$ and circles denote frequencies at which the response of the system is almost reciprocal $(N^F=N^B, \phi^F \approx \phi^B)$. (b) The time-domain response at the red circle, $\omega_f=1.025$. (c) The time-domain response at the blue diamond, $\omega_f=0.99$. (d, e) Spatiotemporal	

Fig. 2.5	Locus of phase nonreciprocity $(N^F = N^B)$ as a function of the asymmetry	
	parameter, μ , at $P=0.15$. (a) Normalized reciprocity bias, R_N , and	
	the phase shift between the forward and backward configurations, $\Delta \phi =$	
	$\phi^F - \phi^B$. (b) The forcing frequency, ω_f , at which phase nonreciprocity occurs.	27
Fig. 2.6	Locus of phase nonreciprocity $(N^F = N^B)$ as a function of the forcing	
	amplitude, P , for $\mu = 2$. (a) Frequency response curves (solid) for three	
	different values of P , superimposed onto backgrounds of different colors for	
	clarity. The dashed, color-coded curve traces the locus of $N^F = N^B$; the	
	color map corresponds to the value of P along this curve. (b) Normalized	
	reciprocity bias, R_N . (c) Nonreciprocal phase shift, $\Delta \phi$	28
Fig. 2.7	Locus of phase nonreciprocity $(N^F = N^B)$ in the optical branch as a func-	
	tion of the forcing amplitude, P , for $\mu = 2$. (a) Frequency response curves	
	for two different values of P . The dashed, color-coded curve traces the locus	
	of $N^F = N^B$; the color map corresponds to the value of P along this curve.	
	(b) The forcing frequency, ω_f , at which phase nonreciprocity occurs. (c)	
	Normalized reciprocity bias, R_N , and nonreciprocal phase shift, $\Delta \phi$, along	
F: 2.0	the locus.	30
Fig. 2.8	Locus of phase nonreciprocity $(N^F = N^B)$ as a function of the damping	
	ratio, ζ_g , at $P = 0.15$. (a) Frequency response curves for two different values	
	of damping. The dashed, color-coded curve traces the locus of $N^F = N^B$;	
	the color map corresponds to the value of ζ_g along this curve. (b) The	
	forcing frequency, ω_f , at which phase nonreciprocity occurs. (c) Normalized	91
E: 2.0	reciprocity bias, R_N , and nonrecircal phase shift, $\Delta \phi$, along the locus	31
Fig. 2.9	Restoring reciprocity $R_N = 0$ for $(P, \mu) = (0.15, 2)$ by tuning a second	
	symmetry-breaking parameter, r_g . (a) Output norms for three different values of the stiffness ratio. The black dashed curve shows the locus of	
	$N^F = N^B$. The green diamond marker denotes the point at which reci-	
	procity is restored. (b) Variation of R_N and $\Delta \phi$ as a function of r_g . The	
	green diamond marker denotes the point at which reciprocity is restored.	
	(c) Time-domain response of the forward and backward configurations at	
	the green diamond marker $(R_N = 0)$	32
	the green diamond marker $(Te_{ij} = 0)$	02
Fig. 3.1	Schematic representation of the 2DoF system	39
Fig. 3.2	(a) Frequency response curves of the system with $P=2, \alpha=1, \mu=1,$ and	
	r=2.5. Time response over one forcing period at the intersections points	
	marked by black circles at (b) $\omega_f = 3.78$, and (c) $\omega_f = 2.18$. The dashed	
	lines indicate unstable regions in the response	41

Fig. 3.3	(a) Locus of phase nonreciprocity $(N^F = N^B)$ as a function of the nonlinear	
	stiffness ratio, α . (b) Nonreciprocal phase shift between the forward and	
	backward configurations, $\Delta \phi = \phi^F - \phi^B$. (c) Frequency response curves of	
	the system for $P=2, r=2.5$ and $\alpha=0.69$. (d) Time response over one	
	forcing period corresponding to the blue diamond marker	43
Fig. 3.4	Locus of phase-preserving nonreciprocity, $\Delta \phi = 0$ for (a) $P = 2$ and $r = 2.5$	
	as a function of the nonlinear stiffness ratio, α , (b) $r=2.5$ and $\alpha=0.5$ as	
	a function of force amplitude, P	44
Fig. 3.5	(a) Frequency response curves of the system with $P=5,\ r=2.5,\ {\rm and}$	
	$\alpha = 0.5$. Time response over one forcing period at the points indicated	
	by square markers: (b) $\omega_f = 3.86$, (c) $\omega_f = 1.89$, (d) $\omega_f = 1.42$, and	
	(e) $\omega_f = 1.13$	45
Fig. 3.6	Locus of phase-preserving nonreciprocity, $\Delta \phi = 0$, as a function of the	
	stiffness ratio, r , computed from the points indicated in Fig. 3.5: (a) the	
	red marker, (b) one of the black markers	47
Fig. 3.7	(a) Frequency response curves of the system with $P=5,\ r=11,\ \mu=$	
	$1, \alpha = 0.5$. Time response at the points indicated by square markers:	
	(b) $\omega_f = 5.46$, (c) $\omega_f = 4.52$ (d) $\omega_f = 1.46$	47
Fig. 3.8	Transient response of the forward and backward configurations over 100	
	forcing periods at $\omega_f=5.46$ starting from the same initial conditions	48
Fig. 4.1	Schematic of the 2DoF system consists of two linear damped oscillators	
0: -:-	coupled with a bilinear spring.	53
Fig. 4.2	Periodic orbits represented by A and C (a) non-unilateral (b) unilateral .	56
Fig. 4.3	(a) Frequency response of the symmetric 2DoF $(r = \mu = 1)$ system for the	
1 10. 110	forward configuration. Thick lines indicate response that exhibits unilat-	
	eral transmission and dashed lines indicate unstable response. Diamond	
	markers indicate period-doubling bifurcation points. The upper right inset	
	shows the unilateral time response at the frequency highlighted by the black	
	square. (b) Unilateral transmission R_u as a function of forcing frequency.	57
Fig. 4.4	Locus of the onset of unilateral transmission $R_u = 1$ as a function of the	
0: -:-	stiffness ratio r for (a) Output amplitude (b) Forcing frequency	59
Fig. 4.5	(a) Frequency response of the asymmetric system $r = 0.28$ for the onset of	
· -	unilateral transmission at the peak frequency (b) Frequency response of the	
	asymmetric system $r = 0.25$ for the onset of unilateral transmission before	
	the peak frequency	59

Fig. 4.6	Frequency response of the system with locus of $R_u = 1.1$ as a function of	
	μ . Thick lines indicate response that exhibits unilateral transmission and	
	dashed lines indicate unstable response	59
Fig. 4.7	Influence of bilinear ratio β on unilateral transmission for $r=1, \mu=3,$	
	$\zeta=0.03,$ and $F=0.15.$ (a) Softening bilinearity, $\beta<1,$ (b) hardening	
	bilinearity, $\beta > 1$	60
Fig. 4.8	(a) Reciprocity bias for the system with $r = 0.25$ and $\mu = 1$. Thick lines	
	indicate response that exhibits unilateral transmission and dashed lines in-	
	dicate unstable response in either the forward or backward configuration.	
	(b) to (d) show the time-domain output displacement at the points indi-	
	cated by the star, circle and diamond markers, respectively	61
Fig. 4.9	(a) DC value of the response for the system with $r = 0.25$ and $\mu = 1$ (b)	
	AC value of the response (c) Unilateral ratio for the forward and backward	
	configurations	62
Fig. 4.10	Periodic structure with a bilinearly coupled unit cell	63
Fig. 4.11	Frequency response of the system for $n=2, \mu=3$ and $r=1$ for (a) forward	
	configuration and (b) backward configuration. Diamonds and pentagrams	
	denote period-doubling and torus bifurcations, respectively. Time-domain	
	response of the system for the forward and backward configurations at (c)	
	$\omega_f = 0.82$ (d) $\omega_f = 1.22$, (e) $\omega_f = 1.41$ and (f) $\omega_f = 2.82$ indicated	
	by vertical lines. In panel (e), $x_1^B(t)$ is computed using direct numerical	
	integration	65
Fig. 4.12	Frequency response curves of the forward and backward configurations for	
8	$\mu = 3, r = 1, \text{ and } \zeta = 0.03 \text{ for (a) } n = 4, \text{ (b) } n = 8, \text{ and (c) } n = 0.03 \text{ for (a) } n = 0.03 \text{ for (b) } n = 0.03 \text{ for (c) } n = 0$	
	16. Diamond markers denote period-doubling bifurcations. Subscript i in	
	$ C_i + A_i $ refers to either n or 1, corresponding to the forward and backward	
	configurations, respectively	67
Fig. 4.13	(a) Frequency response curves of the forward and backward configurations	
0 -	for $n = 16$, $\mu = 3$, $r = 1$, and $\zeta = 0.01$. Time-domain response of the	
	system for the forward and backward configurations at (b) $\omega_f = 1.41$ and	
	(c) $\omega_f = 2.82$. In panel (b), $x_1^B(t)$ is computed using direct numerical	
	integration	68
Fig. 4B.1		
G:	$\zeta = 0.03$ and $\beta = 0.1$ at two forcing amplitudes	71

Chapter 1

Introduction

Reciprocity theorems pertain to the observation that a system's response at point A due to a force at point B is identical to the response at point B when the same force is applied at point A. This fundamental theorem, often stated as a principle, has simplified analysis and design in various fields of engineering and physics for over a century. However, reciprocity inherently limits the control over wave transmission for applications that require directional energy flow or selective wave filtering. To overcome this limitation, nonreciprocal systems are introduced, enabling asymmetric wave transmission and unlocking new possibilities in wave manipulation and energy control. This chapter reviews these concepts.

1.1. Reciprocity

Reciprocity is a fundamental theorem of wave motion that ensures symmetric wave transmission between any two points in a material. In other words, an identical incident wave traveling in opposite directions should produce the same transmitted response in a linear time-invariant system. This principle has been extensively studied since the nineteenth century with contributions from Helmholtz [1] and Rayleigh [2] among many others.

Reciprocity in static systems

Reciprocity in a static system can be understood through Betti's reciprocity theorem. This principle can be effectively illustrated using a simple elastic body, such as the spring-mass system shown in Fig. 1.1. According to Betti's theorem, if a static force F_1 applied at M_1 causes a displacement $u_{2,1}$ at M_2 , and a force F_2 applied at M_2 causes a displacement $u_{1,2}$ at M_1 , then the following reciprocity relation holds:

$$F_{2}.u_{2,1} = F_{1}.u_{1,2} \tag{1.1}$$

The principle behind this relation is that the work done by F_1 on M_2 is equal to the work done by F_2 on M_1 .

Reciprocity in dynamic systems

In elastodynamics, one of the earlier proofs of reciprocity was provided by Rayleigh [2] in the nineteenth century. Fig. 1.2(a) illustrates a reciprocity test performed on a mechanical

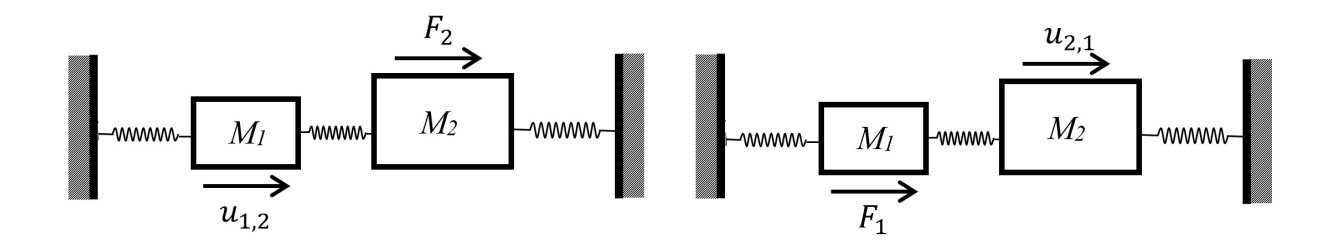


Figure 1.1: 2DoF system used to explain the Betti's reciprocity theorem.

system. The reciprocity principle states that if an excitation force is applied at point A, generating a response at point B (the forward configuration), then applying the same force at B will produce an identical response at A (the backward configuration), assuming that the waveguide is linear and time-invariant. Fig. 1.2(b) shows the time-domain response of the waveguide under a harmonic excitation for forward and backward configurations in one period. As seen in panel (b), this response remains consistent in amplitude, frequency, and phase in opposite directions. Notably, this principle holds even in the presence of heterogeneity and linear damping. Additionally, the response of a mirror-symmetric transmission channel is always reciprocal because of symmetry, even if the conditions of linearity and time invariance are relaxed.

In addition to its numerous theoretical implications [3], reciprocity has played a crucial role in shaping experimental methodologies across multiple disciplines. In vibroacoustics, it has been instrumental in the development of efficient measurement techniques for sound propagation, enabling noise control strategies and source localization methods [4, 5]. In structural dynamics, reciprocity principles underpin modal analysis and Transfer Path Analysis (TPA), allowing engineers to characterize vibration transmission in complex structures with minimal intrusive measurements [6, 7].

Reciprocity theorems have been used to facilitate defect detection and material characterization in non-destructive evaluation techniques, where they help determine the elastic constants and anisotropic material properties [8]. In ultrasonics, reciprocity theorems are widely used in imaging and therapeutic applications, improving transducer calibration, signal focusing, and wave-based sensing techniques [9]. In linear seismology and geophysics, reciprocity governs wave propagation models, enabling the reconstruction of subsurface structures, earthquake source inversions, and seismic interferometry methods [10].

It is important to emphasize that while reciprocity is often associated with spatial symmetry, the two concepts are fundamentally distinct. Spatial symmetry refers to the geometric invariance of a system, whereas reciprocity is a wave-based principle that holds even in

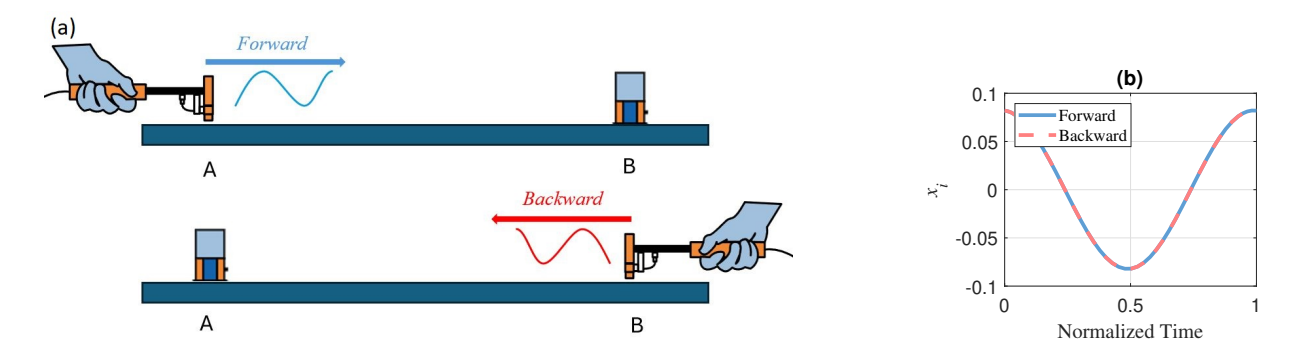


Figure 1.2: (a) Schematic of a waveguide under two wave transmission configurations. (b) Time-domain response of two configurations.

asymmetric media.

1.2. Nonreciprocity

Reciprocity imposes inherent constraints on vibration transmission control because it prevents the wave transmission characteristics between two points from being dependent on the direction of transmission. Consequently, breaking reciprocity can provide control over the direction of wave propagation, enabling or inhibiting wave transmission in specific directions.

For instance, an acoustic diode introduced by Liang et al. [11] demonstrates one of the most celebrated indicators of nonreciprocity by allowing one-way wave transmission using a combination of nonlinear and asymmetric materials. Darabi et al. [12], among many others, expanded on this design by designing a broadband passive nonlinear acoustic diode, utilizing nonlinearity and asymmetric resonators to enhance wave rectification across a wide frequency range, thereby improving energy efficiency and control.

Furthermore, nonreciprocal wave control plays a crucial role in applications where selective sound direction is beneficial, such as noise isolation and communication filtering. Cummer [13] explored methods to enable preferential wave transmission, effectively functioning as acoustic isolators. Energy concentration and localization have also emerged as key applications of nonreciprocity. Wang et al. [14] demonstrated how asymmetric nonlinear lattices can induce irreversible energy transfer, leading to wave trapping and controlled energy localization, useful in applications such as energy harvesting and impact mitigation.

Nonreciprocal systems have also paved the way for topological wave protection [15], where robust, disorder-resistant wave propagation is achieved. Lu et al. [15] explored how topological photonic structures enable backscatter-free wave transmission in electromagnetic systems.

Moreover, nonreciprocal phase shifts [16, 17] have been investigated for applications in sig-

nal processing. Zangeneh-Nejad et al. [16] introduced a Doppler-based acoustic gyrator that manipulates wave phase in a nonreciprocal manner, enabling novel acoustic signal processing techniques. The development of electromagnetic phase shifters has further expanded the scope of nonreciprocal wave manipulation. Hamoir et al. [18] introduced a self-biased nonreciprocal microstrip phase shifter leveraging magnetic nanowires, providing a compact and efficient design for radio frequency applications. Palomba et al. [19] proposed a broadband nonreciprocal phase shifter, demonstrating its effectiveness in microwave engineering and telecommunications.

Reciprocity can be broken through various mechanisms. Three common methods are incorporating moving components or circulating flows within the propagation medium [16, 20], implementing spatiotemporal modulation of the effective properties [21–24], and leveraging nonlinearity [25–28]. The first two methods are active, requiring an external energy source and altering the time-invariant property. Conversely, the third is passive and relies on nonlinearity and spatial asymmetry as key ingredients. A comprehensive review of various physical mechanisms to achieve nonreciprocity in acoustic and elastic media can be found in [17].

1.2.1. Active media

Kinetic media. Kinetic media achieve nonreciprocity by incorporating moving components or circulating flows within the system. Unlike static structures, these media introduce velocity-dependent effects that break time-reversal symmetry, enabling directional wave transmission.

A well-known example of kinetic nonreciprocity is the Doppler-based nonreciprocal acoustic waveguide [16]. As shown in Fig. 1.3(a), this device comprises a fluid flowing at a constant velocity in a fixed direction. Sound waves traveling along and against the flow in the waveguide experience different propagation speeds and consequently different phase shifts, as illustrated in Fig. 1.3(b).

Another well-known example of kinetic nonreciprocity can be observed in a cylindrical cavity connected to three waveguides, where rotating airflow inside the cavity induces nonreciprocity. As shown in Fig. 1.3(c) when the air is stationary, reciprocity is preserved, and an incident wave at one port splits evenly between the other two ports. However, when the airflow within the ring resonator rotates at a specific subsonic speed, as shown in panel (d), reciprocity is strongly broken, leading to a dipolar resonance. In this state, an incoming wave at a given port is transmitted exclusively to one of the two remaining ports, effectively enabling directional wave control [20].

Spatiotemporal modulation. In linear systems, varying one of the effective properties

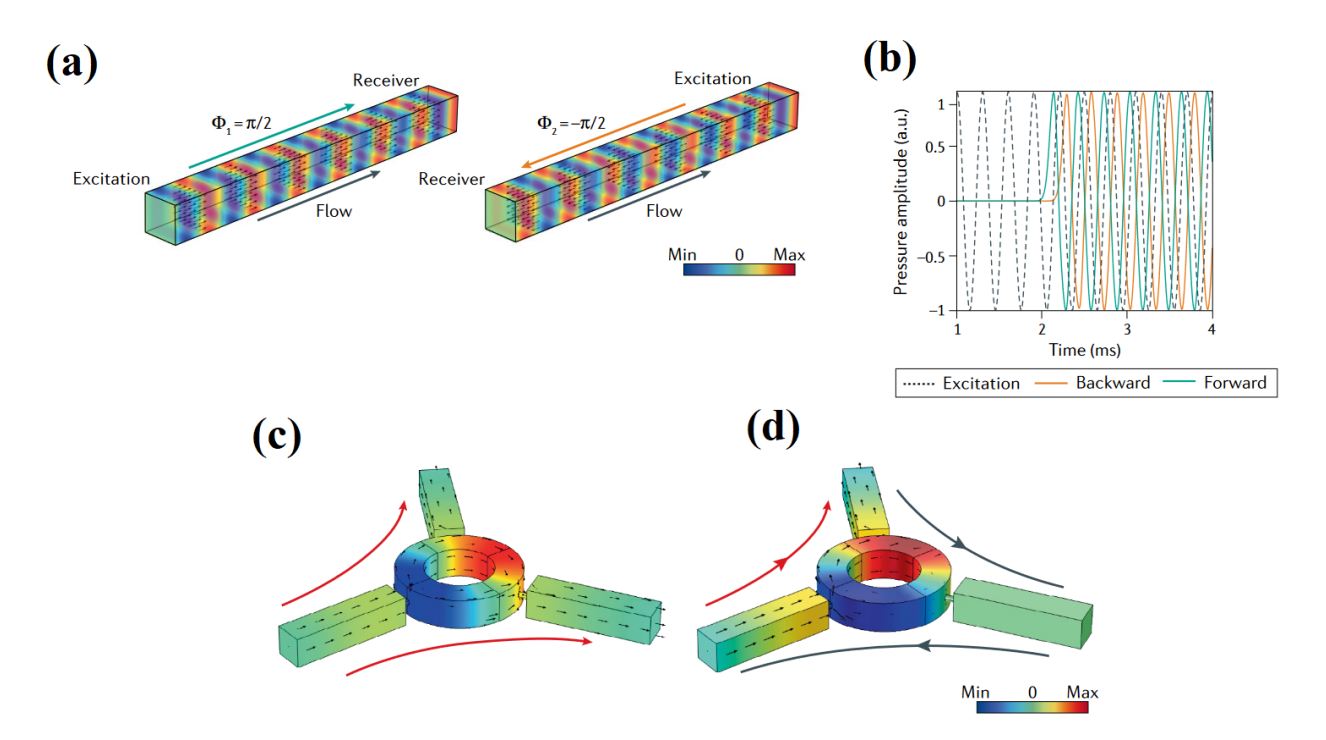


Figure 1.3: [17] Nonreciprocity induced by kinetic media. (a) Doppler-based nonreciprocal acoustic waveguide with unidirectional fluid flow. (b) Response of the acoustic gyrator system in opposite directions. Cylindrical cavity connected to three waveguides with (c) stationary air and (d) rotating airflow.

as a function of both time and space is an established method for achieving nonreciprocal transmission. System's properties modulated in space and time can be either the bulk properties such as spatial variation of the elastic moduli and mass density [29], or the boundary conditions such as interaction coefficients between the structure and attached resonators or the ground [23].

1.2.2. Passive media

Introducing nonlinear forces and spatial asymmetry within a structure offers a passive means to achieve nonreciprocity, eliminating the need for external bias or activation. This dissertation concentrates exclusively on this passive approach.

Nonlinearity in mechanical systems can arise from various sources. Geometric nonlinearity occurs in structures and mechanical systems when deformations become significant enough that linear assumptions fail. This leads to a nonlinear relationship between strain and displacement [30, 31], resulting in stiffness variations that notably affect the dynamic behavior of the system.

Material nonlinearity refers to the behavior of a material that does not have a linear relationship between stress and strain. In simpler terms, when a material is subjected to external forces (stress), the resulting deformation (strain) does not change proportionally, unlike linear materials where this relationship is straightforward and predictable [32]. Material nonlinearity is evident in the inelastic buckling of structures subjected to compressive loads in civil engineering [33] and in the mechanical response of biological and bioinspired materials [34].

Contact-type nonlinearity occurs when two or more bodies interact through contact, resulting in highly nonlinear force-displacement relationships. Factors such as friction, surface roughness, and geometric configurations contribute to this complex behavior. This phenomenon is commonly observed in mechanical systems such as gears, bearings, bolted joints, and impact scenarios, where contact forces continuously change due to loading conditions and surface deformations [35–37].

Nonlinearity can result in nonreciprocal transmission of waves in passive systems that are not mirror-symmetric. As waves propagate through a waveguide, nonlinearity can generate additional harmonics, which may exhibit different transmission characteristics depending on the direction. This property has been applied in acoustic isolators for example [11], where a nonlinear layer is attached to a linear periodic waveguide. When waves approach from the nonlinear side, harmonic generation allows transmission, whereas waves from the linear side are blocked because their harmonics are filtered out.

Another mechanism for nonreciprocal wave propagation is the energy dependence of resonance frequencies [38]. In a waveguide consisting of a linear medium with an asymmetrically placed nonlinear medium, the incident wave amplitudes reaching the nonlinear region differ depending on the direction of propagation. As a result, the nonlinear section processes the received amplitudes differently, leading to direction-dependent transmission. An experimental demonstration of this phenomenon has been observed in a granular chain with localized nonlinearity [39]. Bifurcations, which occur when small parameter changes cause sudden shifts in system behavior, can also lead to nonreciprocity [40, 41].

Bilinear media, where stiffness switches between two values at a critical point, offer another mechanism for nonreciprocal wave transmission. Unlike conventional nonlinear models, bilinear materials may exhibit amplitude-independent nonreciprocity. Spring—mass chains with spatially varying bilinear springs exhibit directional asymmetry, leading to nonreciprocal transmission [28, 42, 43]. Bilinear stiffness, as a key component in one of our research directions, is discussed in detail in Sec. 1.3.

The existence of nonlinear forces is not a sufficient condition for nonreciprocal response to exist. For example, the response of a system or transmission channel that possesses mirror symmetry remains reciprocal even in the presence of strong nonlinearity: the right-to-left transmission path is identical to the left-to-right path by virtue of symmetry. Thus, it is necessary to break the mirror symmetry of the system to enable a nonreciprocal response [38].

Fig. 1.4(a) shows two coupled oscillators connected to the ground by springs with cubic nonlinearity. The asymmetry in the system can be tuned by the ratio between masses (M_2/M_1) . The forward configuration, where M_1 is excited and the response of the M_2 is observed as the output, is compared with the backward configuration, where M_2 is excited and the response of the M_1 is observed. Panel (b) shows the frequency response curve of the symmetric system for $M_1 = M_2$. Even in the presence of nonlinearity, the response of the asymmetric system with $M_2 = 2M_1$. The forward and backward configurations exhibit distinct response curves, demonstrating nonreciprocity, which arises due to the combined effects of nonlinearity and asymmetry. This ratio is selected as a representative example to clearly illustrate the effect of asymmetry; other mass ratios can also lead to nonreciprocity but are not shown here.

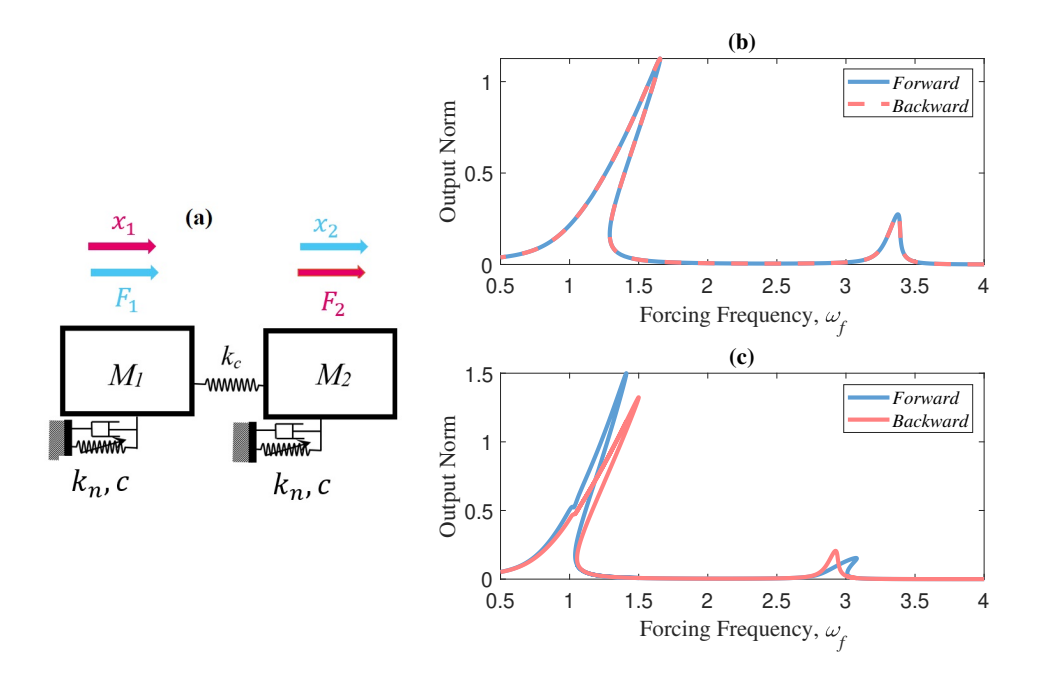


Figure 1.4: (a) Schematic representation of the two-degree-of-freedom (2DoF) system with grounded cubic nonlinear stiffness. Frequency response curve of (b) the symmetric system, $M_2 = M_1$ and (c) the asymmetric system, $M_2 = 2M_1$.

1.3. Bilinear stiffness

Bilinear stiffness describes a system behavior where the effective elasticity undergoes a sudden change beyond a specific deformation threshold. As illustrated in Fig.1.5(a), systems with bilinear stiffness exhibit one stiffness value up to a defined offset s, and transition to a different stiffness value once this threshold is exceeded. This non-smooth behavior leads to complex nonlinear dynamic responses [44].

The influence of bilinear stiffness and damping on vibrational response has been extensively studied for decades [45–54]. This nonlinear characteristic appears in various engineering applications, such as cracked elastic structures [55, 56], vibro-impact drilling systems [57], and systems with intermittent contact [58, 59]. Additionally, there have been extensive studies on wave propagation within bimodular media [60–67]. Studies on discrete vibration systems incorporating bilinear stiffness have discovered intriguing nonlinear behaviors, including output sign inversion [68], directional wave scattering [69], and nonreciprocal wave propagation [27, 28, 70].

1.3.1. Amplitude-independent bilinear force

Bilinear systems can exhibit a special case of nonlinearity where the response remains amplitude-independent. This means that scaling the input force results in a proportionally scaled output, unlike other nonlinearities (e.g., cubic stiffness shown in Fig. 1.4), where response amplitude depends on the magnitude of the input force.

Fig. 1.5(a) illustrates the force-deflection relationship of a bilinear spring, where the restoring force changes slope at x = s, referred to as the bilinearity offset. The parameter $\beta = K_2/K_1$ is defined as the bilinear stiffness coefficient. When the offset is zero (s = 0), the response of the system does not depend on the amplitude of motion. Fig. 1.5(b) depicts a single-degree-of-freedom (SDoF) system, grounded by a bilinear spring, under harmonic excitation. The bilinear restoring force, F(x) in Fig. 1.5(a), does not have odd symmetry with respect to x. This results in a non-zero DC component in the steady-state response. Thus, the displacement of the mass can be approximated as:

$$x = r_0 - r_1 \cos(\omega t + \theta) \tag{1.2}$$

where r_0 is the DC value, r_1 is the AC value, ω is the excitation frequency, and θ represents the phase difference between the response and the harmonic force.

Figs. 1.5(c) and (d) show the frequency response curves of r_1 and r_0 respectively for three different values of the bilinear stiffness coefficients, β . The nondimensional frequency is given

by $\Omega = \omega/\omega_0$ with $\omega_0 = \sqrt{K_1/m}$. When $\beta = 1$ (linear system), the resonant peak appears at $\Omega = 1$ and the DC value is zero. If the tensile stiffness is lower than the compressive stiffness ($\beta = 0.2$), the resonance peak shifts to lower frequencies with increased amplitude. Conversely, for larger tensile stiffness ($\beta > 1$), the resonance peak moves to higher frequencies and decreases in magnitude. In both cases, a nonzero DC component emerges, with its peak occurring at the same frequency as the peak value of the AC component.

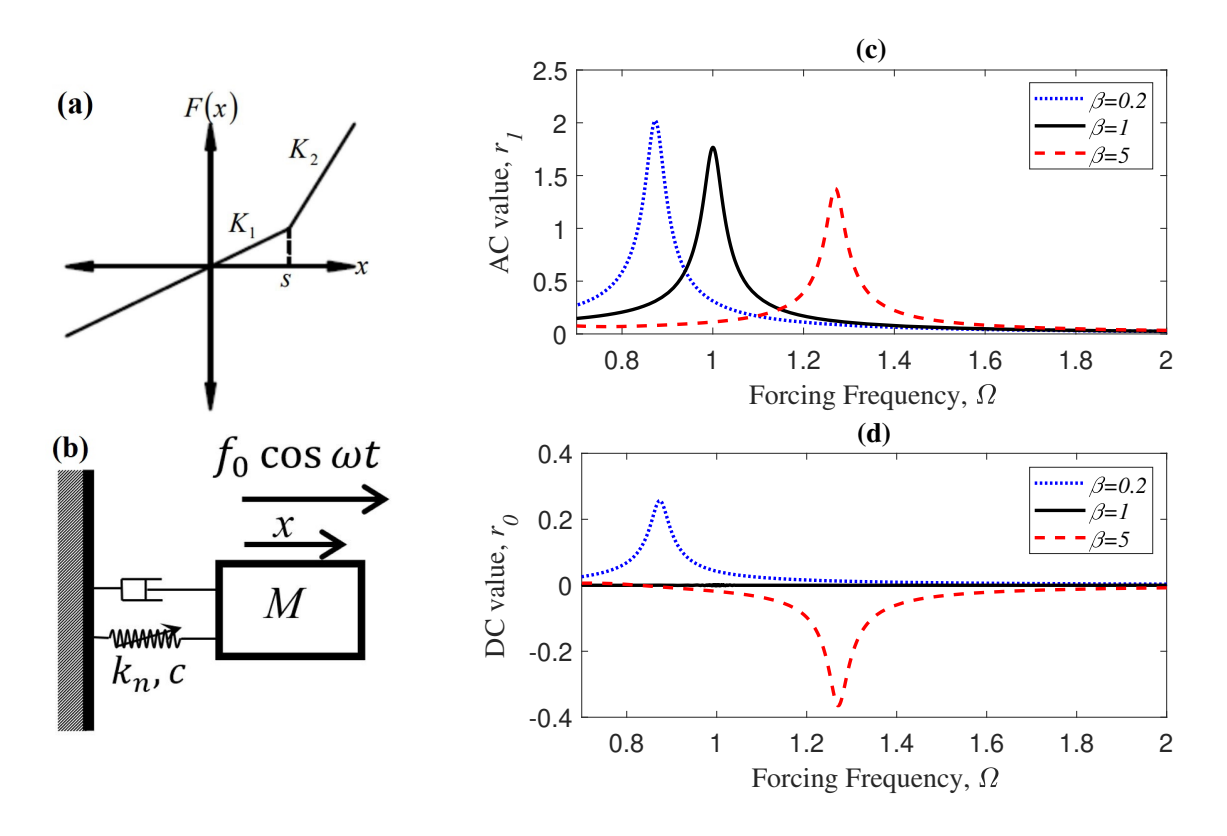


Figure 1.5: (a) Restoring force of a bilinear spring. (b) Schematic representation of the the SDoF vibration system with bilinear stiffness. Frequency response curve of (c) the AC value, and (d) the DC value.

1.3.2. Amplitude-dependent bilinear force

When the offset is nonzero ($s \neq 0$), the response of the system becomes amplitude-dependent. Fig. 1.6 shows the response of the bilinear system from Fig. 1.5(a) for s = 0.6 and $\beta = 5$. As the forcing amplitude increases from a small value, the response of the system remains linear until the displacement amplitude reaches the offset (x = 0.6). Once this threshold is crossed, the effective stiffness increases, shifting the resonant peak to higher frequencies. This behavior is evident in Fig. 1.6(a), where for small force amplitudes ($f_0 = 0.05$, blue line), the system behaves linearly. However, when the force amplitude increases sufficiently

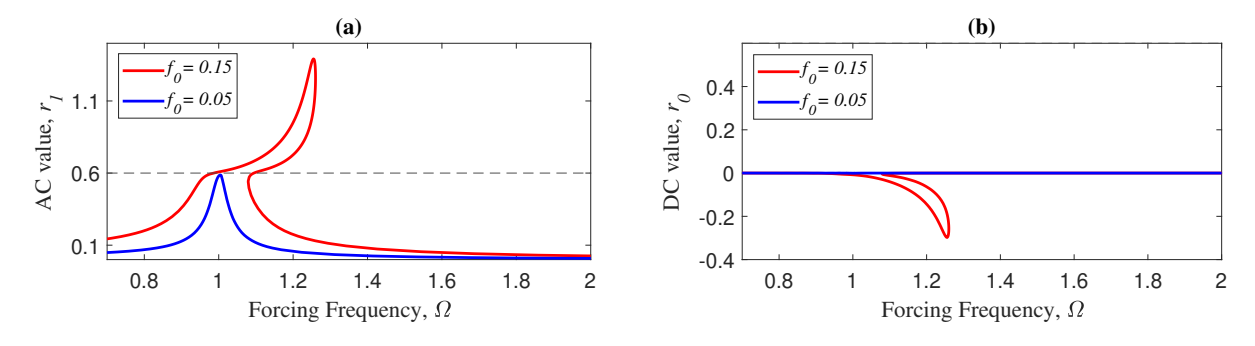


Figure 1.6: Frequency response curve of the single-degree-of-freedom (SDoF) system with bilinear stiffness $\beta = 5$ and an offset s = 0.6. (a) AC value and (b) DC value.

($f_0 = 0.15$, red line), nonlinear effects emerge due to the change in the stiffness slope. As a result, the response curve bends toward higher frequencies, reflecting the hardening effect associated with $\beta > 1$.

1.4. Nonreciprocity in periodic structures

Periodic structures, composed of repeating unit cells, are widely used in engineering and scientific applications due to their unique wave propagation characteristics, which stem from their inherent periodicity [71]. These structures exhibit frequency band gaps that restrict wave propagation within specific frequency ranges. This phenomenon, commonly known as Bragg scattering [72], results from the cumulative interference of waves scattered by each unit cell, leading to wave reflection and localization when the frequency falls within the stop band.

Recent advances in tunable periodic materials [73] have expanded the versatility of these structures. Researchers have designed reconfigurable phononic crystals capable of real-time control over wave propagation. These adaptive materials enable programmable nonreciprocity. In periodic structures, nonlinearity and asymmetry, the two essential requirements for achieving nonlinear nonreciprocity, can be introduced at the unit cell level, resulting in their periodic repetition throughout the structure; see [74–77] for examples of this approach. Alternatively, passive nonreciprocity can be realized by incorporating asymmetry and nonlinearity either locally, (e.g. as a gate or defect) [11, 12, 41, 78, 79], or gradually throughout the system [43].

The ability to control nonreciprocal wave propagation in periodic systems has led to significant advances in areas such as wave filtering, unidirectional energy transport, and vibration isolation [76, 77]. Another promising application of periodic nonreciprocal materials is in topological wave transmission, where edge states within topological band gaps enable highly

robust, backscatter-free propagation [15, 77]. These properties are particularly relevant for signal processing, and noise control, where one-way transmission is desirable. Furthermore, engineered periodic structures play a critical role in nonreciprocal frequency conversion, allowing for energy transfer between different frequency bands through nonlinear interactions [78].

Overall, periodic materials provide an ideal platform for exploiting nonreciprocal dynamics. Using the benefits of periodic structures, researchers are advancing novel metamaterials and phononic devices, leading to significant advances in fields such as acoustic wave engineering, microwave technologies, and optical communications.

1.5. Gaps in the literature

Nonreciprocity is generally studied in terms of the amplitude of transmitted energy in a system. However, there are other overlooked properties of nonreciprocal vibration transmission that warrant detailed investigation. In this chapter, we highlight some of these underexplored phenomena. First, we address the role of the *phase* in nonreciprocal dynamics. Next, we discuss *unilateral transmission*, a unique form of vibration transmission facilitated by induced nonreciprocity in the system.

1.5.1. Influence of phase

The focus of studies on nonlinear nonreciprocity is on maximizing the nonreciprocal energy transfer: the difference in the transmitted energy or amplitude when the locations of the source and receiver are exchanged. Within this context, a highly nonreciprocal response corresponds to unidirectional transmission of energy within a system, which enables targeted energy transfer [80].

However, in addition to the difference in transmitted energies (energy bias), nonreciprocity can be characterized by a difference in the phase of the transmitted vibrations (phase bias), which is often overlooked. Nonreciprocity in the transmitted phase has been a subject of investigation in electronics and optics [81, 82], with recent applications in optical and acoustic waveguides [83–86]. The ability to passively control the direction-dependent transmitted phase of a waveguide may find application in vibration control strategies or in performing certain logic operations [87].

Despite its potential, the role of phase in nonreciprocal systems, particularly in mechanical and vibrational contexts, remains underexplored. Understanding how transmitted phases contribute to nonreciprocity, independent of energy transfer, is a critical step toward designing more efficient and controllable vibration systems. This gap in the literature forms the

foundation of the first part of the present study.

1.5.2. Unilateral Transmission

Unilateral transmission is a wave propagation phenomenon in which the transmitted wave remains exclusively in tension or compression, meaning that deformations relative to the static equilibrium position retain the same sign throughout propagation. This concept was first introduced by Lu and Norris [28], who demonstrated unilateral transmission using a single bilinear stiffness element connecting two waveguides. They derived analytical conditions linking the bilinear spring properties to the emergence of unilateral transmission. While this effect has been explored in wave propagation, its implications in vibration dynamics remain largely unexamined. This gap provides a basis for the second part of the current study.

1.6. Thesis Objectives

Nonreciprocity plays a crucial role in controlling vibration transmission, offering opportunities to design advanced mechanical systems with precisely tailored response characteristics. This thesis investigates three overlooked phenomena related to nonreciprocity that provide new insights into the design of these mechanical systems. The first examines *phase nonreciprocity* (energy-preserving nonreciprocity), where nonreciprocity arises solely from differences in transmitted phases. The second explores *phase-preserving nonreciprocity*, where the transmitted phases remain equal and nonreciprocity is driven only by differences in transmitted energies. The third phenomenon investigates *unilateral transmission*, where transmitted waves remain in tension or compression within nonreciprocal systems.

1.6.1. Phase nonreciprocity

Most studies on nonreciprocity in elastodynamics focus on maximizing nonreciprocal energy transfer, typically quantified by the difference in transmitted amplitude when the locations of the source and receiver are interchanged. In this context, a system is considered highly nonreciprocal if it allows wave transmission in one direction while suppressing it in the opposite direction. In the first part of this thesis, we take on a different perspective to address a question that is primarily overlooked: how does the difference in the transmitted phases (not energies) contribute to nonreciprocity?

To understand the influence of phase, we investigate response regimes that are characterized by nonreciprocal phase shifts but equal transmitted energies: when the locations of the source and receiver are interchanged, the amplitude of transmitted vibrations remains unchanged but the transmitted phases are not equal. We refer to this response regime as *phase*

nonreciprocity because a phase difference between the forward (left-to-right) and backward (left-to-right) configurations is the only contributor to nonreciprocity.

Our objective is to examine phase nonreciprocity in a periodic waveguide. This will be achieved through a parametric study, analyzing the effects of system parameters such as input energy, energy dissipation, and spatial asymmetry on phase nonreciprocity. We focus on the steady-state response of a nonlinear periodic system under harmonic excitation. In this context, the phase of the response represents the angular offset between displacement (or another response variable) and the external harmonic force, indicating whether the response leads or lags the excitation.

1.6.2. Phase-preserving nonreciprocity

We further explore the role of phase in nonreciprocity by addressing another question: can nonreciprocal response regimes exist where the transmitted phases remain equal, but the transmitted energies differ? We refer to such regimes as *phase-preserving nonreciprocity*. By investigating phase-preserving nonreciprocity, we aim to determine whether energy bias alone, without any contribution from phase, can lead to nonreciprocal behavior. This investigation reveals yet another fundamental aspect of how phase influences the breaking of reciprocity.

To achieve this, a parametric study will be conducted on a coupled oscillator system under harmonic excitation. The goal is to fine-tune the system parameters, primarily the asymmetry parameters, to identify response regimes where the system exhibits phase-preserving nonreciprocity.

1.6.3. Unilateral transmission

The primary objective of this part of the study is to investigate unilateral transmission within mechanical vibration systems, with a particular focus on how system parameters influence this phenomenon. Unilateral transmission is when the transmitted vibrations remain in a either purely tensile or purely compressive state. To achieve unilateral transmission, the system requires a nonlinear stiffness function that lacks odd symmetry. This asymmetry introduces a DC component in the response of the system, enabling the unilateral transmission. As discussed in Sec. 1.3, bilinear stiffness is a strong candidate for this effect, as its inherent asymmetry naturally leads to the presence of a DC component (in a Taylor expansion of a bilinear force, the coefficient of the quadratic term is typically not small compared to that of the cubic term). We seek to investigate how bilinear stiffness contributes to unilateral transmission. Our objective is to examine a model consisting of two coupled oscillators with

bilinear coupling, to understand how this nonlinearity affects the steady-state response of the system under harmonic excitation.

Previous studies on bilinear coupling have primarily examined nonreciprocity in terms of variations in transmitted energy in opposite directions [25, 43, 88–90]. In contrast, our objective is to specifically explore nonreciprocity in the context of unilateral transmission. We aim to identify and characterize other direction-dependent response behaviors, such as the emergence of higher harmonics, period-doubling, and quasiperiodic dynamics—phenomena that have not been extensively studied in the literature.

A further objective is to extend our analysis to periodic lattice materials with tunable properties, as advancements in their fabrication offer new avenues for controlling wave propagation [73]. The goal here is to explore how the periodic structure composed of bilinearly coupled units influences transmission behavior, particularly in the context of unilateral transmission. This will include a parametric study to assess the impact of lattice size and energy dissipation on the observed transmission characteristics.

1.7. Thesis Outline

This thesis is organized in five chapters and is written according to the manuscript-based thesis regulations stated in the *Thesis Preparation Guide*.

Chapter 2 explores nonreciprocal phase shifts in a nonlinear periodic waveguide. We investigate the effects of nonlinearity and asymmetry within the unit cell and perform a parametric study to characterize phase nonreciprocity under steady-state conditions. We identify conditions where reciprocal response emerges despite broken mirror symmetry, highlighting the crucial role of phase in nonlinear nonreciprocity.

Chapter 3 investigates phase-preserving nonreciprocity in coupled nonlinear systems under harmonic excitation. We examine how energy bias alone, without the influence of the phase, can produce nonreciprocity and demonstrate how two independent symmetry-breaking parameters enable this effect.

Chapter 4 explores unilateral transmission in systems with bilinear coupling, where transmitted waves remain in pure tension or compression. We analyze how breaking the mirror symmetry of the system enables unilateral transmission near primary resonance and enables nonreciprocal dynamics. The study extends to bilinear periodic structures, examining the role of system size and energy dissipation on transmission characteristics.

Chapter 5 summarizes the major contributions and conclusions, together with recommenda-

tions for possible future work.

Chapter 2

Nonreciprocal phase shifts in a nonlinear periodic waveguide

2.1. Introduction

Reciprocity refers to a symmetry property of a vibrating system that dictates that transmitted vibrations from point A to point B are identical in amplitude, frequency and phase to those from point B to point A. In other words, the transmission characteristics between two points do not depend on the direction. This property has been studied and utilized in applications since the nineteenth century, with contributions from Helmholtz [1] and Rayleigh [2] among others. In addition to its numerous theoretical implications [3], reciprocity has enabled various experimental approaches, for example in vibroacoustics [4, 5], structural dynamics [6, 7], defect detection and determination of elastic constants [8], ultrasonics [9] and seismology and geophysics [10].

Waveguides are structures designed to guide and manipulate the propagation of waves within a confined region. They are ubiquitous in various areas of science and technology [91–93]. The operation of waveguides are typically restricted by reciprocity, meaning that their propagation characteristics are independent of the direction of wave travel; perhaps the most widely known exception to this are diodes in electronics.

In mechanical systems, there exist several ways for the dynamic response to exhibit non-reciprocal characteristics [17]. The presence of nonlinear forces within the structure is a common way to realize nonreciprocity in a passive way, i.e., with no need for external bias or activation. In this work, we focus exclusively on this approach. Comprehensive discussion of other approaches to realize nonreciprocity are found elsewhere [17, 94, 95].

Among the appealing features of nonlinear nonreciprocity is that it makes the transmission characteristics between two points in a waveguide dependent on the direction of wave propagation. Thus, nonreciprocity could provide control over the direction of wave propagation, enabling or inhibiting wave transmission in specific directions. For instance, Liang et al. proposed an acoustic diode by combining a superlattice with a highly nonlinear medium, demonstrating a pronounced rectifying effect in the energy flux within a specific frequency range [11]. Boechler et al. employed a defective granular chain composed of spherical beads to achieve nonreciprocal transmission thresholds for harmonic excitation within a bandgap [41]. The response of a nonlinear system is generally dependent on the energy of the system (amplitude of motion), but there do exist response regimes that are independent of the energy

level as well. For example, Lu and Norris used bilinear stiffness to realize a diode-like waveguide, in which waves with distinct patterns are transmitted in different directions regardless of the wave amplitude [43].

The existence of nonlinear forces is not a sufficient condition for nonreciprocal response to exist. For example, the response of a system or transmission channel that possesses mirror symmetry remains reciprocal even in the presence of strong nonlinearity: the right-to-left transmission path is identical to the left-to-right path by virtue of symmetry. Thus, it is necessary to break the mirror symmetry of the system to enable a nonreciprocal response [38]. In periodic systems, our focus in this work, nonlinearity and asymmetry can be introduced at the level of the unit cell, thereby appearing periodically throughout the structure; see [74–77] for examples implementing this approach. Alternatively, nonlinear nonreciprocity is achieved by incorporating asymmetry either locally (such as a gate or defect) [11, 12, 41, 78, 79] or gradually throughout the system [43, 96].

The focus of studies on nonlinear nonreciprocity is on maximizing the nonreciprocal energy transfer: the difference in the transmitted energy or amplitude when the locations of the source and receiver are exchanged. Within this context, a highly nonreciprocal response corresponds to unidirectional transmission of energy within a system, which enables targeted energy transfer [80]. In this work, we take on a different perspective to address a question that is primarily overlooked: how does the difference in the transmitted phases (not energies) contribute to nonreciprocity?

To understand the influence of phase, we investigate response regimes that are characterized by nonreciprocal phase shifts but equal transmitted energies: when the locations of the source and receiver are interchanged, the amplitude of transmitted vibrations remains unchanged but the transmitted phases are not equal. We refer to this response regime as *phase nonreciprocity* because a phase difference between the forward (left-to-right) and backward (left-to-right) configurations is the only contributor to nonreciprocity. Creating nonreciprocity in the transmitted phase has been a subject of investigation in electronics and optics for some time now [81, 82] with recent applications in optical and acoustic waveguides [83–85]. The ability to passively control the direction-dependent (nonreciprocal) transmission phase of a waveguide may find application in vibration control strategies or in performing certain logic operations [97].

Phase nonreciprocity in mechanical systems is already reported in systems with two degrees of freedom that have well-separated modes [98]. Here, we extend and expand this work to periodic waveguides, where there exists modal overlap within a pass band. We perform a parametric study to investigate the influence of forcing amplitude, damping and asymmetry

on phase nonreciprocity. We focus exclusively on the steady-state response of a nonlinear periodic system to external harmonic excitation. In this context, the phase of the response refers to the angular relationship between the displacement (or another response variable) and the harmonic excitation force. This phase difference represents the delay or advance of the steady-state response relative to the excitation force over one cycle of oscillation. Phase nonreciprocity, therefore, refers to the scenario in which the phase of the response (but not its energy) changes if the locations of the source and receiver are interchanged.

We conduct our study on a periodic system that comprises eight unit cells, each with two degrees of freedom. Nonlinearity and asymmetry are both introduced within the unit cell. The source of nonlinearity is the cubic restoring force that grounds every mass in the system. The ratio of the two masses and the two springs in the unit cell act as two symmetry-breaking parameters in this study. We compute the locus of phase nonreciprocity and characterize the response using the nonreciprocal phase shift.

It is already known that asymmetry is a necessary but insufficient condition for realizing nonreciprocity in nonlinear systems [99–101]. In the context of phase nonreciprocity, a zero nonreciprocal phase shift corresponds to a reciprocal response. We thereby utilize this approach to systematically find parameters that enable a non-trivial reciprocal response in a nonlinear system with broken mirror symmetry.

Because superposition does not hold for nonlinear systems, the findings of this study cannot be directly extended to the response of the same system under other types of excitation. See [102–104] for examples of recent studies that explore nonlinear nonreciprocity in systems subjected to impulse excitation. In such cases, investigating the nonlinear normal modes (NNMs) could offer valuable insight, particularly for characterizing transient dynamics and understanding the underlying structure of the system's response independent of the specific excitation [102].

Section 2.2 introduces the details of the setup and solution methodology. We discuss the frequency response curves of the system in Section 2.3 and introduce phase nonreciprocity. We present the results of our parametric study of phase nonreciprocity in Section 2.4, where we use the mass ratio as the symmetry-breaking parameter. In Section 2.5, we discuss how to use the stiffness ratio to restore reciprocity even in the absence of mirror symmetry. We conclude in Section 2.6 by an overview of our findings.

2.2. Problem Setup

Fig. 2.1 shows a schematic representation of the periodic system we study in this work. The structure comprises eight identical unit cells, with fixed boundaries at the two ends. Each

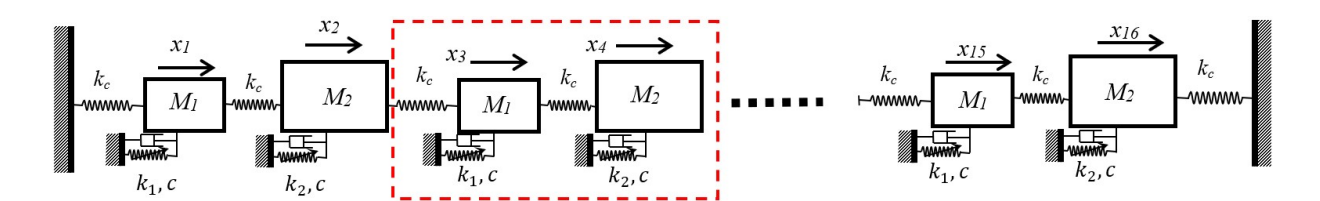


Figure 2.1: Schematic of the finite periodic structure. The red dashed box shows the unit cell, which consists of two linear oscillators coupled with a linear stiffness and grounded by a nonlinear spring and a linear damping.

cell consists of two masses, M_1 and $M_2 = \mu M_1$, which are coupled by a linear spring k_c . The mass M_1 is anchored to the ground by a spring with cubic nonlinearity, $k_1 = k_g + k_n \delta^2$, where δ represents the spring deformation from the static equilibrium position. The mass M_2 is anchored to the ground with a similar nonlinear spring of constant $k_2 = k'_g + k_n \delta^2$. The linear components of the two grounding springs are different, but the coefficient of the cubic term is the same for the two springs. Adjacent unit cells are coupled by the same linear spring that couples M_1 and M_2 within each cell. Energy loss is implemented in the model by identical linear viscous dampers of constant c that connect each mass to the ground. The periodic system is subject to harmonic external force of amplitude F and frequency ω_f (not shown).

The mirror symmetry of the system can be broken within a unit cell by changing the ratio of the two masses, $\mu = M_2/M_1$, or by changing the ratio of the two grounding springs, $r = k'_q/k_q$.

2.2.1. Governing equations

As outlined in Appendix 2A, the equations of motion for the system shown in Fig. 2.1 can be written using non-dimensional parameters as

$$\bar{x}_{2i-1}'' + 2K_c\bar{x}_{2i-1} - K_c(\bar{x}_{2i-2} + \bar{x}_{2i}) + \bar{x}_{2i-1} + K_n\bar{x}_{2i-1}^3 + 2\zeta_g\bar{x}_{2i-1}' = F_{2i-1}\cos\omega_f\tau$$

$$\mu\bar{x}_{2i}'' + 2K_c\bar{x}_{2i} - K_c(\bar{x}_{2i+1} + \bar{x}_{2i-1}) + r_g\bar{x}_{2i} + K_n\bar{x}_{2i}^3 + 2\zeta_g\bar{x}_{2i}' = F_{2i}\cos\omega_f\tau$$
(2.1)

The subscripts i = 1, ..., 8 denote the counter of unit cells. We use $\bar{x}_0(t) = 0$ and $\bar{x}_{17}(t) = 0$ to represent the fixed boundaries at the two ends of the structure. With the exception of F_1 and F_{16} , all the forcing amplitudes are zero.

Testing for reciprocity requires comparing the response of the system for two different configurations of the input-output locations. We study the end-to-end transmission characteristics of the finite periodic system in this work. Accordingly, we define (i) the *forward* configuration with $F_1 = P$ and $F_{16} = 0$, in which the output is the displacement of the last (right-most)

mass, $\bar{x}_{16}^F(t)$; (ii) the *backward* configuration with $F_1 = 0$ and $F_{16} = P$, in which the output is the displacement of the first (left-most) mass, $\bar{x}_1^B(t)$. The response of the system is reciprocal if and only if $\bar{x}_{16}^F(t) = \bar{x}_1^B(t)$.

2.2.2. Methodology

Systems with cubic nonlinear elasticity, also known as Duffing oscillators, have long been known to exhibit a rich nonlinear behavior and bifurcation structure [105, 106]. In this work, we exclusively focus on the weakly nonlinear response regime of the system in Fig. 2.1, described by Eq. (2.1). In particular, the steady-state response of the system remains harmonic in this regime and the only bifurcations encountered are the saddle-node bifurcation of periodic orbits at the turning points of the frequency response curves. These points are characterized visually by the vertical tangencies of the frequency response curves or, more precisely, to points at which one of the Floquet multipliers of the system exits the unit circle on the positive real axis [105].

In this light, we adopt a harmonic representation for the steady-state response of Eq. (2.1) as

$$\bar{x}_i(t) = X_i \cos(\omega_f t + \phi_i) \tag{2.2}$$

for j=1,...,16. The response is harmonic with its frequency imposed by the external force but different amplitude and phase from those of the external excitation. Eq. (2.2) is then substituted in Eq. (2.1) to convert the governing equations from a set of nonlinear ordinary differential equations to a set of nonlinear algebraic equations for the unknown amplitudes, X_j , and phases, ϕ_j . The steady-state response of the system is obtained by solving the ensuing set of algebraic equations; we use the Matlab package COCO for this purpose [107]. The linear stability analysis of the response is determined by computing the Floquet multipliers of the system [108]. Detailed formulation of the numerical technique, the harmonic balance method, along with descriptions of its more sophisticated implementations can be found elsewhere [109, 110].

For ease of future reference, we define the output displacements for the forward and backward configurations, $\bar{x}_{16}^F(t)$ and $\bar{x}_1^B(t)$, as follows

$$\bar{x}_{16}^F(t) = A^F \cos(\omega_f t + \phi^F) \tag{2.3a}$$

$$\bar{x}_1^B(t) = A^B \cos(\omega_f t + \phi^B) \tag{2.3b}$$

We refer to $A^{F,B}$ and $\phi^{F,B}$ as the output or transmitted amplitude and phase of the forward or backward configurations. Within this framework, nonreciprocal phase shift occurs when $A^F = A^B$ and $\phi^F \neq \phi^B$.

While this study employs numerical continuation methods to capture the steady-state dynamics of the nonlinear periodic waveguide, it is important to acknowledge that classical analytical or semi-analytical techniques could also be applied, particularly in the weakly nonlinear regime characterized by small-amplitude motions and cubic nonlinearities.

Methods such as the Method of Multiple Scales and the Lindstedt-Poincaré technique are widely used in the literature to derive approximate analytical solutions that reveal the leading-order effects of nonlinearity on frequency shifts, stability boundaries, and phase relationships [111]. These techniques can offer valuable physical insights and are computationally efficient for systems with a small number of degrees of freedom.

2.2.3. Response norms

To quantify the response of the system, we define the output norms for the forward (N^F) and backward (N^B) configurations as

$$N^{F} = \frac{1}{T} \int_{0}^{T} \left(\bar{x}_{16}^{F}(t)\right)^{2} dt \tag{2.4a}$$

$$N^{B} = \frac{1}{T} \int_{0}^{T} (\bar{x}_{1}^{B}(t))^{2} dt$$
 (2.4b)

where $T=2\pi/\omega_f$ is the period of excitation. We use displacement-based norms, proportional to potential energy, to focus on steady-state frequency response amplitude [99, 101]. A reciprocity test based on these norms overlooks the influence of phase change on breaking reciprocity. This is because the norms defined in Eq. (2.4) are proportional to the energy in the output of the system. Specifically, with our focus on the frequency-preserving response regime, we have $N^F=(A^F)^2/2$ and $N^B=(A^B)^2/2$. Looking back to Eq. (2.3), $N^F=N^B$ implies $A^F=A^B$ but puts no restrictions on the relation between ϕ^F and ϕ^B .

Even though the response of the system remains harmonic in the parameter ranges discussed in this work, we continue using the output norms defined in Eq. (2.4) instead of the response amplitudes A^F and A^B . This keeps our approach consistent with our previous work [70, 98, 99], where the analysis is not restricted to the harmonic response. In this case, an integral-based norm is more suitable to the analysis based on continuation of periodic orbits [98] or optimization tools [101], and also because there is no definition of response amplitude for anharmonic signals that is universally adopted in the literature.

To find a solution branch that exhibits phase nonreciprocity, we first need to find a set of parameters at which the transmitted energies are equal in the forward and backward configurations. We then compute the locus of phase nonreciprocity from this initial point by adding $N^F = N^B$ as a constraint.

To quantify the degree of nonreciprocity in the response, we define the reciprocity bias as

$$R = \frac{1}{T} \int_0^T (\bar{x}_{16}^F(t) - \bar{x}_1^B(t))^2 dt$$
 (2.5)

The response of the system is reciprocal if and only if R = 0. Note that the norm defined in Eq. (2.5) captures the changes in both amplitude and phase. In the frequency-preserving response regime, we have the simplified form $R = N^F + N^B - A^F A^B \cos(\phi^F - \phi^B)$.

When needed, we normalize the reciprocity bias with the output norms,

$$R_N = \frac{R}{N^B + N^F} \tag{2.6}$$

to eliminate the apparent increase in reciprocity that is caused merely by higher response amplitudes.

2.3. Frequency Response Curves

We start by studying the frequency response curves of the system: the output norms, N^F and N^B , as a function of the forcing frequency, ω_f . We keep moderate coupling, $K_c = 1$, throughout the work to avoid the overlapping of the two passbands of the system. The nonlinear stiffness is of the hardening type, $K_n = 1$. We consider moderate damping, $\zeta_g = 0.03$, except in section 2.4.3 where we explore the role of damping on phase nonreciprocity. We choose P = 0.15 for the forcing amplitude throughout this section; we study the role of P in section 2.4.2.

To better appreciate the role of symmetry in enabling a nonreciprocal response, we present the response of the mirror-symmetric system in Fig. 2.2. Owing to the mirror symmetry of the system ($\mu = 1$, r = 1), the forward and backward configurations are identical. This corresponds to the identical frequency response curves in Fig. 2.2 despite the presence of nonlinearity. Note that the response is nonlinear even though the typical 'bends' in the frequency response curves are not present for this particular set of system parameters; breaking the mirror symmetry results in nonreciprocity without the need for increasing the value of P.

Fig. 2.3 shows the frequency response curves of the system after we break the mirror symmetry of the unit cell by changing the mass ratio, $\mu = 2$. Notice that the periodic system with different masses exhibits a band gap where the output norm is very small; roughly for $1.3 < \omega_f < 1.7$. This is because the unit cell of the lattice has two degrees of freedom when $\mu \neq 1$. The lower branch (first pass band) is known as the acoustic (in-phase) branch, which corresponds to the collection of natural frequencies at which the adjacent masses move in

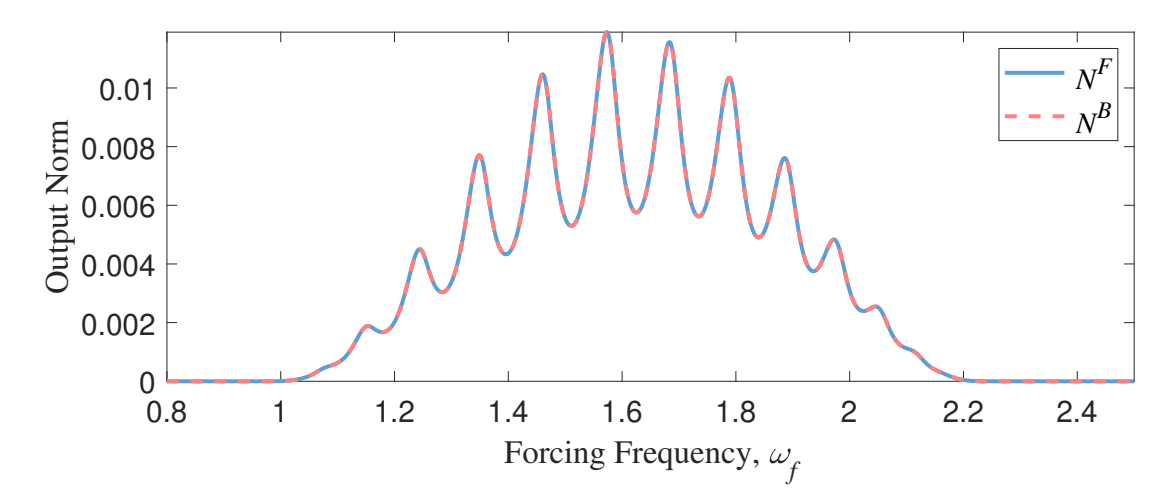


Figure 2.2: Output norms (Eq. 2.4) at P = 0.15 for the system with mirror symmetry $(\mu = 1)$

phase with each other. The upper branch (second pass band) is known as the optical (out-of-phase) branch, corresponding to mode shapes at which adjacent masses move out of phase with each other. As a result, damping has a larger influence on the optical branch and the amplitudes of the acoustic branch are relatively higher. The resonances of the optical branch are corresponding more highly damped.

As expected, breaking the mirror symmetry of the system enables the response of the system to become nonreciprocal. This is, of course, most conspicuous near the resonance frequencies because the amplitude of motion is relatively higher. The response away from resonances is linear owing to its small amplitude and necessarily reciprocal. Even near the resonances, however, we notice there are frequencies at which the two frequency response curves intersect $(N^F = N^B)$, indicating equal amplitudes in the forward and backward configurations.

The grey circles in Fig. 2.3 indicate the intersection points of the two frequency response curves. Some of these intersections occur near resonances and some near anti-resonances of the system. To understand the difference between these points, we refer to the reciprocity bias, R, shown in Fig. 2.4(a).

Fig. 2.4(a) indicates the points at which the forward and backward transmissions have the same amplitude, $N^F = N^B$, with two different markers. The circle markers in the valleys correspond to frequencies at which the response of the system is almost reciprocal. Fig. 2.4(b) shows the output displacement at the red circle ($\omega_f = 1.025$) in the time domain. These points occur near the local minima of the frequency response curves, which correspond to the anti-resonances of the system. Because of the relatively low amplitude of the response,

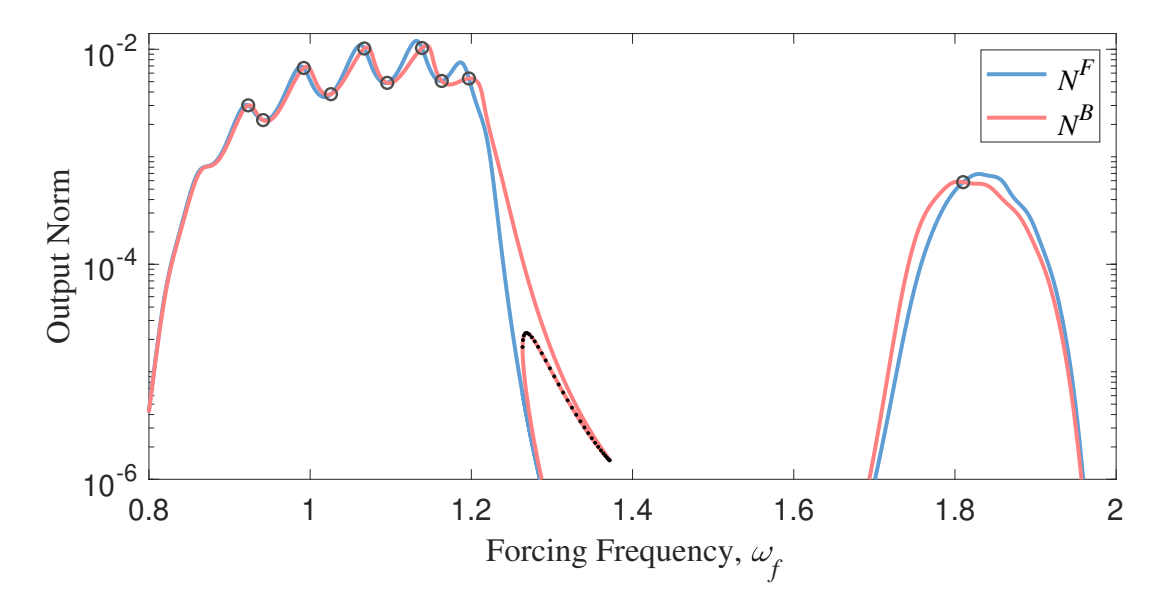


Figure 2.3: Frequency response curves at P = 0.15 for the system with broken mirror symmetry, $\mu = 2$. The grey circles show points at which $N^F = N^B$. The black dots indicate unstable regions in the response.

the system behaves almost linearly near these points and almost reciprocally as a result. In practice, these points are not of much importance due to their low response amplitudes.

The diamond markers in Fig. 2.4(a) correspond to frequencies at which $N^F = N^B$ in the vicinity of the resonances of the nonlinear system. Even though the amplitude of the transmitted vibrations is equal for the forward and backward configurations, these points occur near the local maxima of the reciprocity bias. Fig. 2.4(c) shows the time-domain response at the blue diamond ($\omega_f = 0.99$), revealing that the only difference between the forward and backward configurations is in the transmitted phases: $\phi^F \neq \phi^B$. We refer to this state as the state of phase nonreciprocity and to $\Delta \phi = \phi^F - \phi^B$ as the nonreciprocal phase shift of the response [98].

Figs. 2.4(d) and (e) show the spatiotemporal variation of the steady-state amplitude at the point indicated by the blue diamond (phase nonreciprocity). We observe that energy is indeed *not* localized within the system, as typically expected of steady-state vibrations near a resonant frequency.

Before moving on to a detailed analysis of phase nonreciprocity in section 2.4, we note in Fig. 2.4(a) that the value of R corresponding to the bent portion of the curve (1.3 < ω_f < 1.4) is markedly smaller than those at the diamond markers. Given the large difference between the norms in this portion of the response curve, a relatively lower value of R indicates

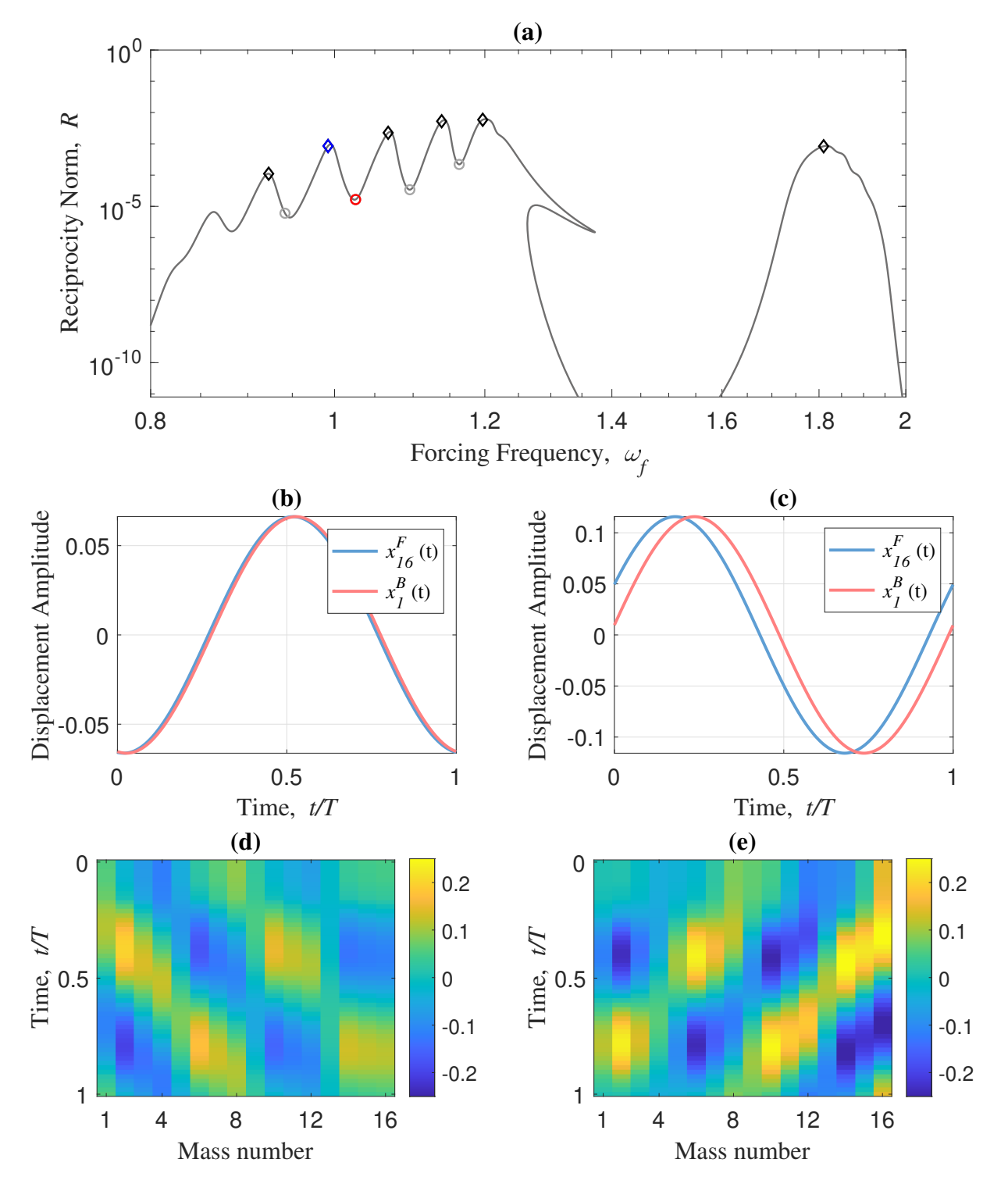


Figure 2.4: Nonreciprocal dynamics for P=0.15 and $\mu=2$. (a) The reciprocity norm, R, with the markers indicating $N^F=N^B$. Diamonds denote phase nonreciprocity ($N^F=N^B$, $\phi^F\neq\phi^B$) and circles denote frequencies at which the response of the system is almost reciprocal ($N^F=N^B$, $\phi^F\approx\phi^B$). (b) The time-domain response at the red circle, $\omega_f=1.025$. (c) The time-domain response at the blue diamond, $\omega_f=0.99$. (d, e) Spatiotemporal variation of the steady-state response at the blue diamond for the forward and backward configurations, respectively; cf. panel (c). 25

the significant contribution of nonreciprocal phase shifts to nonreciprocity. The influence of phase, a key focus of the present work, is typically overlooked in the analysis of nonreciprocity in nonlinear systems.

2.4. Phase Nonreciprocity

To better understand phase nonreciprocity, we perform a parametric study of the system while imposing the constraint $N^F = N^B$. Specifically, we investigate the effect of the asymmetry of the system as controlled by the mass ratio, μ , the influence of the forcing amplitude, P, and damping effects, ζ_g . The mass ratio, μ , remains the only source of asymmetry in this section $(r_g = 1)$. We postpone discussing the effect of two competing symmetry-breaking parameters to section 2.5.

2.4.1. Influence of asymmetry (mass ratio, μ)

We study the influence of asymmetry on phase nonreciprocity by computing the locus of $N^F = N^B$ as a function of the mass ratio for $1 \le \mu \le 10$. Fig. 2.5 shows this locus for different parameters. Panel (a) shows the variation of the normalized reciprocity bias, R_N , and the nonreciprocal phase shift, $\Delta \phi$. As expected, the response is reciprocal at $\mu = 1$ because the system is mirror-symmetric at that point. Increasing the asymmetry of the system results in an increase in the degree of nonreciprocity, as indicated by the increasing value of R_N . Because nonreciprocity is due to $\Delta \phi \neq 0$, the nonreciprocal phase shift increases along this locus as well. Panel (b) shows that the frequency at which phase nonreciprocity occurs moves to lower values as the mass ratio increases. This can be understood by noting the increased mass of the system – the non-dimensional masses of the unit cell are 1 and μ .

2.4.2. Influence of the forcing amplitude (*P*)

To investigate the influence of the forcing amplitude on phase nonreciprocity, we keep $\mu = 2$ and compute the locus of $N^F = N^B$ as a function of P. Different loci are obtained depending on which of the diamond markers in Fig. 2.4(a) is being traced. We choose the intersection marked by the blue diamond for further investigation.

Fig. 2.6(a) shows the frequency response curves at three values of P; these are superimposed onto backgrounds of different colors for clarity. The frequency response curves at P = 0.15 are reproduced from Fig. 2.2. Starting from the intersection point at $\omega_f \approx 0.99$ indicated by the blue diamond marker, the dashed curve traces the locus of $N^F = N^B$ as a function of P. Moving from the blue marker toward lower values of P, we see the trace reaching the frequency response curves at P = 0.05. The intersection point is still near a resonance

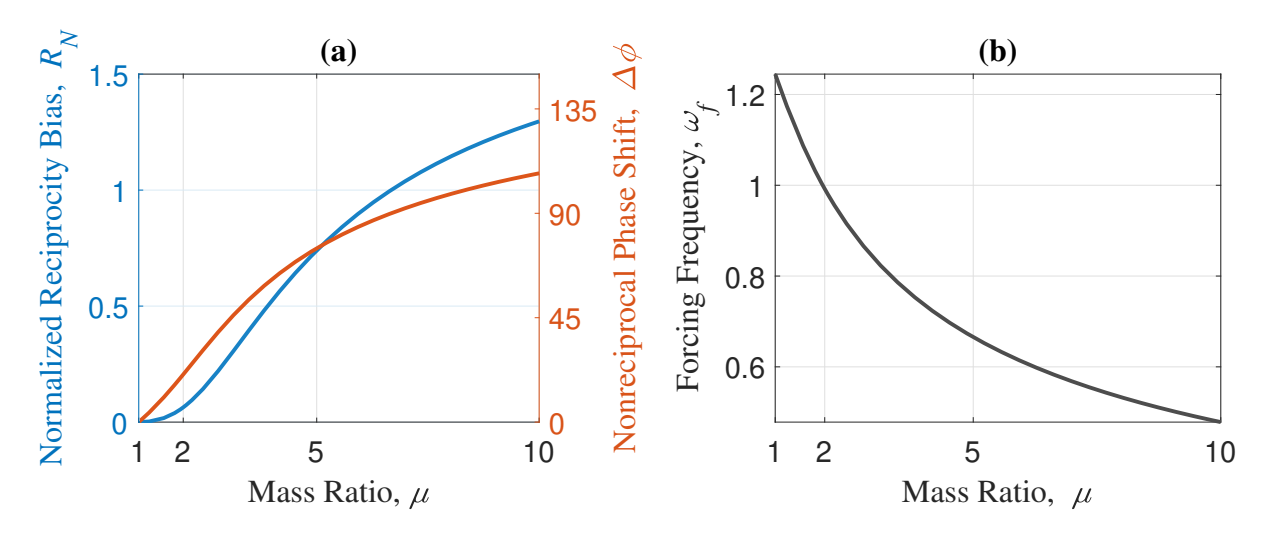


Figure 2.5: Locus of phase nonreciprocity $(N^F = N^B)$ as a function of the asymmetry parameter, μ , at P = 0.15. (a) Normalized reciprocity bias, R_N , and the phase shift between the forward and backward configurations, $\Delta \phi = \phi^F - \phi^B$. (b) The forcing frequency, ω_f , at which phase nonreciprocity occurs.

frequency of the system.

Tracing the same locus toward increasing values of P, we reach an interaction point of the frequency response curves at P=0.52. We note here that the intersection is somewhat off-resonance for the forward configuration and near an anti-resonance for the backward configuration. The locus of phase nonreciprocity continues up to a maximum forcing amplitude of $P\approx 0.5231$, above which the two frequency response curves do not intersect in this frequency range. Intersections at higher values of P are not overruled, of course, but their discussion falls outside the scope of the present work. This is in part because we can no longer guarantee the harmonicity of the response; a different numerical algorithm would be required in this case [98].

Moving along the locus of phase nonreciprocity beyond the turning point at $P \approx 0.5231$, the value of P decreases until we reach the intersection point with the second frequency response curves at P = 0.15, near an anti-resonance of the system at $\omega_f \approx 1.025$. The locus continues to a second intersection point with the frequency response curves at P = 0.05, again close to an anti-resonance frequency of the system.

We can now summarize the behavior of the locus of phase nonreciprocity for the intersection point indicated by the blue diamond. The locus starts at a resonance frequency at low forcing amplitudes and continues near the same resonance frequency as the value of P increases. As the nonlinear effects become more prominent and the degree of nonreciprocity increases,

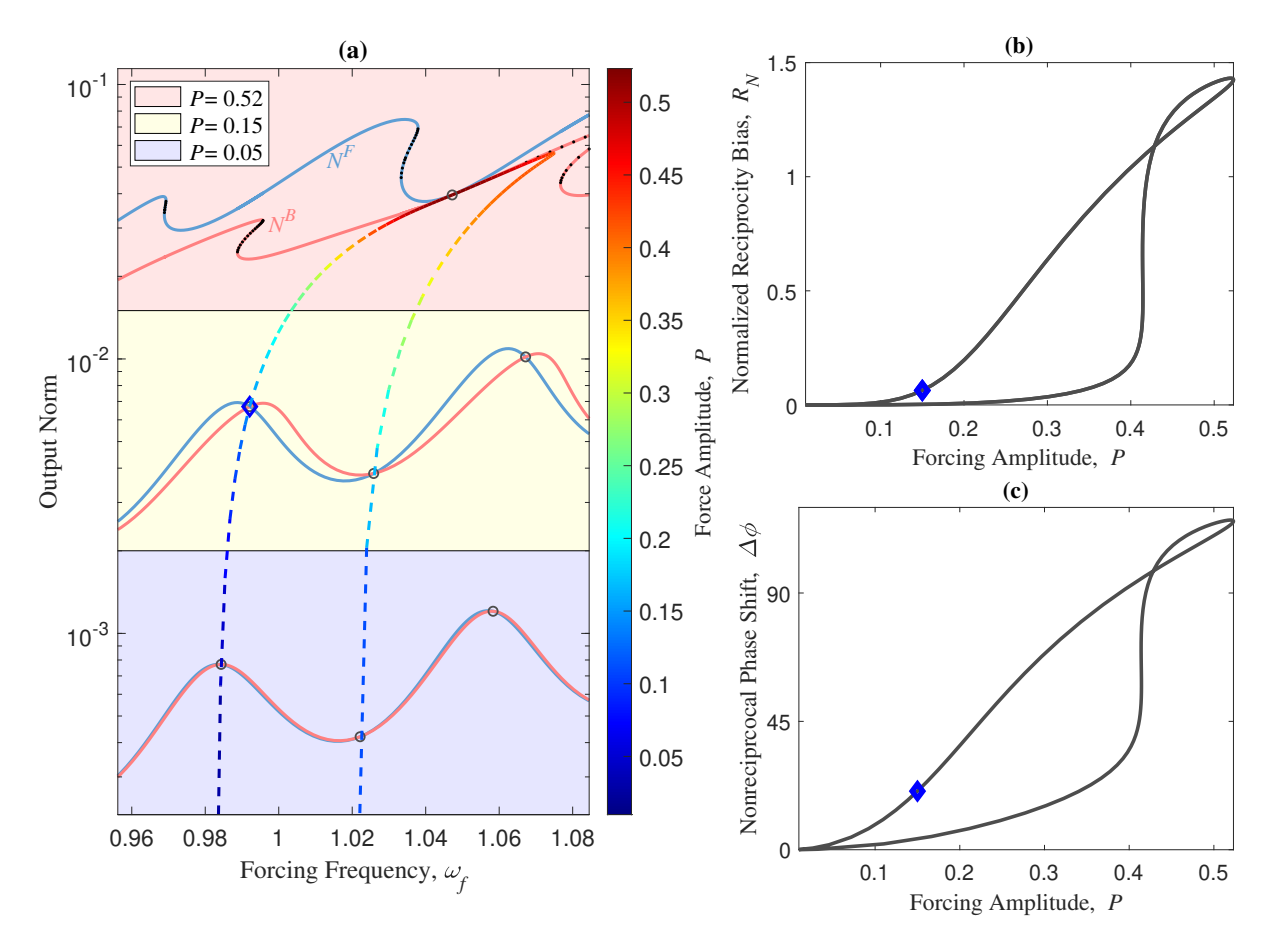


Figure 2.6: Locus of phase nonreciprocity $(N^F = N^B)$ as a function of the forcing amplitude, P, for $\mu = 2$. (a) Frequency response curves (solid) for three different values of P, superimposed onto backgrounds of different colors for clarity. The dashed, color-coded curve traces the locus of $N^F = N^B$; the color map corresponds to the value of P along this curve. (b) Normalized reciprocity bias, R_N . (c) Nonreciprocal phase shift, $\Delta \phi$.

the locus starts moving away from the resonance frequency and toward an anti-resonance frequency. The transition occurs through a turning point, after which the locus is near an anti-resonance frequency for both the forward and backward configurations. As shown in panel (b), for a given forcing amplitude, two distinct phase shift values exist. These correspond to two consecutive intersection points along the response curve, each representing a valid steady-state solution. The loci of these solutions, traced as a function of the forcing amplitude, eventually merge at P=0.52. We observed a similar pattern for the other loci in the acoustic branch.

Panels (b) and (c) in Fig. 2.6 show the locus of phase nonreciprocity in the (P, R_N) and $(P, \Delta \phi)$ planes, respectively. We see that the degree of nonreciprocity, as expected, is rela-

tively higher along the portion of the locus that is near a resonance frequency of the system (higher response amplitude). The transition of the locus from the vicinity of a resonance frequency to the vicinity of an anti-resonance frequency is markedly evident in these panels by the sharp drop in R_N just above P = 0.4. Furthermore, the fact that R_N follows $\Delta \phi$ so closely is a reminder that breaking of reciprocity is solely due to a nonreciprocal phase shift: $N^F = N^B$ while $\phi^F \neq \phi^B$.

There is only one intersection of the frequency response curves at the optical branch near $\omega_f \approx 1.8$. Fig. 2.7(a) shows the frequency response curves at two values of the forcing amplitude: P = 0.15, which is the base configuration reproduced from Fig. 2.3, and P = 0.70, which is chosen such that the response of the system remains harmonic and stable. The dashed curve shows the locus of $N^F = N^B$ for $0.01 \le P \le 0.7$. For higher values of P, the locus becomes unstable because the backward configuration loses stability through a Neimark-Sacker bifurcation; analysis of this operating regime falls outside the scope of this work.

Moving along the locus of nonreciprocity Fig. 2.7(a), the output norm increases until $\omega_f \approx 1.87$, after which it begins to decrease again. This decrease is accompanied by the intersection point moving away from the resonance frequency of the system, similar to what we observed for the acoustic branch. Fig. 2.7(b) shows the projection of the locus onto the (P, ω_f) plane. This locus is somewhat 'bumpy'. To explain this, we note that the modes within the optical branch are more damped than their acoustic counterparts; recall Fig. 2.3. Thus, as the forcing amplitude increases in Fig. 2.7(b), the locus traverses multiple modes of the system, which results in the observed behavior. The locus becomes relatively flat only after the locus has passed through the modes in the optical branch. This can be confirmed by observing the individual phases ϕ^F and ϕ^B .

Fig. 2.7(c) shows that the normalized nonreciprocity bias, R_N , reaches a local maximum near $P \approx 0.36$, which corresponds to $\omega_f \approx 1.87$. This trend is mirrored in the nonreciprocal phase shift, $\Delta \phi$, because nonreciprocity is solely due to the phase difference. Accordingly, the maximum value of R_N corresponds to $\Delta \phi = \pi$. The nonreciprocal phase shift, together with R_N , gradually decreases as the locus of phase nonreciprocity moves away from the resonant region of the forward and backward response curves.

2.4.3. Influence of damping (ζ_g)

Fig. 2.8 shows the influence of damping on the locus of phase nonreciprocity at P = 0.15. Panel (a) shows the frequency response curves at two values of the damping ratio, ζ_g , which are superimposed onto backgrounds of different colors for clarity. The frequency response

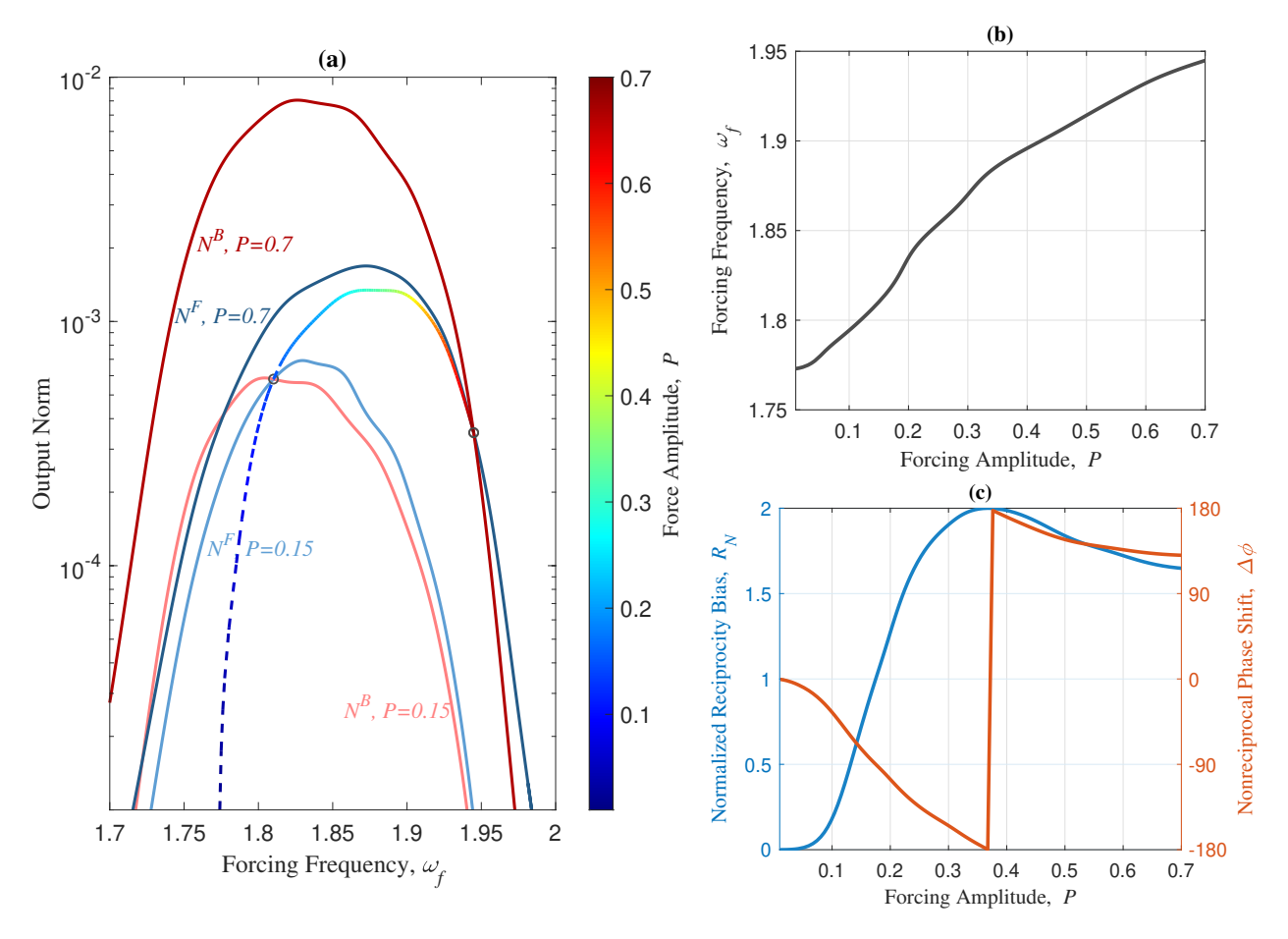


Figure 2.7: Locus of phase nonreciprocity $(N^F = N^B)$ in the optical branch as a function of the forcing amplitude, P, for $\mu = 2$. (a) Frequency response curves for two different values of P. The dashed, color-coded curve traces the locus of $N^F = N^B$; the color map corresponds to the value of P along this curve. (b) The forcing frequency, ω_f , at which phase nonreciprocity occurs. (c) Normalized reciprocity bias, R_N , and nonreciprocal phase shift, $\Delta \phi$, along the locus.

curves at P=0.15 are reproduced from Fig. 2.2. We have traced the locus of $N^F=N^B$ (dashed curve) from two intersection points, at $\omega_f\approx 0.99$ (blue diamond) and at $\omega_f\approx 1.025$ (red circle); the color map corresponds to the value of ζ_g along this locus. Moving in the direction of increasing damping, we observe that the two loci merge together through a turning point at $\zeta_g\approx 0.055$; panel (b) shows the projection of the locus onto the (ζ_g,ω_f) plane. We observe in the frequency response curves in panel (a) that, as ζ_g increases, the influence of nonlinear forces is becoming increasingly smaller, making the response more linear gradually. We recall that the overall effect of increasing damping is, indeed, to merge the two frequency response curves because it diminishes the relative effect of nonlinearity and, colloquially speaking, linearizes the response of the system.

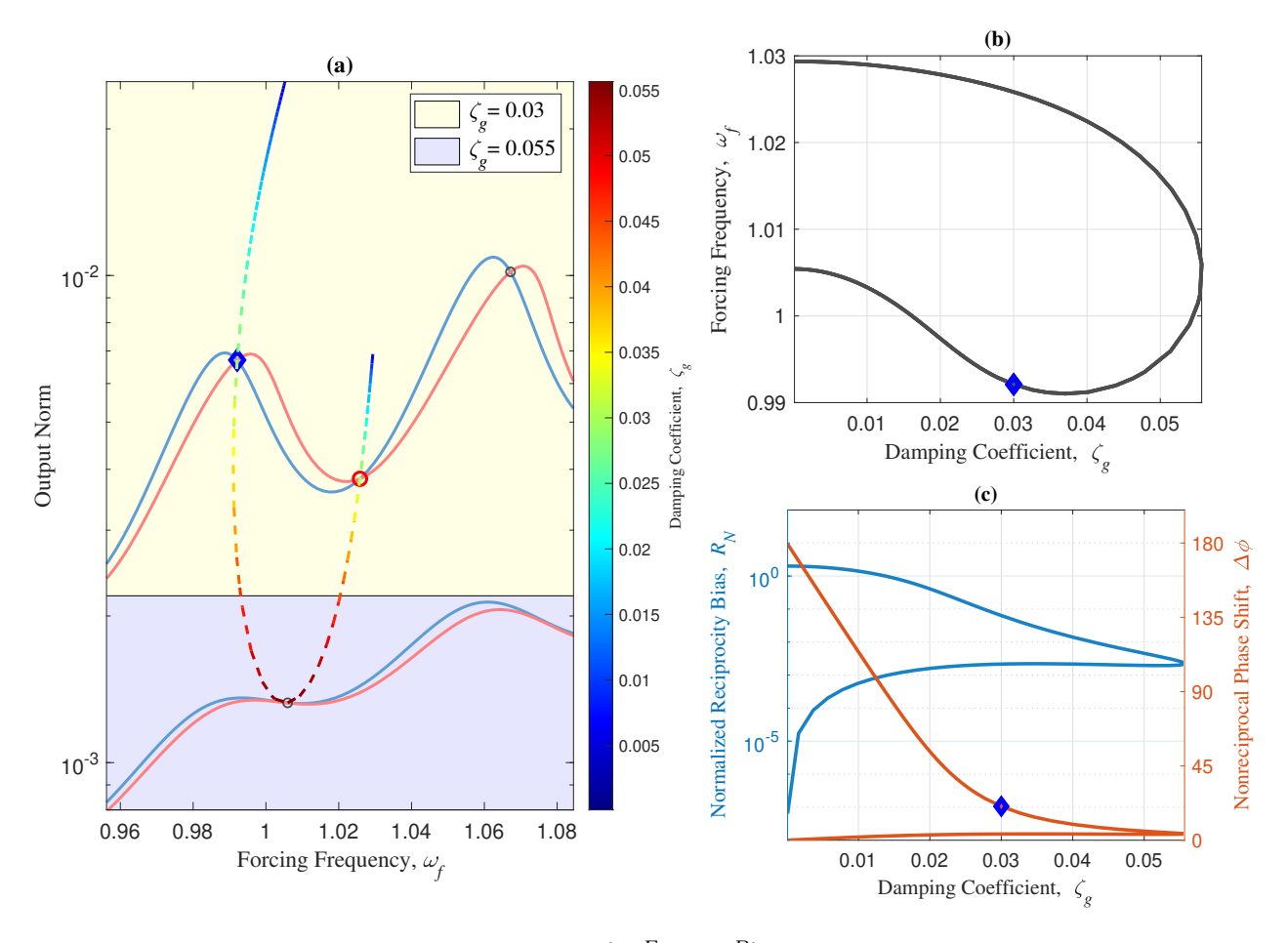


Figure 2.8: Locus of phase nonreciprocity $(N^F = N^B)$ as a function of the damping ratio, ζ_g , at P = 0.15. (a) Frequency response curves for two different values of damping. The dashed, color-coded curve traces the locus of $N^F = N^B$; the color map corresponds to the value of ζ_g along this curve. (b) The forcing frequency, ω_f , at which phase nonreciprocity occurs. (c) Normalized reciprocity bias, R_N , and nonreciprocal phase shift, $\Delta \phi$, along the locus.

Fig. 2.8 (c) shows the evolution of the normalized reciprocity norm, R_N , and the nonreciprocal phase shift, $\Delta \phi$, along the locus of phase nonreciprocity. We note that as the value of ζ_g increases, both R_N and $\Delta \phi$ diminish rapidly until the turning point. As the value of ζ_g decreases toward zero, the locus of phase nonreciprocity terminates either at $(\Delta \phi, R_N) = (0, 0)$ or at $(\Delta \phi, R_N) = (\pi, 2)$. The end point with $\Delta \phi = 0$ corresponds to a matching of the anti-resonance frequencies of the forward and backward configurations, while $\Delta \phi = \pi$ corresponds to a matching of their resonances.

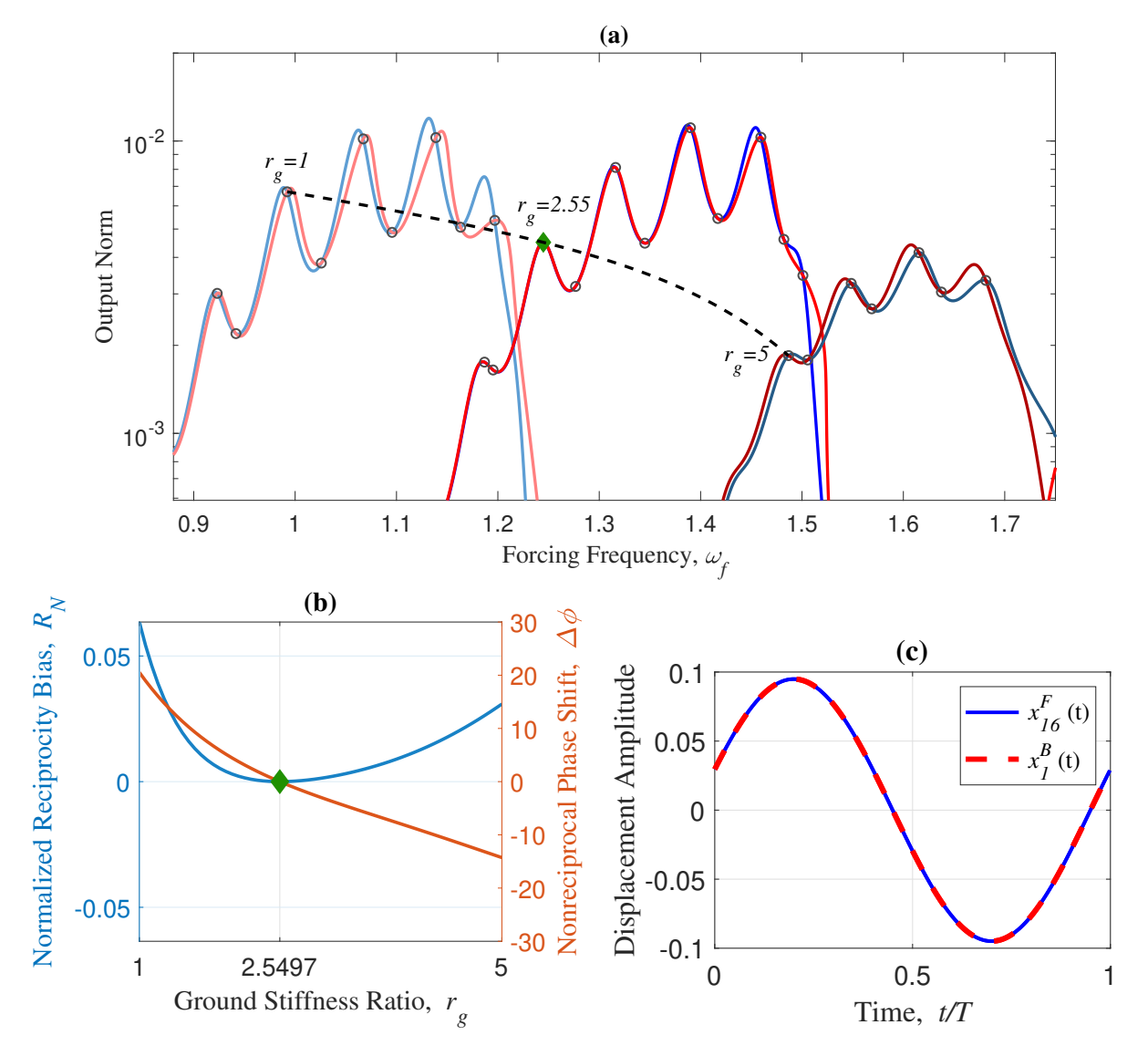


Figure 2.9: Restoring reciprocity $R_N = 0$ for $(P, \mu) = (0.15, 2)$ by tuning a second symmetry-breaking parameter, r_g . (a) Output norms for three different values of the stiffness ratio. The black dashed curve shows the locus of $N^F = N^B$. The green diamond marker denotes the point at which reciprocity is restored. (b) Variation of R_N and $\Delta \phi$ as a function of r_g . The green diamond marker denotes the point at which reciprocity is restored. (c) Time-domain response of the forward and backward configurations at the green diamond marker $(R_N = 0)$.

2.5. Restoring reciprocity using two symmetry-breaking parameters

The forward and backward configurations have equal output norms for phase nonreciprocity, $N^F = N^B$. If, additionally, the nonreciprocal phase shift can be set to zero, $\Delta \phi = 0$, then the output displacements are identical and we retrieve a reciprocal response, R = 0

0. To achieve this, a second symmetry-breaking parameter (other than μ) is required to counterbalance the effect of the existing asymmetry and restore reciprocity [99]. The two symmetry-breaking parameters thus act together to maintain reciprocity in a system with broken mirror symmetry. We use the stiffness ratio, r_g , as the second symmetry-breaking parameter. From a practical perspective, we note that it is possible to independently tune the effective mass and stiffness parameters of a mechanical system [112].

Fig. 2.9(a) shows frequency response curves for the system with $\mu = 2$ at P = 0.15 at three different values of r_g . The frequency response curves on the left side correspond to $r_g = 1$, where μ is the only symmetry-breaking parameter. The dashed black curve traces the locus of phase nonreciprocity that emanates from the intersection point near $\omega_f \approx 0.99$ as the value of r_g increases.

Fig. 2.9(b) shows the corresponding values of the normalized reciprocity norm, R_N , and nonreciprocal phase shift, $\Delta \phi$, along the locus of phase nonreciprocity. We note that the value of R_N becomes zero near $r_g \approx 2.55$, indicating a reciprocal response. Because R_N is a non-negative number, we use $\Delta \phi$ to confirm whether the response is indeed reciprocal. The nonreciprocal phase shift has a zero-crossing near $r_g \approx 2.55$, which confirms reciprocity. Fig. 2.9(c) shows the corresponding reciprocal response in the time domain.

We return to Fig. 2.9(a) to observe the frequency response curves at $r_g \approx 2.55$. We observe that the forward and backward configurations have similar norms in the vicinity of the resonance frequency where reciprocity is restored; *i.e.*, near the intersection point at $\omega_f \approx 1.24$. Similar findings are reported in a system of coupled oscillators [99]. When r_g is further increased, the two frequency response curves drift apart again. Phase nonreciprocity persists, but the response is no longer reciprocal ($\Delta \phi \neq 0$).

2.6. Conclusions

We presented a computational analysis of nonreciprocal vibration transmission in a discrete model of a nonlinear periodic material. Nonlinearity and asymmetry are the two required ingredients for realizing nonreciprocity in this setting. Nonlinearity appeared in the grounding elasticity as a cubic spring (symmetric restoring force). Asymmetry appeared at the substructure level in two ways: the ratios of the effective inertia and effective linear elasticity of the two units. We focused on the weakly nonlinear steady-state response of the system to a harmonic excitation; *i.e.*, the frequency-preserving regime. We presented scenarios in which there is a phase difference between the transmitted vibrations in the forward and backward configurations ($\phi^F \neq \phi^B$), while the energies transmitted in the opposite directions remain equal ($N^F = N^B$). Thus, nonreciprocity is due *solely* to the nonreciprocal

phase shifts $(\Delta \phi = \phi^F - \phi^B)$ in the transmitted vibrations. We call this the state of *phase nonreciprocity*.

We performed a parametric study of phase nonreciprocity in the nonlinear waveguide, investigating the influence of the forcing amplitude, damping ratio, and degree of asymmetry on the nonreciprocal phase shifts. In particular, by tuning two independent symmetry-breaking parameters (mass ratio and stiffness ratio), we have shown that it is possible to restore reciprocity in the vicinity of a resonance frequency of the system. We achieved this by finding a nontrivial set of parameters at which $\Delta \phi = 0$ along the locus of phase nonreciprocity. The results indicate that although breaking the symmetry of the system is a necessary requirement for enabling nonreciprocal dynamics, it is not strictly a sufficient condition. Furthermore, these results showcase the potential of asymmetry to serve as an additional design parameter, especially in systems that rely on symmetry but are inherently asymmetric due to unavoidable imperfections. We hope that these findings contribute to enhancing the performance of devices that operate based on nonlinear nonreciprocity.

Appendices

2A. Appendix A: Non-dimensional Equations of Motion

The governing equations for the system in Fig. 2.1 can be written as:

$$M_1\ddot{x}_{2i-1} + 2k_c x_{2i-1} - k_c (x_{2i-2} + x_{2i}) + k_g x_{2i-1} + k_n x_{2i-1}^3 + c\dot{x}_{2i-1} = f_{2i-1}\cos\omega_f t$$

$$M_2\ddot{x}_{2i} + 2k_c x_{2i} - k_c (x_{2i+1} + x_{2i-1}) + k_g' x_{2i} + k_n x_{2i}^3 + c\dot{x}_{2i} = f_{2i}\cos\omega_f t$$
(2A.1)

where i=1,...,8 is the counter of the unit cells, k_c is the coupling stiffness, k_g and k_g' are the coefficients of the linear grounding springs for M_1 and M_2 , and c is the linear viscous damping connecting each mass to the ground. We divide the equations by k_g and introduce the non-dimensional parameters $\tau = \omega_0 t$, $\omega_0^2 = k_g/M_1$, $\Omega = \omega_f/\omega_0$ to obtain

$$M_{1}\omega_{0}^{2}/k_{g}x_{2i-1}'' + 2k_{c}/k_{g}x_{2i-1} - k_{c}/k_{g}(x_{2i-2} + x_{2i}) + x_{2i-1} + k_{n}/k_{g}x_{2i-1}^{3} + 2\zeta_{g}x_{2i-1}' = f_{2i-1}/k_{g}\cos\Omega\tau$$

$$M_{2}\omega_{0}^{2}/k_{g}x_{2i}'' + 2k_{c}/k_{g}x_{2i} - k_{c}/k_{g}(x_{2i+1} + x_{2i-1}) + k_{g}'/k_{g}x_{2i} + k_{n}/k_{g}x_{2i}^{3} + 2\zeta_{g}x_{2i}' = f_{2i}/k_{g}\cos\Omega\tau$$

$$(2A.2)$$

where $x' = dx/d\tau = (dx/dt)/\omega_0$, $x'' = d^2x/d\tau^2 = (d^2x/dt^2)/\omega_0^2$ and $\zeta_g = (c\omega_0)/(2k_g)$. We define the non-dimensional displacement and force as $\bar{x} = x/d$ and $F = f/(dk_g)$, where d is a characteristic displacement of the system. This results in

$$\bar{x}_{2i-1}'' + 2K_c\bar{x}_{2i-1} - K_c(\bar{x}_{2i-2} + \bar{x}_{2i}) + \bar{x}_{2i-1} + K_n\bar{x}_{2i-1}^3 + 2\zeta_g\bar{x}_{2i-1}' = F_{2i-1}\cos\Omega\tau$$

$$\mu\bar{x}_{2i}'' + 2K_c\bar{x}_{2i} - K_c(\bar{x}_{2i+1} + \bar{x}_{2i-1}) + r_g\bar{x}_{2i} + K_n\bar{x}_{2i}^3 + 2\zeta_g\bar{x}_{2i}' = F_{2i}\cos\Omega\tau$$
(2A.3)

where $\mu = M_2/M_1$, $K_c = k_c/k_g$, $K_n = d^2k_c/k_g$ and $r_g = k'_g/k_g$. Eq. (2A.3) is the non-dimensional form of Eq. (2A.1). Eq. (2A.3) is the same as Eq. (2.1) in the main text, where

we have dropped the overbar in \bar{x} and replaced τ with t for ease of reference.

Chapter 3

Phase-preserving nonreciprocal dynamics in coupled nonlinear oscillators

3.1. Introduction

Reciprocity refers to the symmetry property of wave and vibration phenomena that guarantees transmission characteristics between two points do not depend on the direction of travel. This concept has been extensively studied and applied since the nineteenth century, with seminal contributions from Helmholtz [1] and Rayleigh [2], among many others. Beyond its significant theoretical implications [3], reciprocity has underpinned diverse experimental methodologies in fields such as vibroacoustics [4, 5], structural dynamics [6, 7], defect detection, determination of elastic constants [8], ultrasonics [9], and seismology [10].

For a device to allow for different transmission properties in opposite directions, it needs to operate beyond the bounds of reciprocity. Nonreciprocity plays a crucial role in the functioning of well-established communication devices such as isolators and circulators [95]. A celebrated example of nonreciprocity in vibration and acoustics is the mechanical or acoustic diode, which restricts waves to travel in only one direction [41, 113, 114]. Nonreciprocity also facilitates wave filtering and frequency conversion. To name a few examples from one-dimensional systems, high-efficiency, broadband acoustic waveguides capable of converting wave frequencies have been proposed for potential applications in sonar and ultrasound imaging [115], resonators with reconfigurable bandwidth properties have been developed [116], and nonreciprocity has played an important role in enabling and enhancing energy localization and irreversible energy transmission in mechanical systems [80, 117].

Nonreciprocal dynamics in mechanical systems can arise through several different mechanisms [17]. One approach (active) involves time-dependent modulation of the effective properties by means of external controls, such as introducing kinetic motion or applying spatiotemporal modulations [29, 118, 119]. Another approach (passive) relies on nonlinear forces within the system [38, 76, 101]. Nonlinearity introduces various mechanisms that drive nonreciprocity, including the dependence of the response on the amplitude of motion, generation of higher harmonics, and various bifurcations. Regardless of the approach, a system with mirror symmetry cannot support a nonreciprocal response because symmetry ensures the transmission between the two points is identical in both directions. Thus, breaking the mirror symmetry is a necessary (but not sufficient [99]) condition for enabling nonreciprocity.

We focus exclusively on nonreciprocal dynamics in nonlinear systems in this work. Structural asymmetry may be introduced locally within the system in form of a defect [41], periodically throughout the structure [12, 120], as an effective gate by combining two mirror-symmetric sub-structures [28, 79], or by incorporating nonreciprocal internal forces [77]. In all cases, the most salient indicator of nonreciprocity is the ability of a system to support unidirectional (diode-type) transmission. This occurs when there is a large difference between the energies transmitted in opposite directions. This prominent feature of nonreciprocity has driven the primary interest in the study of nonreciprocal dynamics.

In addition to a difference in transmitted energies (energy bias), nonreciprocity is accompanied by a difference in the phase of the transmitted vibrations (phase bias). The phase bias, however, is often overlooked. The extreme case of this phenomenon occurs when the transmitted energies between two points remain unchanged upon interchanging of the source and receiver, but there is still a difference in the transmitted phases. This effect, phase non-reciprocity, has been shown for the steady-state response to external harmonic excitation, both for a system with two degrees of freedom (coupled waveguides) [98] and a spatially periodic system [121]. The resulting nonreciprocal phase shift is the only contributor to nonreciprocity in this case.

In this work, while still focusing on the role of phase in nonreciprocity, we tackle a different question: do nonreciprocal response regimes exist that are characterized by equal transmitted phases but different transmitted energies? We refer to such response regimes as *phase-preserving nonreciprocity*. Energy bias has been the most common indicator of nonreciprocity so far. Phase-preserving nonreciprocity will determine whether an energy bias alone (without contribution from phase) can lead to nonreciprocity. Thereby, this investigation highlights yet another aspect of the contribution of phase in breaking reciprocity.

Nonreciprocity in the transmitted phase has been a subject of investigation in electronics and optics [81, 82], with recent applications in optical and acoustic waveguides [83–86]. The ability to passively control the direction-dependent transmitted phase of a waveguide may find application in vibration control strategies or in performing certain logic operations [87].

We use a lumped-parameter model to investigate phase-preserving nonreciprocity. Lumped-parameter models represent the phenomenon in systems that can be adequately modeled as a combination of scalar wave fields and coupled oscillators. These models have been widely used in acoustics and vibrations to describe wave propagation and resonance phenomena. In phononic crystals and metamaterials, lumped-parameter models are capable of presenting a concise description of complex physics such as formation of Bragg and sub-Bragg bandgaps [122, 123], bandgaps induced by inertial amplification [124], directional bandgaps

in spatiotemporally modulated systems [125–127], amplitude-dependent bandgaps in nonlinear systems [128, 129], cloaking [130], flat bands [131] and topological effects [131–133], to name a few examples. The present work is carried out within the same context.

Following the previous work on phase nonreciprocity [98, 121], we investigate phase-preserving nonreciprocity in the steady-state response of two nonlinear oscillators to external harmonic excitation. Our methodology for finding phase-preserving nonreciprocity relies on first establishing phase nonreciprocity as an intermediate operating point. Here, the phase of the response refers to the angular relationship between the steady-state displacement and the external force, which represents the delay or advance between the input and output of the system over one cycle of oscillation. Phase-preserving nonreciprocity, therefore, refers to the scenario in which this phase shift remains unchanged when the locations of the source and receiver are interchanged.

Section 3.2 introduces the system under investigation and the solution methodology. Section 3.3 presents the procedure that enables us to find a family of system parameters that lead to phase-preserving nonreciprocity. This involves finding response regimes that exhibit phase nonreciprocity and reciprocal dynamics. Section 3.4 presents the main results on phase-preserving nonreciprocity. We summarize our findings in Section 3.5.

3.2. Problem Setup

Fig. 3.1 shows a schematic representation of the two-degree-of-freedom (2DoF) system we study in this work. The system consists of two masses, M_1 and $M_2 = \mu M_1$, that are coupled by a linear spring of constant k_3 . The mass M_1 is anchored to the ground by a spring with cubic nonlinearity, $k_1 = k_{g1} + k_{n1}\delta^2$, where δ represents the spring deformation from its static equilibrium position. The mass M_2 is also anchored to the ground with a similar nonlinear spring of constant $k_2 = k_{g2} + k_{n2}\delta^2$. Energy dissipation is modeled by a linear viscous damping mechanism, represented by a dashpot of constant c connecting each mass to the ground. The system is subject to an external harmonic force of amplitude F and frequency ω_f (not shown).

The mirror symmetry of the system is controlled by the ratio of the two masses, $\mu = M_2/M_1$, the ratio of the two grounding linear springs, $r = k_{g2}/k_{g1}$, or the ratio of the nonlinear spring coefficients, $\alpha = k_{n2}/k_{n1}$. We note that independent tuning of the linear and nonlinear portions of the effective elasticity of the system is already reported in the literature [112, 134].

As outlined in Appendix 3A, the equation of motion of the system can be expressed in

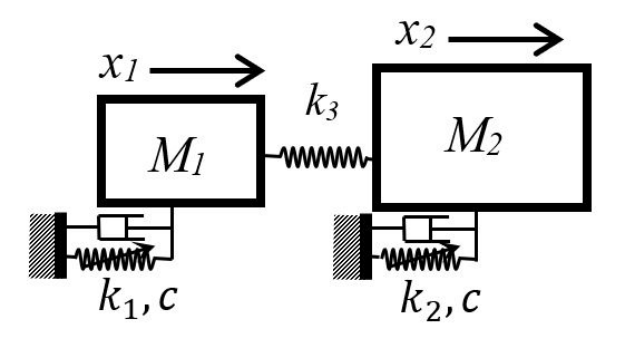


Figure 3.1: Schematic representation of the 2DoF system.

non-dimensional parameters as follows:

$$\ddot{x}_1 + k_c(x_1 - x_2) + x_1 + k_N x_1^3 + 2\zeta \dot{x}_1 = F_1 \cos \omega_f t$$

$$\mu \ddot{x}_2 + k_c(x_2 - x_1) + r x_2 + \alpha k_N x_2^3 + 2\zeta \dot{x}_2 = F_2 \cos \omega_f t$$
(3.1)

where k_c represents the strength of coupling, k_N the strength of the cubic nonlinearity, and ζ is the damping ratio. Throughout this work, we consider moderate damping, $\zeta = 0.05$. We use a system with hardening nonlinearity to present our results, $k_N = 1$. We consider strong coupling between the units, $k_c = 5$, to avoid the overlapping of the two modes of the system.

To investigate nonreciprocity, we analyze the steady-state response of the system under two different configurations for the input-output locations. Specifically, we define: (i) the forward configuration, where $F_1 = P$ and $F_2 = 0$, and the output is the displacement of the right mass, x_2^F ; and (ii) the backward configuration, where $F_1 = 0$ and $F_2 = P$, with the output being x_1^B . The response of the system is reciprocal if and only if $x_2^F(t) = x_1^B(t)$.

We use the following norms to quantify the response of the system for the forward (N^F) and backward (N^B) configurations:

$$N^{F} = \frac{1}{T} \int_{0}^{T} (x_{2}^{F}(t))^{2} dt$$
 (3.2a)

$$N^{B} = \frac{1}{T} \int_{0}^{T} (x_{1}^{B}(t))^{2} dt$$
 (3.2b)

where $T = 2\pi/\omega_f$ is the period of excitation. These integral-based measures are proportional to the energy in the output of the system and are commonly used in the study of nonlinear nonreciprocity [101].

We use numerical continuation, as implemented in COCO [107], to compute the steady-state response of the system as a family of periodic orbits that satisfy a suitable boundary-value

formulation [135]. Thus, the computed solutions are not necessarily harmonic. The stability of the response is determined by the Floquet multipliers associated with each periodic orbit.

Classical analytical methods, such as the Method of Multiple Scales and the Lindstedt-Poincaré technique, are well-established tools for capturing leading-order effects of cubic nonlinearities, including frequency shifts, stability changes, and bifurcations[136]. These methods have been successfully applied to Duffing systems in numerous studies to derive approximate analytical expressions for steady-state responses. While this work does not implement these methods explicitly, they remain valuable for gaining physical intuition in the weakly nonlinear regime.

However, these methods typically rely on small nonlinearity assumptions and may not fully capture the multi-harmonic and strongly nonlinear behaviors explored in this work. Therefore, we adopted numerical continuation methods, which offer a more general computational framework capable of resolving both weak and strong nonlinear responses without restrictive assumptions. A systematic comparison with analytical approximations is identified as a promising direction for future research to further strengthen the interpretation and generalization of the findings.

We define the phase of the response based on the first harmonic component of the output; i.e. the Fourier coefficients corresponding to $2\pi/\omega_f$. Appendix 3B provides more details on this process. This choice is motivated by the fact that we primarily operate the system in the weakly nonlinear regime where contributions from the higher-order harmonics are not significant. This is also known as the frequency-preserving response regime. For ease of reference, parameters ϕ^F and ϕ^B denote the phase of the forward and backward output displacements, respectively.

3.3. Controlling the Transmitted Phase and Energy

We are looking for a systematic computational procedure to find parameters at which the system exhibits phase-preserving nonreciprocity $(N^F \neq N^B, \phi^F = \phi^B)$. We achieve this by first obtaining a response characterized by phase nonreciprocity $(N^F = N^B, \phi^F \neq \phi^B)$ and then a reciprocal response $(N^F = N^B, \phi^F = \phi^B)$.

3.3.1. Phase Nonreciprocity

Fig. 3.2(a) shows the frequency response curve of the system at P=2. We have used r=2.5 to break the mirror symmetry of the system and enable nonreciprocity in this section, while keeping $\mu=\alpha=1$. Nonreciprocity is most conspicuous near the primary resonances because the amplitude of motion is relatively higher there. The response away from resonances is

similar to that of a linear system owing to the small amplitudes, and reciprocal as a result.

There are forcing frequencies at which the two frequency response curves intersect $(N^F = N^B)$, indicating equal amplitudes in the forward and backward configurations. Figs. 3.2(b) and (c) show the time-domain response at the two intersection points near $\omega_f = 2.18$ and $\omega_f = 3.78$, respectively. Despite having equal amplitudes, the response at these forcing frequencies are nonreciprocal because the transmitted phase in the forward and backward configurations are different, $\phi^F \neq \phi^B$. We refer to this as the state of phase nonreciprocity and to $\Delta \phi = \phi^F - \phi^B$ as the nonreciprocal phase shift of the response.

We note that at both intersection points identified in Fig. 3.2 the response of the system is unstable in one of the configurations. In our approach, phase nonreciprocity is an intermediate state in finding parameters that lead to phase-preserving nonreciprocity. We can tolerate an unstable response at this stage as long as the final state of phase-preserving nonreciprocity is stable. A detailed discussion of stable states of phase nonreciprocity near the primary resonances of the system is available elsewhere [98, 121].

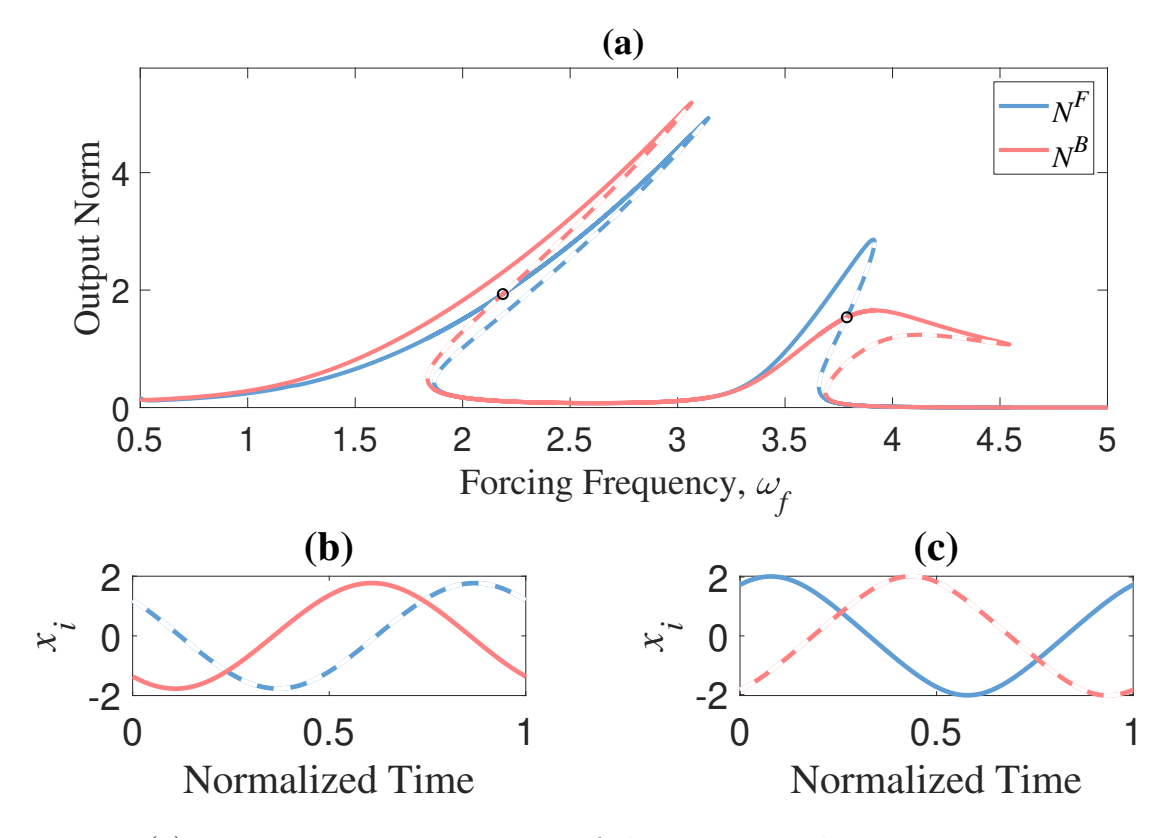


Figure 3.2: (a) Frequency response curves of the system with P=2, $\alpha=1$, $\mu=1$, and r=2.5. Time response over one forcing period at the intersections points marked by black circles at (b) $\omega_f=3.78$, and (c) $\omega_f=2.18$. The dashed lines indicate unstable regions in the response.

3.3.2. Restoring Reciprocity

In a system that exhibits phase nonreciprocity $(N^F = N^B)$, if the nonreciprocal phase shift becomes zero $(\Delta \phi = 0)$, then the output displacements become identical $(x_2^F = x_1^B)$ and we retrieve a reciprocal response. To achieve this, a second symmetry-breaking parameter (other than r) is required to counterbalance the effect of the existing asymmetry and restore reciprocity [99]. The two symmetry-breaking parameters thus act together to maintain reciprocity in a system with broken mirror symmetry. We use the nonlinear stiffness ratio, α , as the second symmetry-breaking parameter in this section.

Fig. 3.3(a) shows the locus of phase nonreciprocity $(N^F = N^B)$ as a function of α for the intersection point at $\omega_f = 3.78$. Panel (b) shows the variation of the nonreciprocal phase shift, $\Delta \phi$, along this locus. The blue diamond at $\alpha \approx 0.69$ marks the point at which reciprocity is restored: $N^F = N^B$ and $\Delta \phi = 0$. Panel (c) shows the frequency response curves of the system for r = 2.5 and $\alpha = 0.69$. The response of the system is nonreciprocal everywhere in this frequency range except at the point marked by the blue diamond, where the response is reciprocal, as shown in panel (d). The reciprocal response is stable and occurs near a primary resonance of the system. More details about restoring reciprocity in a nonlinear system with broken mirror symmetry can be found elsewhere [99, 121].

We will use the reciprocal response at the diamond marker to find a family of parameters that lead to phase-preserving nonreciprocity.

3.4. Phase-Preserving Nonreciprocity

3.4.1. Influence of the forcing amplitude

To find a family of solutions that exhibits phase-preserving nonreciprocity, we start from the reciprocal response of a system with broken mirror symmetry (diamond marker in Fig. 3.3). Keeping the phase constraint, $\phi^F = \phi^B$, we compute the steady-state response manifold as a function of the nonlinear stiffness ratio, α . This is shown in Fig.3.4(a).

The response exhibits phase-preserving nonreciprocity at all the points along the locus in Fig.3.4(a); however, the difference between N^F and N^B remains very small throughout the locus. To increase the difference in the transmitted amplitudes of the forward and backward configurations, we fix $\alpha = 0.5$ (indicated by the black square marker) and increase the forcing amplitude P as we keep $\Delta \phi = 0$. Fig.3.4(b) shows that the difference between the transmitted energies can increase at higher values of the forcing amplitude. In this range of parameters, the maximum difference between N^F and N^B in the stable region of the response occurs near P = 5, marked by the red square.

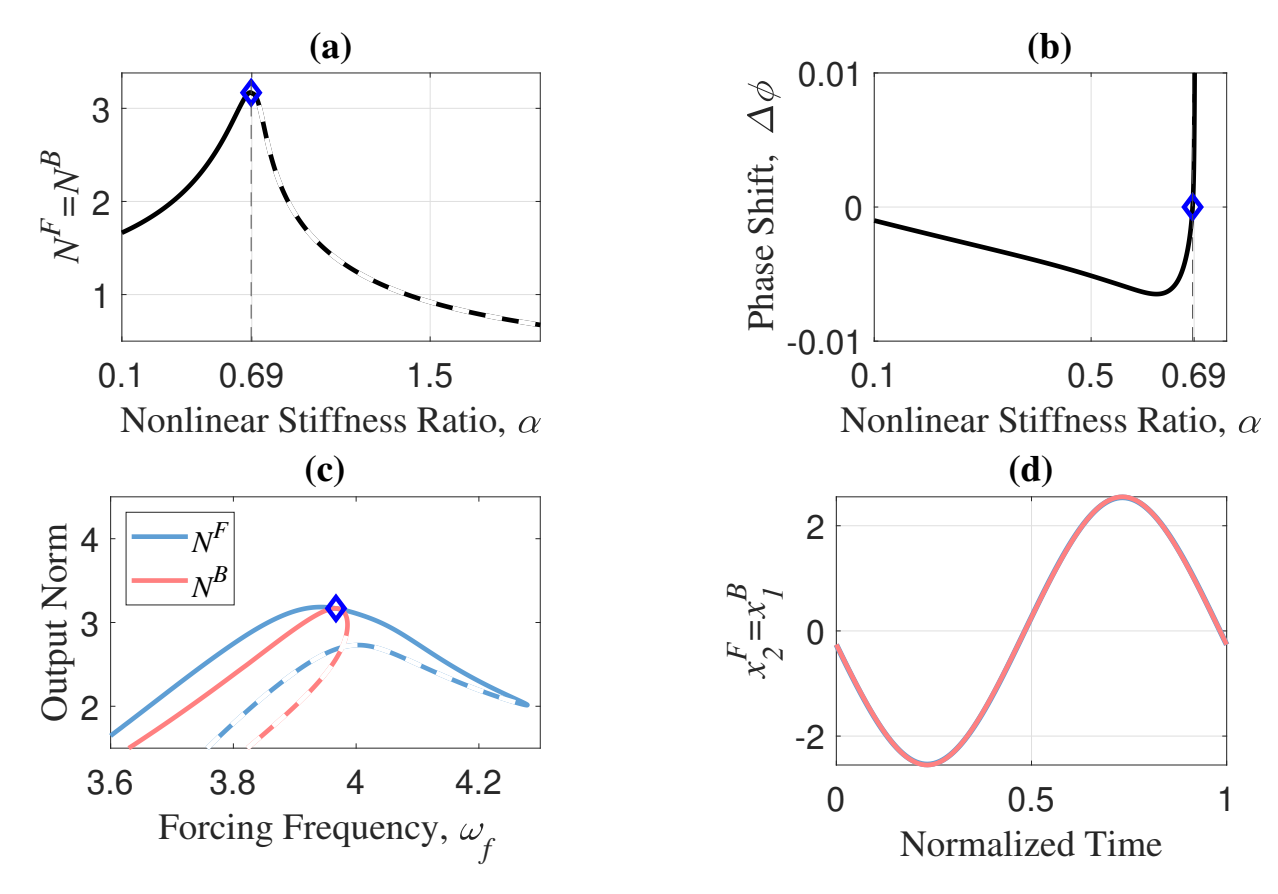


Figure 3.3: (a) Locus of phase nonreciprocity $(N^F = N^B)$ as a function of the nonlinear stiffness ratio, α . (b) Nonreciprocal phase shift between the forward and backward configurations, $\Delta \phi = \phi^F - \phi^B$. (c) Frequency response curves of the system for P=2, r=2.5 and $\alpha=0.69$. (d) Time response over one forcing period corresponding to the blue diamond marker.

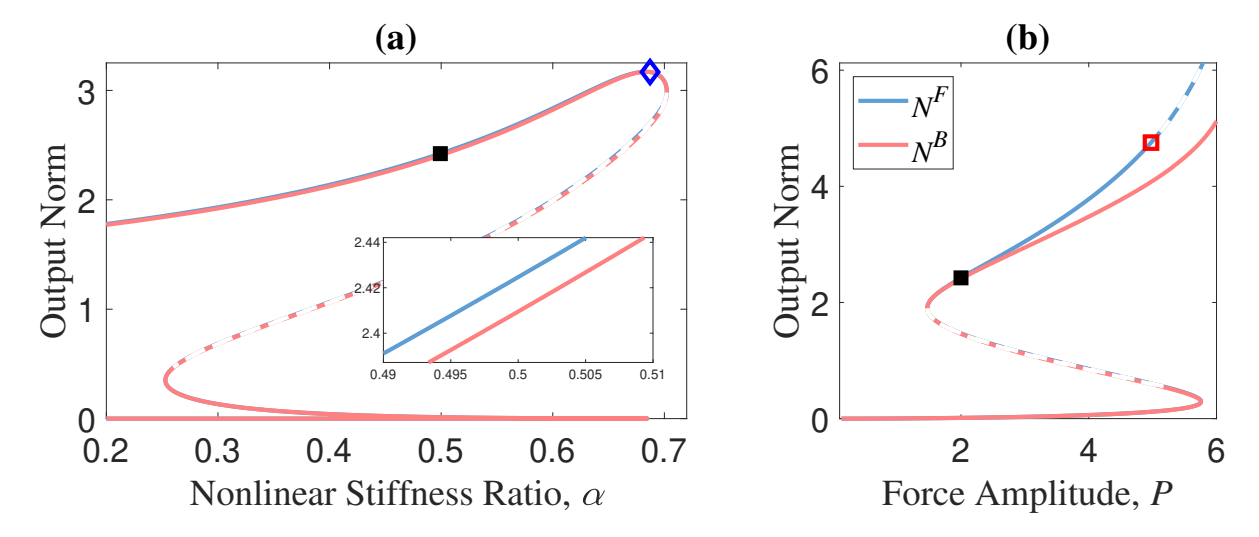


Figure 3.4: Locus of phase-preserving nonreciprocity, $\Delta \phi = 0$ for (a) P = 2 and r = 2.5 as a function of the nonlinear stiffness ratio, α , (b) r = 2.5 and $\alpha = 0.5$ as a function of force amplitude, P.

Fig. 3.5(a) shows the frequency response curves of the system for r = 2.5, $\alpha = 0.5$, and P = 5. The red square marks the point with phase-preserving nonreciprocity obtained in Fig.3.4(b). Fig. 3.5(b) shows the time-domain response at this point: the output displacements are harmonic and have the same phases, but the response is nonreciprocal. The amplitude of the output displacement is 7% higher in the forward configuration in this case.

There are three other forcing frequencies at which the system exhibits phase-preserving non-reciprocity, marked by black squares in Fig. 3.5(a). Panel (c) shows the time-domain response at $\omega_f = 1.89$, which is near the first primary resonance. Similar to the situation in panel (a), the amplitude difference is small. In panels (d) and (e), phase-preserving nonreciprocity is accompanied by the appearance of higher harmonics in the forward configuration due to the proximity to a 3:1 internal resonance near $\omega_f \approx 1.2$. We note that the phase difference is zero only for the first harmonics.

3.4.2. Influence of the linear stiffness ratio

We use the linear stiffness ratio, r, to find parameters at which the phase-preserving non-reciprocity is accompanied by a larger difference in the transmitted amplitudes. Fig. 3.6(a) shows the locus of phase-preserving nonreciprocity, $\Delta \phi = 0$, as a function of r. The red square marker corresponds to the same point as in Fig. 3.5(a). The green square marker at r = 11 indicates a point within the stable range of the locus at which the difference between the amplitudes of the forward and backward configurations is the largest. Fig. 3.6(b) shows the locus of $\Delta \phi = 0$ for the points near the first primary resonance of the system that are

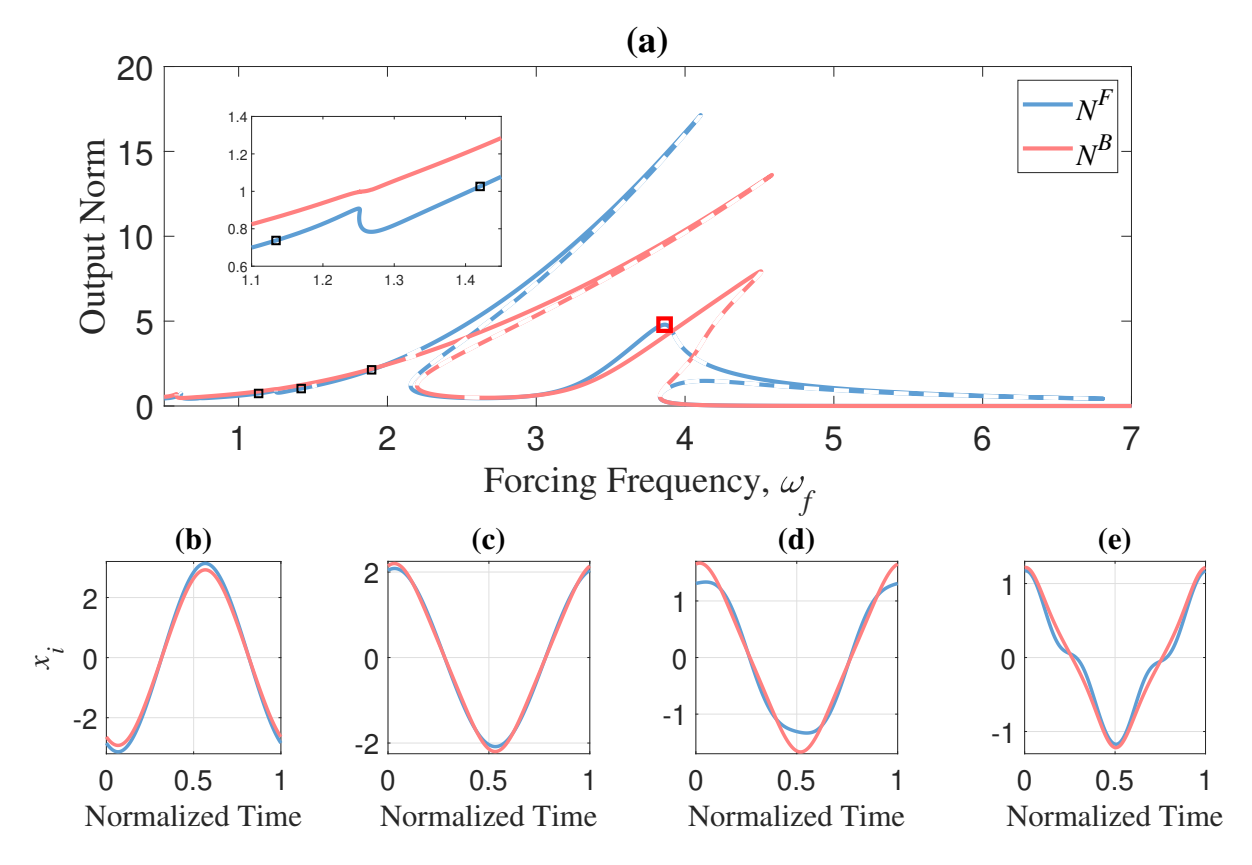


Figure 3.5: (a) Frequency response curves of the system with P=5, r=2.5, and $\alpha=0.5.$ Time response over one forcing period at the points indicated by square markers: (b) $\omega_f=3.86,$ (c) $\omega_f=1.89,$ (d) $\omega_f=1.42,$ and (e) $\omega_f=1.13.$

marked by black squares in Fig. 3.5(a). The locus of phase-preserving nonreciprocity forms a closed loop that passes through these points.

Fig. 3.7(a) shows the frequency response curve of the system for r=11, $\alpha=0.5$, and P=5, which corresponds to the parameter values for the green square marker in Fig. 3.6(a). Remarkably, the green square marker lies on an isolated portion of the response curve (an isola) for the forward configuration; we could not find an isola in the response curve of the backward configuration in this frequency range. Panel (b) shows the time-domain response of the system at the green square marker, showing a significant difference in the amplitudes of the forward and backward configurations.

Fig. 3.7(a) includes other points that exhibit $\Delta \phi = 0$, indicated by the blue square markers. Panel (c) shows the time-domain response at $\omega_f = 4.52$, where the difference in the transmitted amplitudes is negligible; the response happens to be almost reciprocal at this point. Panel (d) shows the time-domain response at $\omega_f = 1.46$, which is one of the two square markers close to the 3:1 internal resonance of the system near $\omega_f \approx 1.43$ – see the inset in Fig. 3.7(a). The response at the other square marker ($\omega_f = 1.41$) is very similar and is not shown. The contribution from the third harmonic in Fig. 3.7(d) is stronger than in Figs. 3.5(d) and (e). It is clear from the asymmetry of the response in Fig. 3.7(d) that the third harmonics in this case have different phases between the forward and backward configurations. This is because we have only enforced phase preservation for the first harmonic.

Fig. 3.8 shows the transient response of the forward and backward configurations for initial conditions within the basin of attraction of the green blue marker in Fig. 3.6(a). As expected, the steady-state response in the forward configuration settles on the isola ($N^F \approx 2.50$ and an amplitude of 2.25), while the steady-state response in the backward configuration lies on the main frequency curve ($N^B \approx 0.85$ and an amplitude of 1.30).

It is worth noting that the system considered here is intentionally designed to isolate and investigate phase-preserving nonreciprocity. While the findings provide valuable insights into the role of asymmetry and nonlinearity, caution should be exercised when extending these results to other nonlinear systems with different configurations or boundary conditions. This is because achieving phase-preserving nonreciprocity typically requires carefully tailored parametric designs specific to the system under consideration.

3.5. Conclusions

We conducted a computational analysis of nonreciprocal vibration transmission in a nonlinear mechanical system with two degrees of freedom. We focused on the steady-state response of the system to external harmonic excitation. Nonlinearity appeared in the grounding

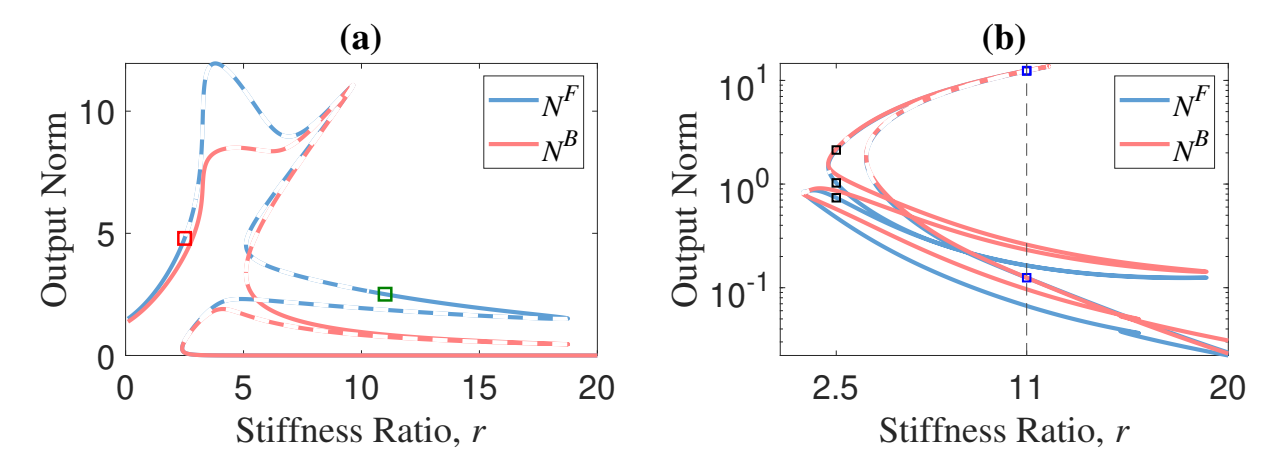


Figure 3.6: Locus of phase-preserving nonreciprocity, $\Delta \phi = 0$, as a function of the stiffness ratio, r, computed from the points indicated in Fig. 3.5: (a) the red marker, (b) one of the black markers.

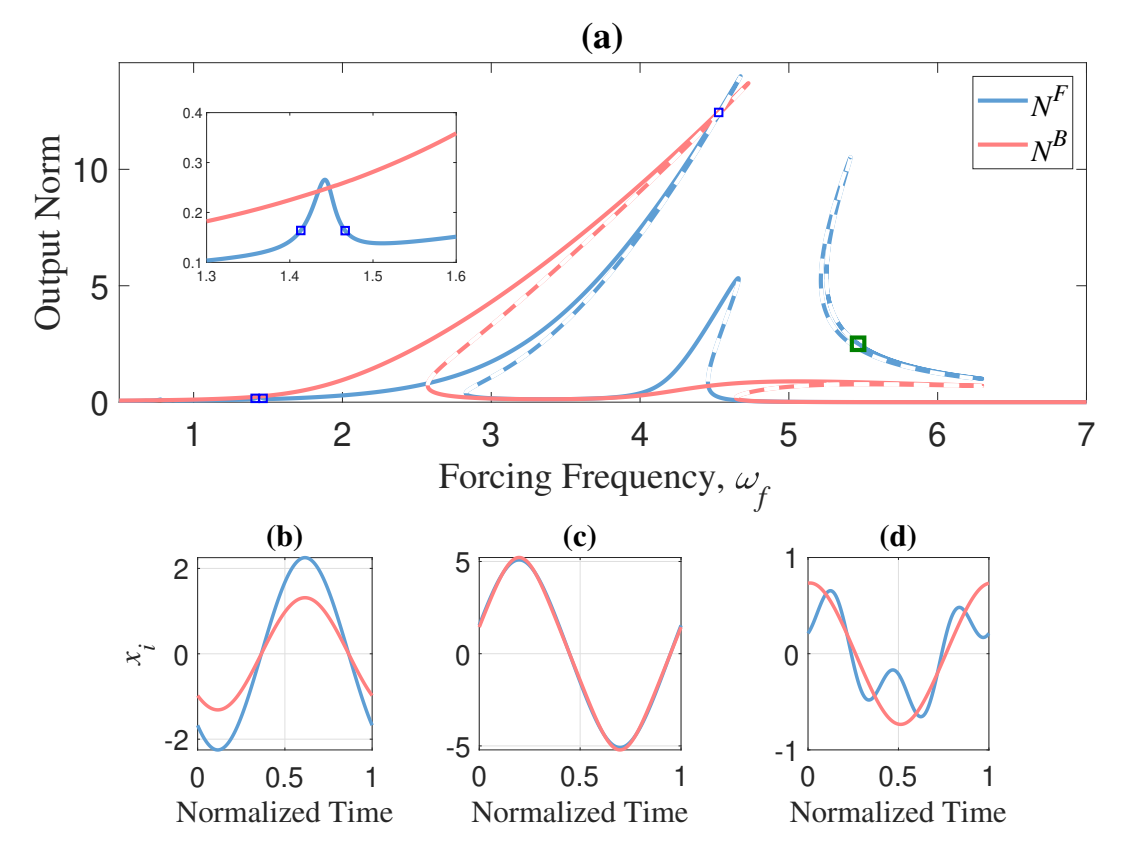


Figure 3.7: (a) Frequency response curves of the system with $P=5, r=11, \mu=1, \alpha=0.5$. Time response at the points indicated by square markers: (b) $\omega_f=5.46$, (c) $\omega_f=4.52$ (d) $\omega_f=1.46$.

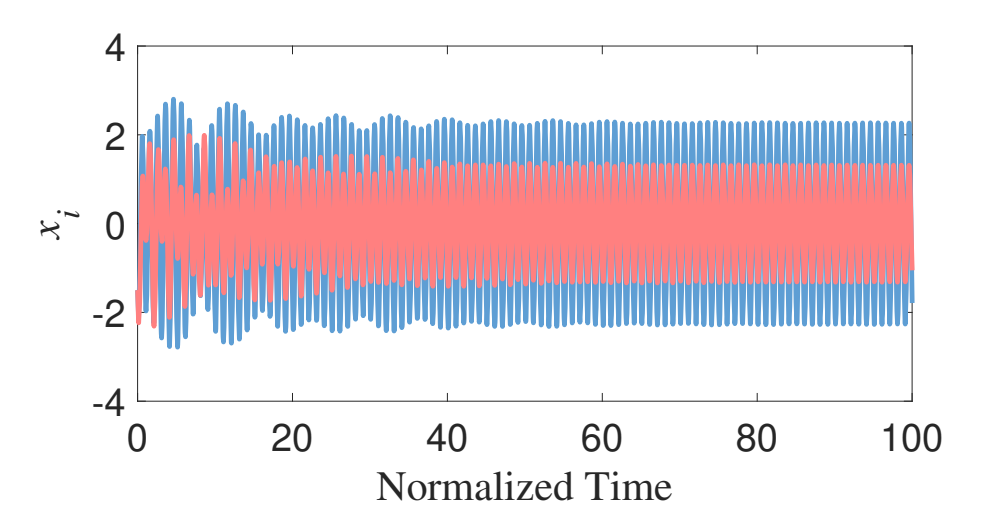


Figure 3.8: Transient response of the forward and backward configurations over 100 forcing periods at $\omega_f = 5.46$ starting from the same initial conditions.

nonlinear elasticity of each degree of freedom. The mirror symmetry of the system was controlled by two independent symmetry-breaking parameters. Within this context, our primary focus was on highlighting the role of transmitted phase in breaking reciprocity.

Nonreciprocity is most commonly associated with and identified by a large energy bias in the transmitted energy when the locations of the source and receiver are interchanged $(N^F \neq N^B)$. This energy bias is almost always accompanied by a difference in the transmitted phase $(\phi^F \neq \phi^B)$. It is possible to have response regimes in which breaking of reciprocity is solely due to a difference in the transmitted phases and not the transmitted energies $(N^F = N^B, \phi^F \neq \phi^B)$. In this work, we showed that it is possible to have response regimes in which an energy bias is not accompanied by a phase bias $(N^F \neq N^B, \phi^F = \phi^B)$. We provide a systematic approach for realizing such regimes of phase-preserving nonreciprocity by tuning two independent symmetry-breaking parameters of the system.

Our findings indicate that breaking of reciprocity is most commonly accompanied by a simultaneous bias in the transmitted energy and phase. Energy bias alone, with no contribution from phase, can still lead to nonlinear nonreciprocity, albeit at very finely tuned sets of system parameters. This highlights the significant role of phase in breaking reciprocity, a feature that is often overlooked. We hope that our findings prove useful in the design and application of nonreciprocal devices in energy harvesting and mechanical signal processing.

Appendices

3A. Non-dimensional Equations of Motion

The governing equations for the system in Fig. 3.1 can be written as:

$$M_1\ddot{x}_1 + k_3(x_1 - x_2) + k_{g1}x_1 + k_{n1}x_1^3 + c\dot{x}_1 = f_1\cos\omega_f t$$

$$M_2\ddot{x}_2 + k_3(x_2 - x_1) + k_{g2}x_2 + k_{n2}x_2^3 + c\dot{x}_2 = f_2\cos\omega_f t$$
(3A.1)

where k_3 is the coupling stiffness. k_{n1} and k_{n2} are the coefficients of the nonlinear grounding stiffness for M_1 and M_2 . k_{g1} and k_{g2} are the coefficients of the linear grounding springs for M_1 and M_2 , and c is the linear viscous damping connecting each mass to the ground. We divide the equations by k_{g1} and introduce the non-dimensional parameters $\tau = \omega_0 t$, $\omega_0^2 = k_{g1}/M_1$, $\Omega = \omega_f/\omega_0$ to obtain

$$M_{1}\omega_{0}^{2}/k_{g1}x_{1}'' + k_{3}/k_{g1}(x_{1} - x_{2}) + x_{2i-1} + k_{n1}/k_{g1}x_{1}^{3} + 2\zeta_{g}x_{1}' = f_{1}/k_{g1}\cos\Omega\tau$$

$$M_{2}\omega_{0}^{2}/k_{g1}x_{2}'' + k_{3}/k_{g1}(x_{2} - x_{1}) + k_{g2}/k_{g1}x_{2} + k_{n2}/k_{g1}x_{2}^{3} + 2\zeta_{g}x_{2}' = f_{2}/k_{g1}\cos\Omega\tau$$
(3A.2)

where $x' = dx/d\tau = (dx/dt)/\omega_0$, $x'' = d^2x/d\tau^2 = (d^2x/dt^2)/\omega_0^2$, and $\zeta_g = (c\omega_0)/(2k_{g1})$. We define the non-dimensional displacement and force as $\bar{x} = x/d$ and $F = f/(dk_{g1})$, where d is a characteristic displacement of the system. This results in

$$\bar{x}_1'' + k_c(\bar{x}_1 - \bar{x}_2) + \bar{x}_1 + k_N \bar{x}_1^3 + 2\zeta_g \bar{x}_1' = F_1 \cos \Omega \tau$$

$$\mu \bar{x}_2'' + k_c(\bar{x}_2 - \bar{x}_1) + r_g \bar{x}_2 + \alpha k_N \bar{x}_2^3 + 2\zeta_g \bar{x}_2' = F_2 \cos \Omega \tau$$
(3A.3)

where $\mu = M_2/M_1$, $k_N = d^2k_{n1}/k_{g1}$, $\alpha = k_{n2}/k_{n1}$, $k_c = k_3/k_{g1}$, and $r_g = k_{g2}/k_{g1}$. Eq. (3A.3) is the non-dimensional form of Eq. (3A.1). Eq. (3A.3) is the same as Eq. (3.1) in the main text, where we have dropped the overbar in \bar{x} and replaced τ with t, and Ω with ω_f for ease of reference.

3B. Extraction of the Phase of the First Harmonic

In this appendix, we outline the procedure for extracting the phase of the first harmonic from a periodic response using Fourier series decomposition.

A general periodic response x(t) with period T can be expanded in terms of its Fourier series as

$$x(t) = a_0 + \sum_{n=1}^{\infty} \left(a_n \cos(n\omega t) + b_n \sin(n\omega t) \right), \tag{3B.1}$$

where $\omega = \frac{2\pi}{T}$ is the fundamental frequency, and the Fourier coefficients are given by

$$a_n = \frac{2}{T} \int_0^T x(t) \cos(n\omega t) dt,$$

$$b_n = \frac{2}{T} \int_0^T x(t) \sin(n\omega t) dt.$$
(3B.2)

To extract the phase of the first harmonic (n = 1), we consider the first-order terms:

$$x_1(t) = a_1 \cos(\omega t) + b_1 \sin(\omega t). \tag{3B.3}$$

This can be rewritten in an equivalent phase-amplitude form:

$$x_1(t) = A_1 \cos(\omega t - \phi_1), \tag{3B.4}$$

where the amplitude A_1 and phase ϕ_1 are determined as

$$A_1 = \sqrt{a_1^2 + b_1^2},\tag{3B.5}$$

$$\tan(\phi_1) = b_1/a_1 \tag{3B.6}$$

Thus, the phase of the first harmonic is directly obtained from the ratio of the Fourier coefficients a_1 and b_1 .

Chapter 4

Unilateral vibration transmission in mechanical systems with bilinear coupling

4.1. Introduction

It is generally preferred in engineering to design vibrating machines and devices to operate in the linear regime, where their behavior is more easily predictable. Nonlinearity, within this framework, is often associated with unwanted complexity. However, nonlinearity is unavoidable in several engineering systems such as systems with friction joints or clearances [37, 137]. On the other hand, nonlinearity can be introduced intentionally to a vibrating system with the goal of achieving new response characteristics [138–140]. There is therefore a need to understand the nonlinear behavior of vibrating systems from both theoretical and practical perspectives.

Nonlinearity can originate from the material properties of a system (material nonlinearity) [30], from large deformations (geometrical nonlinearity) [31] or from the interaction force between multiple sub-systems such as friction in joints (contact nonlinearity) [37]. In this work, we focus on a particular type of nonlinearity known as bilinear elasticity or bilinear stiffness.

Bilinear stiffness refers to a system characteristic where the effective elasticity changes at a certain degree of elastic deformation, exhibiting one stiffness value up to a threshold called the offset, and a different stiffness value beyond that threshold. This unique nonlinearity can be found in systems such as a cracked beam [56], in vibro-impact drilling systems [57], or in systems with intermittent contact [58, 59]. Systems featuring bilinear elasticity are known for their non-smooth behavior (sudden change between two states), leading to intricate nonlinear dynamic response characteristics [44]. Vibration systems with bilinear stiffness may exhibit unique dynamic behavior not readily found in other types of nonlinearity. Therefore, it is important to understand the associated dynamics and vibration transmission characteristics of such systems.

The study of bilinear stiffness and its impact on the vibration characteristics of mechanical systems has a long history [45–48]. Extensive research has explored various aspects of vibration characteristics influenced by bilinear stiffness and damping [49–54]. In this work, we focus on a response characteristic that can be triggered effectively by bilinear stiffness:

unilateral transmission.

Unilateral transmission is a response characteristic where the transmitted wave remains purely in tension or compression; *i.e.*, the corresponding deformations from the static equilibrium position remain consistently positive or negative. Lu and Norris [28] were the first, to the best of our knowledge, to demonstrate unilateral transmission using a single bilinear stiffness connecting two waveguides. They derived equations that describe the relationship between the parameters of the bilinear spring and the conditions necessary for achieving unilateral transmission. Despite the intriguing nature of unilateral transmission, this phenomenon has not been explored in details in the context of vibration dynamics Our main goal is to investigate unilateral transmission in the context of vibration transmission in mechanical systems, with a focus on understanding the influence of different system parameters on this phenomenon.

We investigate unilateral transmission using an archetypal system of two coupled oscillators. Each oscillator may be viewed as the amplitude equation for linear waves propagating in a waveguide. Bilinearity is introduced through the coupling spring; this is the only source of nonlinearity in this work. We focus exclusively on steady-state vibration transmission in response to an external harmonic force. We find that breaking the mirror symmetry of the system facilitates unilateral transmission by allowing it to occur near a primary resonance.

A consequence of breaking the mirror symmetry of the system is that it enables nonreciprocal dynamics [17]. Nonreciprocity in systems with bilinear coupling has already been reported, primarily with a focus on attaining a significant difference in transmitted energies in opposite directions [25, 43, 88–90]. Here, we investigate nonreciprocity in the context of unilateral transmission. We show that nonreciprocal unilateral transmission may occur either in one transmission direction or both. In addition, we report on other nonreciprocal features of the response such as direction-dependent appearance of higher harmonics, periodic-doubled response or quasiperiodic dynamics, some of which are not presented often in the literature.

Inspired by recent advances in the manufacturing of periodic lattice materials with tunable dynamic properties [73], we extend our analysis to a periodic lattice made from repetition of bilinearly coupled units. We investigate the wave propagation characteristics of a periodic material with a bilinear unit cell, with a focus on analyzing unilateral transmission. We then conduct a parametric study to investigate the influence of the number of units and of energy dissipation on unilateral transmission in the periodic lattice.

Section 4.2 presents the problem formulation and solution methodology. We discuss unilateral transmission for bilinearly coupled systems in Section 4.3. We extend the analysis to a

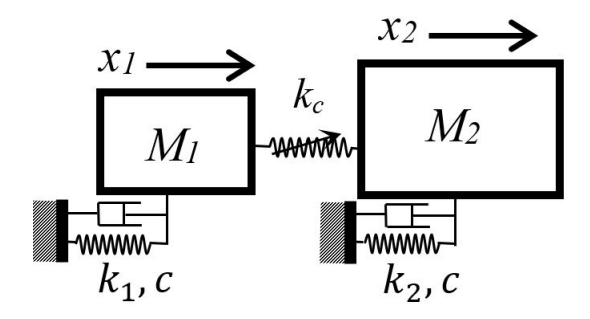


Figure 4.1: Schematic of the 2DoF system consists of two linear damped oscillators coupled with a bilinear spring.

periodic structure made from bilinearly coupled units in Section 4.4. We review our main findings and conclude in Section 4.5.

4.2. Problem setup

4.2.1. Governing equations

Fig. 4.1 shows the schematics of the two-degree-of-freedom (2DoF) vibration system we study in this section. The system consists of two masses, M_1 and $M_2 = \mu M_1$, connected by a bilinear spring k_c . The two masses are anchored to the ground by linear springs k_1 and k_2 . Energy loss is accounted for by identical linear viscous dampers with a constant c, connecting each mass to the ground. The system is subject to external harmonic excitation with amplitude F and frequency ω_f , which acts on one of the two masses depending on the transmission scenario. The symmetry of the setup can be controlled by either the mass ratio $\mu = \frac{M_2}{M_1}$ or the ratio of the grounding springs $r = \frac{k_2}{k_1}$.

As outlined in Appendix 4A, the equations of motion for the system shown in Fig. 4.1 can be written using non-dimensional parameters as

$$\ddot{x}_1 + K_c(x_1 - x_2) + x_1 + 2\zeta \dot{x}_1 = F_1 \cos \omega_f t$$

$$\mu \ddot{x}_2 + K_c(x_2 - x_1) + rx_2 + 2\zeta \dot{x}_2 = F_2 \cos \omega_f t$$
(4.1)

where

$$K_c = \begin{cases} \beta k, & x_2 - x_1 > 0 \\ k, & x_2 - x_1 < 0 \end{cases}$$
 (4.2)

The parameter K_c represents the bilinear stiffness, which results in a nonsmooth (piecewise smooth) force in the system. This is the origin of nonlinearity in our system. We define β as the bilinear ratio. The coupling stiffness (therefore the coupling force) is considered

softening when $\beta < 1$ and hardening when $\beta > 1$. The damping ratio is denoted by ζ and the forcing frequency by ω_f .

In the proceeding sections, we study the end-to-end vibration transmission characteristics of Eq. (4.1). For this purpose, we define (i) the forward configuration with $F_1 = P$ and $F_2 = 0$, in which the output is the steady-state displacement of the last (right-most) mass, $x_2^F(t)$; (ii) the backward configuration with $F_1 = 0$ and $F_2 = P$, in which the output is the steady-state displacement of the first (left-most) mass, $x_1^B(t)$. To quantify the degree of nonreciprocity of the response, we define the reciprocity bias, R, as

$$R = \frac{1}{T} \int_0^T \left(x_2(t)^F - x_1(t)^B \right)^2 dt \tag{4.3}$$

where $T=2\pi/\omega_f$ is the forcing period. We have R=0 if and only if the response is reciprocal.

4.2.2. Solution methodology

The bilinear stiffness represents a strong nonlinearity. The nonsmooth nature of this non-linear force poses challenges for the analysis of the system. It is possible to obtain analytical expressions in the frequency-preserving (weakly nonlinear) operating regime of the system [141]. This approach is cumbersome for systems with many degrees of freedom, however. Direct numerical computation of the response of the system is also time-consuming for performing a parametric study.

Given that our focus is exclusively on the steady-state response of the system to harmonic excitation, we will use continuation techniques to compute the response of the bilinear system. We approximate the bilinear stiffness by the following smooth function:

$$K_c = \frac{k(\beta - 1)}{\pi} \arctan(B(x_2 - x_1)) + \frac{k(\beta + 1)}{2}$$
(4.4)

It is possible to capture the nonsmooth nature of the bilinear force with no approximation, but the associated cost is increasing the computation time. The accuracy of this approximation (regularization) depends on the value of the regularization parameter, B. Higher values of B result in a sharper transition around the transition point between the two values of the stiffness, k and βk , at the cost of making the equations numerically stiffer. We have chosen B = 1000 for all the results presented in this work. This will be validated by comparing the results with those from an event-driven numerical integration scheme. When the transition between the two values of stiffness occurs at zero deformation, we refer to this case as bilinear stiffness with no offset. The steady-state response of a bilinear system with no offset

is independent of the value of the forcing amplitude [52]. For the low to moderate values of forcing amplitude that we consider in this work, the response is indeed independent of the forcing amplitude – see Appendix 4B. When the offset is not zero, the response below a certain threshold is linear (amplitude independent) until the bilinearity is triggered; see [70] for an example.

We use the software package COCO [107] to compute the steady-state response of the system under harmonic excitation as a family of periodic orbits with period $T = 2\pi/\omega_f$ that satisfy a suitable boundary-value problem [135]. This is particularly suitable for our system because we anticipate the response to be anharmonic within the parameter ranges that we explore. The (local) stability of the response is determined by the Floquet multipliers associated with each periodic orbit.

Because the restoring force in the bilinear spring, $f(x_2-x_1) = K_c(x_2-x_1)$, is not symmetric with respect to its deformation, $f(d) \neq f(-d)$, there will be a drift (DC term) in the steady-state response of the system; *i.e.* the oscillations may not be centered around the static equilibrium points of the two masses. To account for this, we define the DC value C_i around which each mass i oscillates as

$$C_{i} = \frac{\operatorname{Max}(x_{i}(t)) + \operatorname{Min}(x_{i}(t))}{2}$$
(4.5)

We define the amplitude of the oscillation or the AC value for each mass as

$$A_{i} = \frac{\operatorname{Max}(x_{i}(t)) - \operatorname{Min}(x_{i}(t))}{2}$$

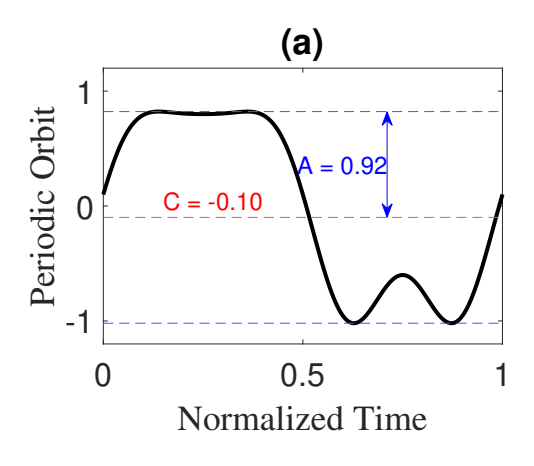
$$(4.6)$$

which represents the maximum deflection of each mass from its static equilibrium position.

We note that the choice of amplitude parameters is not unique. Our goal here is to use parameters that help determine when a response is unilateral. Fig. 4.3 shows how parameters A and C in Eqs. (4.5-4.6) represent two examples of anharmonic periodic solutions. Panel (a) shows a periodic response that is not unilateral; *i.e.*, |A| > |C|. Panel (b) shows a unilateral response for which |A| < |C|. Of course, these norms also work well when the response is harmonic. We can therefore use the ratio of C to A in the output displacement to determine whether the transmitted vibration is unilateral.

For unilateral transmission to occur, the output must exhibit a minimum value greater than zero or a maximum value less than zero. In other words, the transmitted vibration displacement must be exclusively positive or negative. Using the norms A and C from Eqs. (4.5-4.6), we define the unilateral ratio as

$$R_u = \frac{|C_i|}{|A_i|} \tag{4.7}$$



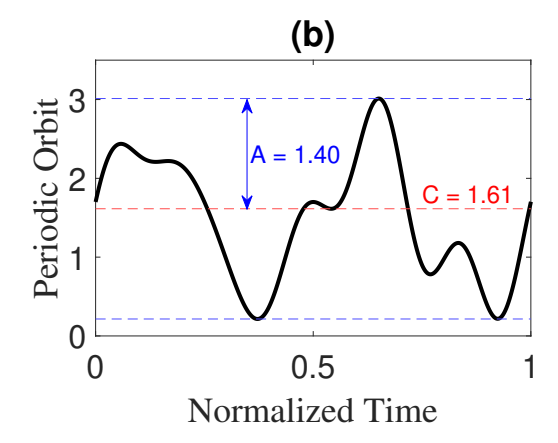


Figure 4.2: Periodic orbits represented by A and C (a) non-unilateral (b) unilateral

where i = 2 for the forward configuration and i = 1 for the backward configuration. Thus, $R_u > 1$ represents unilateral transmission and $R_u = 1$ corresponds to the onset of unilateral transmission.

4.3. Bilinearly coupled oscillators

4.3.1. Unilateral transmission in a symmetric system

We first focus on unilateral transmission in a 2DoF system with mirror symmetry (identical oscillators), characterized by $\mu = 1 = r$. There is no difference between the left-to-right and right-to-left transmission characteristics in this case and the response of the system is (trivially) reciprocal by virtue of the mirror symmetry. We consider the case of softening bilinearity, $\beta < 1$, in which the system is stiffer in compression than in tension. This type of bilinear force can be found in coupled structures assembled with bolted joints [142].

Fig. 4.3 (a) shows the frequency response function of the output of the system for P = 0.15, $\zeta = 0.03$, k = 1, $\beta = 0.1$, and $r = \mu = 1$. The unilateral ratio, R_u , is monitored to find regions with unilateral transmission; these regions are indicated by thicker lines. The top right inset shows the steady-state output displacement of the system during one period $(2\pi/\omega_f)$ at the onset of unilateral transmission, $R_u = 1$, near $\omega_f \approx 2.03$. The displacement is always positive in sign (purely in extension) and does not cross the zero line (static equilibrium position). The unstable range below the first primary resonance $(0.84 < \omega_f < 0.92$, shown in the bottom left inset) corresponds to a branch of period-doubled solutions that emanate from period-doubling (PD) bifurcation points indicated by diamond markers. The PD branch is computed and plotted as a gray line in Fig. 4.3(a), and its validity is confirmed using a custom event-driven direct numerical integration implemented in MATLAB. This method employs MATLAB's ode45 solver with an event detection function

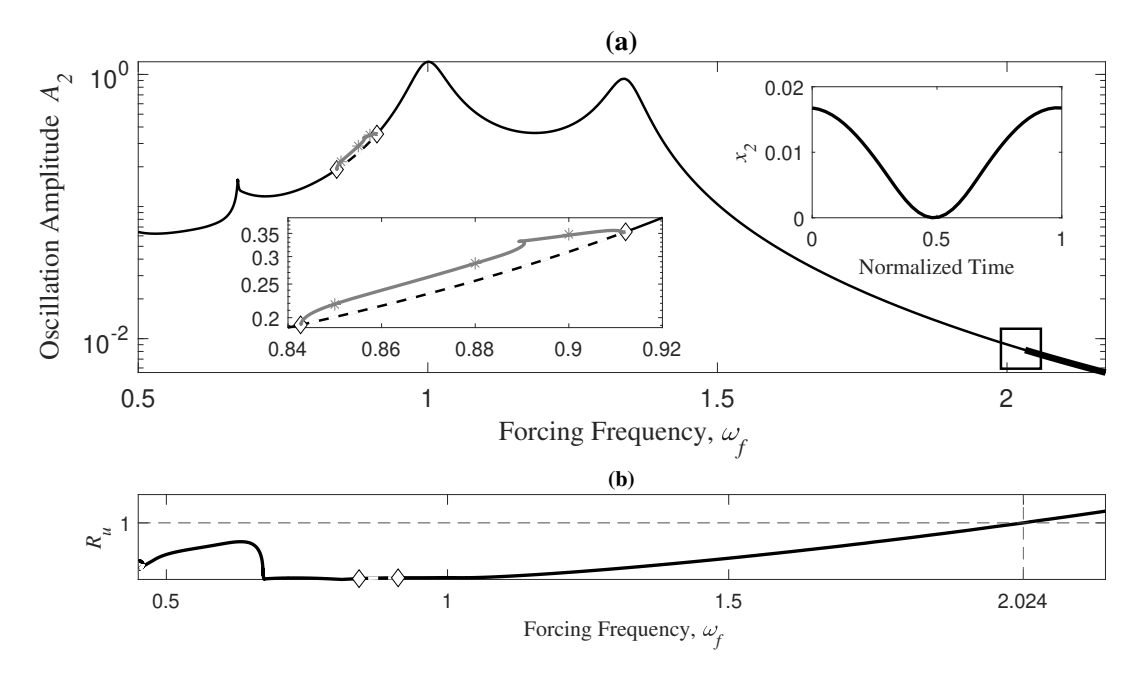


Figure 4.3: (a) Frequency response of the symmetric 2DoF $(r = \mu = 1)$ system for the forward configuration. Thick lines indicate response that exhibits unilateral transmission and dashed lines indicate unstable response. Diamond markers indicate period-doubling bifurcation points. The upper right inset shows the unilateral time response at the frequency highlighted by the black square. (b) Unilateral transmission R_u as a function of forcing frequency.

that accurately captures the switching behavior of the bilinear stiffness by detecting when the displacement crosses the offset threshold. The period-doubled solutions (not shown) are not unilateral. Similar branches of period-doubled solutions have been reported in systems with bilinear elasticity [143]. Fig. 4.3 (b) shows the unilateral ratio in the same range of the forcing frequency.

Although it is possible for the symmetric system to exhibit unilateral transmission, this characteristic occurs far from the system's resonance region. The response of the system has a very low amplitude and operating a mechanical system off-resonance is inefficient and often unproductive in practice. We were not able to find near-resonance unilateral transmission in the symmetric system by changing the bilinear ratio β (including hardening), damping ratio ζ or forcing amplitude P. It is possible to overcome this issue, however, by breaking the mirror symmetry of the system.

4.3.2. Unilateral transmission in an asymmetric system

To find an asymmetric system that exhibits unilateral transmission near its primary resonances, we compute the locus of the onset of unilateral transmission, $R_u = 1$, as a function of one of the symmetry-breaking parameters. Fig. 4.4(a) shows the output amplitude (forward configuration) at the onset of unilateral transmission as a function of the stiffness ratio, r. We observe that lower values of the stiffness ratio (softer grounding stiffness for M_1) lead to higher output amplitudes at the onset of unilateral transmission. The maximum output occurs near r = 0.28, which aligns the onset of unilateral transmission to the peak frequency. Fig. 4.4(b) shows the variation of the forcing frequency along the same locus ($R_u = 1$). The response at the forcing frequencies that lie above this locus, highlighted by a red background, exhibit unilateral transmission.

Fig. 4.5(a) shows the frequency response function of the asymmetric system with r = 0.28. The inset shows the output displacement at the resonance peak indicated by the square over one forcing period. This point corresponds to the onset of unilateral transmission, which is characterized by the minimum value of the time-domain response grazing the static equilibrium position at zero.

Because the onset of unilateral transmission occurs precisely at the second peak frequency, $R_u > 1$ on one side of the peak and $R_u < 1$ on the other side. Fig. 4.4 suggests that selecting a lower value for the stiffness ratio (r < 0.28) can shift the onset of unilateral transmission to a lower forcing frequency such that unilateral transmission covers the peak frequency on both sides. Fig. 4.5(b) shows the frequency response function of the system for r = 0.25. As expected, the region of stable unilateral response covers a wider frequency range around the peak frequency. The value of the unilateral ratio is 10% larger than 1 at the peak ($R_u = 1.1$). We also note that the onset of unilateral transmission has a strong dependence on the stiffness ratio, especially near the peak frequency.

We followed the same procedure for finding unilateral transmission occurring near a resonance of the system, this time using the other symmetry-breaking parameter, μ , the mass ratio. To ensure that the region of unilateral transmission covers both sides of the peak frequency, we set $R_u = 1.1$ based on the observations from Fig. 4.5(b). Fig. 4.6 shows the frequency response of the system with r = 1 for three values of μ : 1, 2, and 3. The red line indicates the locus where $R_u = 1.1$. For $\mu = 3$, the response demonstrates that unilateral transmission occurs around the second resonance peak. Comparing Fig. 4.6 with Fig. 4.5(b) reveals that both the mass ratio r and the stiffness ratio μ can be used to achieve unilateral transmission near the system's second primary resonance.

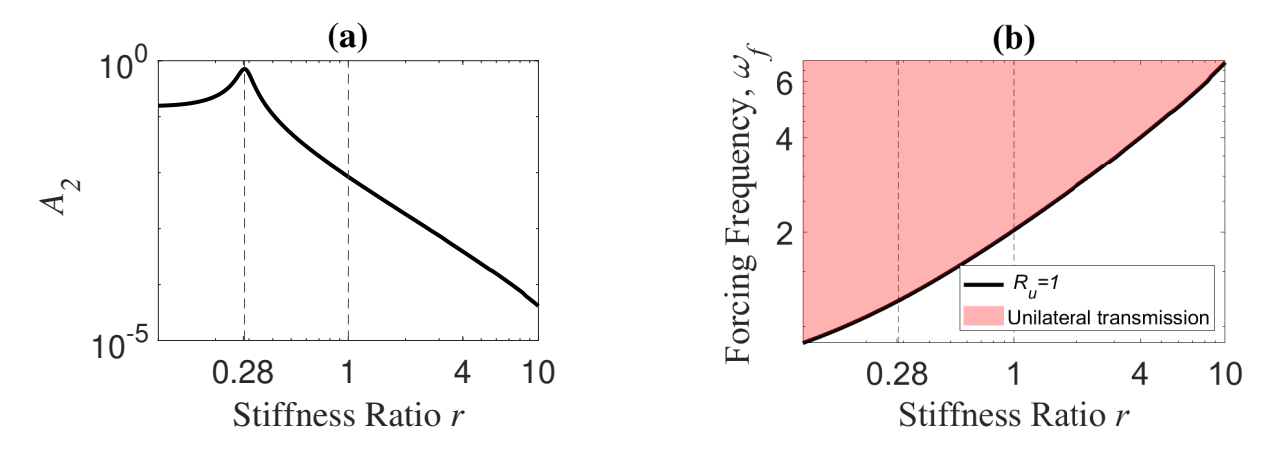


Figure 4.4: Locus of the onset of unilateral transmission $R_u = 1$ as a function of the stiffness ratio r for (a) Output amplitude (b) Forcing frequency.

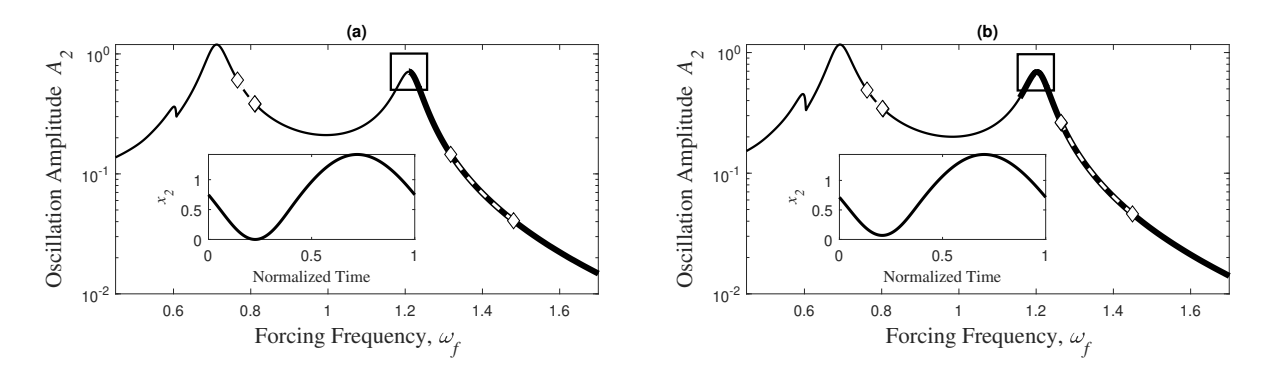


Figure 4.5: (a) Frequency response of the asymmetric system r=0.28 for the onset of unilateral transmission at the peak frequency (b) Frequency response of the asymmetric system r=0.25 for the onset of unilateral transmission before the peak frequency

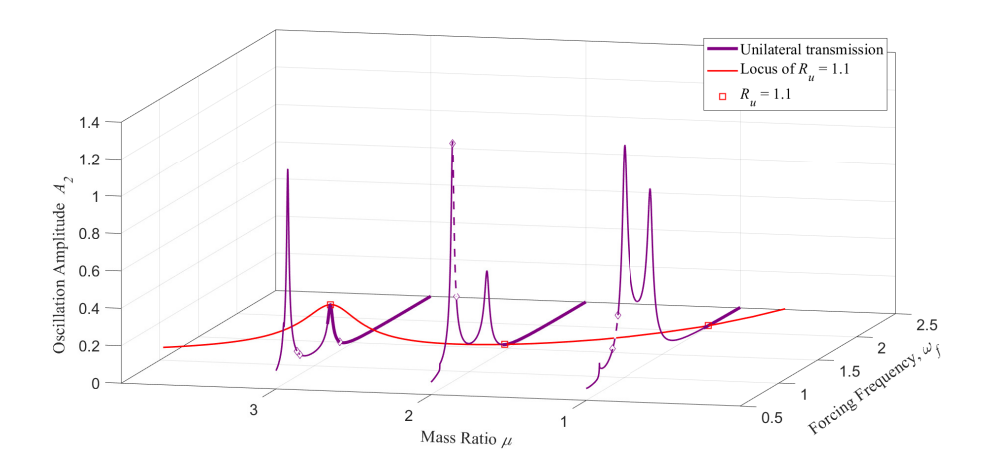


Figure 4.6: Frequency response of the system with locus of $R_u = 1.1$ as a function of μ . Thick lines indicate response that exhibits unilateral transmission and dashed lines indicate unstable response.

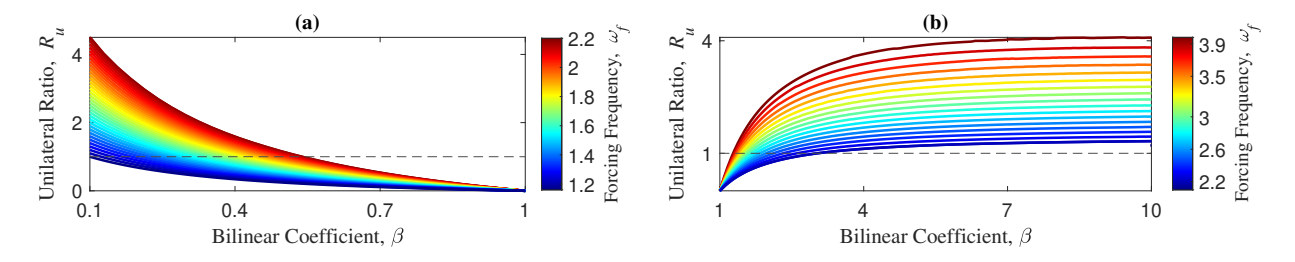


Figure 4.7: Influence of bilinear ratio β on unilateral transmission for r = 1, $\mu = 3$, $\zeta = 0.03$, and F = 0.15. (a) Softening bilinearity, $\beta < 1$, (b) hardening bilinearity, $\beta > 1$.

4.3.3. Influence of the bilinear ratio

The bilinear stiffness is the only source of nonlinearity in our system. To investigate the influence of bilinearity on unilateral transmission, we focus on the frequency range 1.16 $< \omega_f < 2.2$, where unilateral transmission occurs for the system with r = 1 and $\mu = 3$; recall Fig. 4.6. This range is discretized into several frequencies. At each frequency, we compute the variation of the unilateral ratio (R_u) as a function of the bilinear ratio (β) .

Fig. 4.7(a) shows a contour plot of R_u as a function of β for the case of softening bilinearity $(\beta < 1)$. As β increases, the frequency range with $R_u > 1$ becomes smaller, as indicated by the shrinking color range above the $R_u = 1$ line. As β approaches 1, the system becomes linear and the unilateral ratio approaches zero for all forcing frequencies. As expected, all the curves converge to $(\beta, R_u) = (1, 0)$. Fig. 4.7(b) shows a similar behavior for a hardening bilinear spring $(\beta > 1)$. As the bilinear ratio (degree of nonlinearity) increases, there is an increasingly larger range of forcing frequencies over which unilateral transmission occurs.

4.3.4. Nonreciprocal Unilateral Transmission

We obtained near-resonance unilateral transmission in the system with broken mirror symmetry; Section 4.3.2. Because the system is nonlinear and asymmetric, it is therefore possible to find parameters that lead to nonreciprocal response. This property holds even though the response of the system is independent of the forcing amplitude in the parameter range that we consider in this work. Here, we investigate the possibility of nonreciprocal unilateral transmission of vibrations for the 2DoF system.

Fig. 4.8(a) shows the reciprocity bias, R, for the system with $(\mu, r) = (1, 0.25)$. As expected, the system exhibits nonreciprocal response. Figures 4.8(b) to (d) show the time-domain response of the system at the local maxima of R, indicated by a star, circle and diamond respectively. In both panels (b) and (c), the response of the forward configuration is primarily harmonic while that of the backward configuration has significant contributions form the

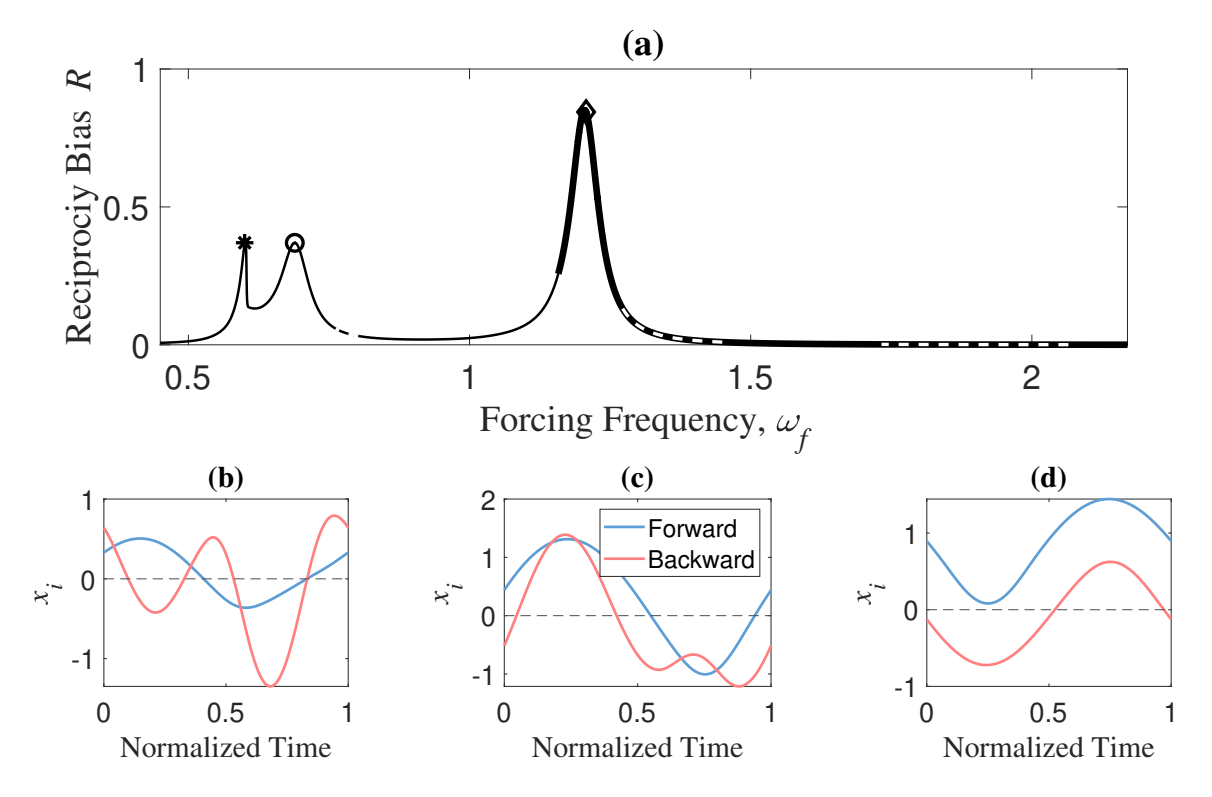


Figure 4.8: (a) Reciprocity bias for the system with r = 0.25 and $\mu = 1$. Thick lines indicate response that exhibits unilateral transmission and dashed lines indicate unstable response in either the forward or backward configuration. (b) to (d) show the time-domain output displacement at the points indicated by the star, circle and diamond markers, respectively.

second harmonic. Thus, we observe harmonic generation only in one direction. At the global maximum of the reciprocity bias, panel (c), we observe unilateral nonreciprocal transmission. This corresponds to the second primary resonance of the system where the masses move out of phase, thereby engaging the bilinear spring significantly.

Figures 4.9(a) and (b) show the DC and AC components of the output displacement, respectively. The DC component is responsible for enabling unilateral transmission. At the diamond marker in Fig. 4.9(a,b), there is a significant difference between the DC values in the forward and backward configurations, while the AC values are similar for the two configurations. Figures 4.9(c) shows the variation of the unilateral ratio, R_u , over the same interval of the forcing frequency. As expected, the onset of unilateral transmission in the forward configuration is accompanied by the increase in the DC value of the output displacement.

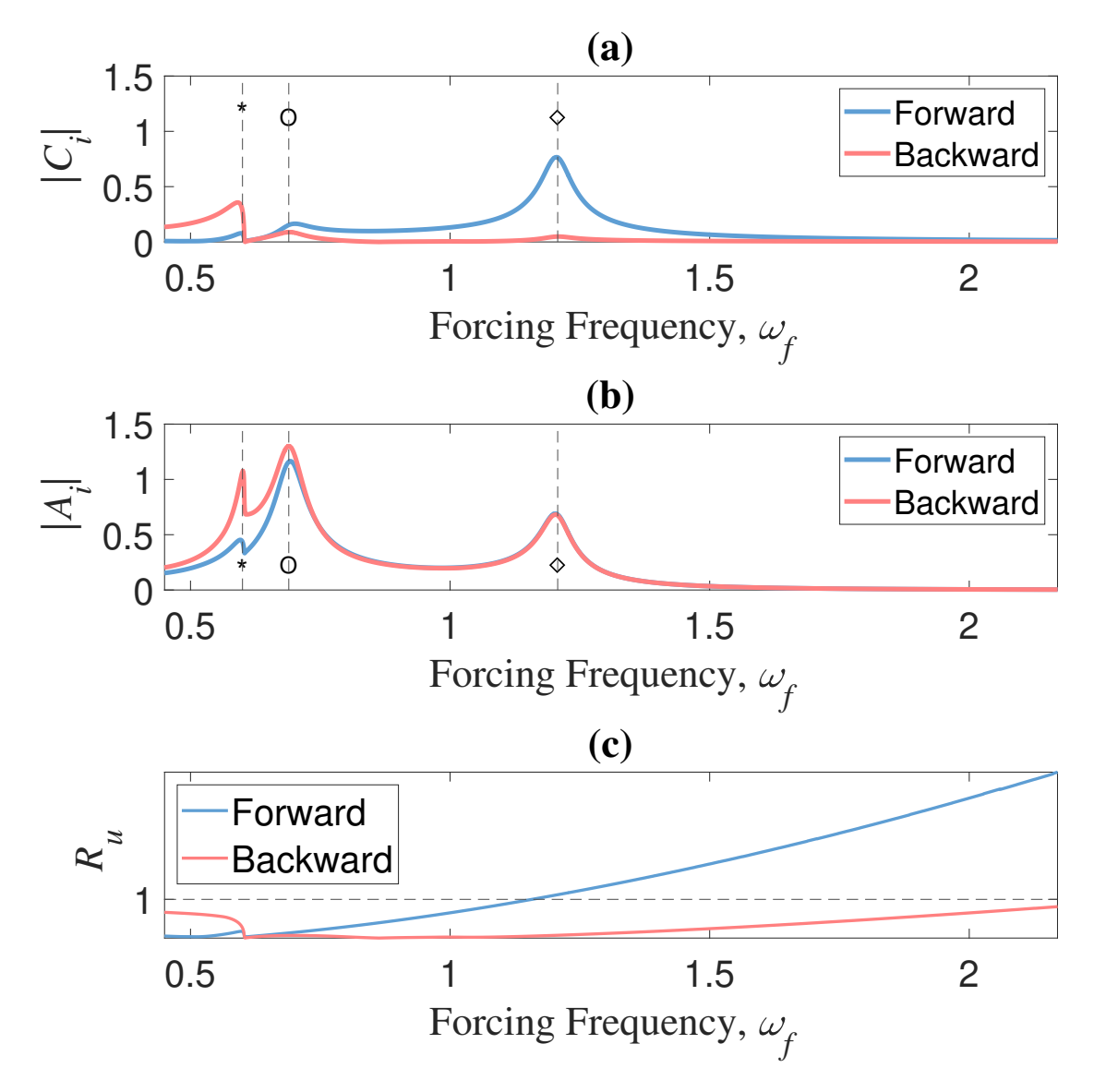


Figure 4.9: (a) DC value of the response for the system with r=0.25 and $\mu=1$ (b) AC value of the response (c) Unilateral ratio for the forward and backward configurations

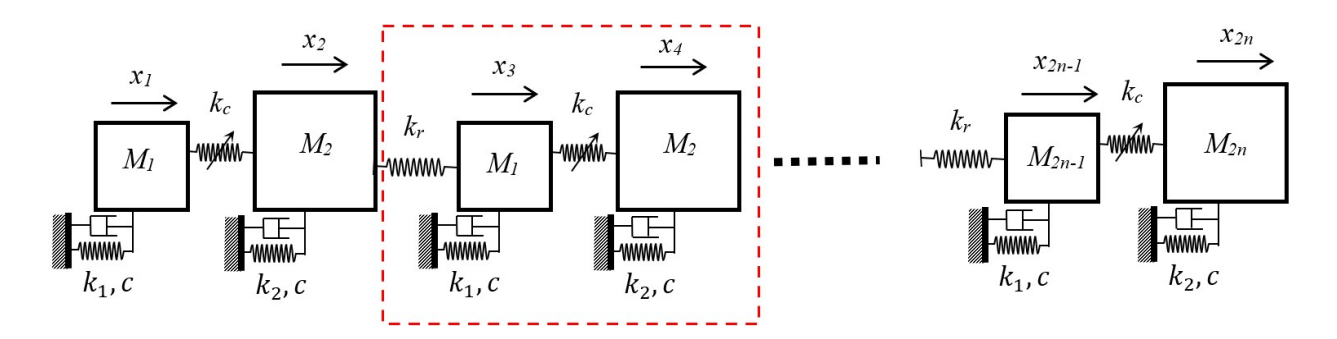


Figure 4.10: Periodic structure with a bilinearly coupled unit cell

4.4. Periodic Structure with Bilinearly Coupled Units

Fig. 4.10 shows a periodic lattice composed of n unit cells. The unit cells are the same as the 2DoF system in Fig. 4.1, with adjacent units coupled to each other with a linear spring of non-dimensional stiffness k_r . In Section 4.2, we found sets of system parameters that lead to stable unilateral transmission within a unit cell near a peak frequency. Building on this design, we investigate unilateral vibration transmission in the end-to-end steady-state response of the periodic structure in Fig. 4.10 to external harmonic excitation. In particular, we highlight the influence of two key parameters of the periodic system on its vibration transmission characteristics: the number of units and energy dissipation.

For the results presented in this section, each unit cell featured an asymmetry in the mass ratio only, $(\mu, r) = (3, 1)$, and a softening bilinear ratio of $\beta = 0.1$. This is similar to the case studied in Sec. 4.3.2, Fig. 4.6. The non-dimensional constant of the spring connecting adjacent unit cells is $k_r = 5$, resulting in well separated band of resonances in the finite periodic structure.

4.4.1. Influence of the number of units

We investigate unilateral transmission in lattices of 2, 4, 8, and 16 unit cells. Extension of the results to infinitely long systems requires a different methodology and lies beyond the scope of the present work.

Fig. 4.11(a) and (b) illustrate the response of the periodic structure with two unit cells (n = 2, 4DoF in total) for the forward and backward configurations, respectively. As in previous sections, unilateral response is indicated in the frequency response function by thicker lines. Four distinct frequency peaks are identified by vertical lines, and their corresponding time response for the forward and backward configurations are shown in Fig. 4.11(c)-(f).

Near the second resonant peak ($\omega_f = 0.82$), the system undergoes a PD bifurcation in both

forward and backward configurations, as seen in Fig. 4.11 (c). The corresponding branches of period-doubled solutions are shown in the insets in panels (a) and (b). At the two subsequent peaks, shown in panels (d) and (e), the system exhibits nonreciprocal unilateral transmission: the response is unilateral only in the forward configuration. At $\omega_f = 1.41$, panel (e), the backward configuration has undergone a torus bifurcation, resulting in the quasi-periodic response. At $\omega_f = 2.82$, panel (f), the response of the system is nonreciprocal but unilateral for both forward and backward configurations.

We note that the system exhibits several other bifurcations. The bifurcation structures in the forward and backward configurations are different from each other, as indicated by the markers in Fig. 4.11(a)-(b). As a case in point, there is a pair of period-doubling bifurcations occurring near $\omega_f \approx 1.65$. The branch of the period-doubled solution is shown for the backward configuration in panel Fig. 4.11(b), which undergoes secondary bifurcations. We have found period-doubling bifurcations to generally increase the amplitude of motion especially when they occur away from a primary resonance.

Figures 4.12(a)-(c) display the response of the periodic structure for n = 4, n = 8, and n = 16, respectively. The insets highlight the frequency response curves for the in-phase modes (acoustic band). All systems undergo period-doubling bifurcations near $\omega_f \approx 0.82$. As an example, the inset in Fig. 4.12(a) shows the ensuing branch of period-double solutions for the system with n = 4. The periodic-doubled solutions are not reciprocal (time-domain response not shown).

The peak near $\omega_f \approx 2.82$ corresponds to the out-of-phase modes (optical band). The *n* modes appear as one damped peak because of the modal overlap caused by damping; see [121] for a similar situation. As expected, the response amplitude at the output decreases with increasing the number of unit cells because of damping. This is more pronounced in the optical band because adjacent masses move out of phase with each other in this frequency range.

For n = 4, shown in Fig.4.12(a), the system exhibits unilateral transmission at $\omega_f = 1.22$, $\omega_f = 1.41$ and $\omega_f = 2.82$. The system with n = 2 exhibited a similar behavior (Fig.4.11(a) and (b)). The first two (lower) frequencies correspond to nonreciprocal unilateral transmission, where the response is unilateral in the forward configuration, while the third (higher) frequency exhibits unilateral transmission in both the forward and backward configurations.

For n = 8, Fig. 4.12(b), the backward configuration no longer exhibits unilateral transmission at any of the three forcing frequencies in Fig. 4.12(a). However, the response of the forward configuration remains unilateral at these frequencies. We observe that the response of the

system is unilateral over a shorter range of frequencies as a result of increasing the number of units.

Fig. 4.12(c) shows the response of the system with n = 16, where unilateral transmission no longer occurs near any of the peaks. This is attributed to the increased energy dissipation in the longer periodic structure.

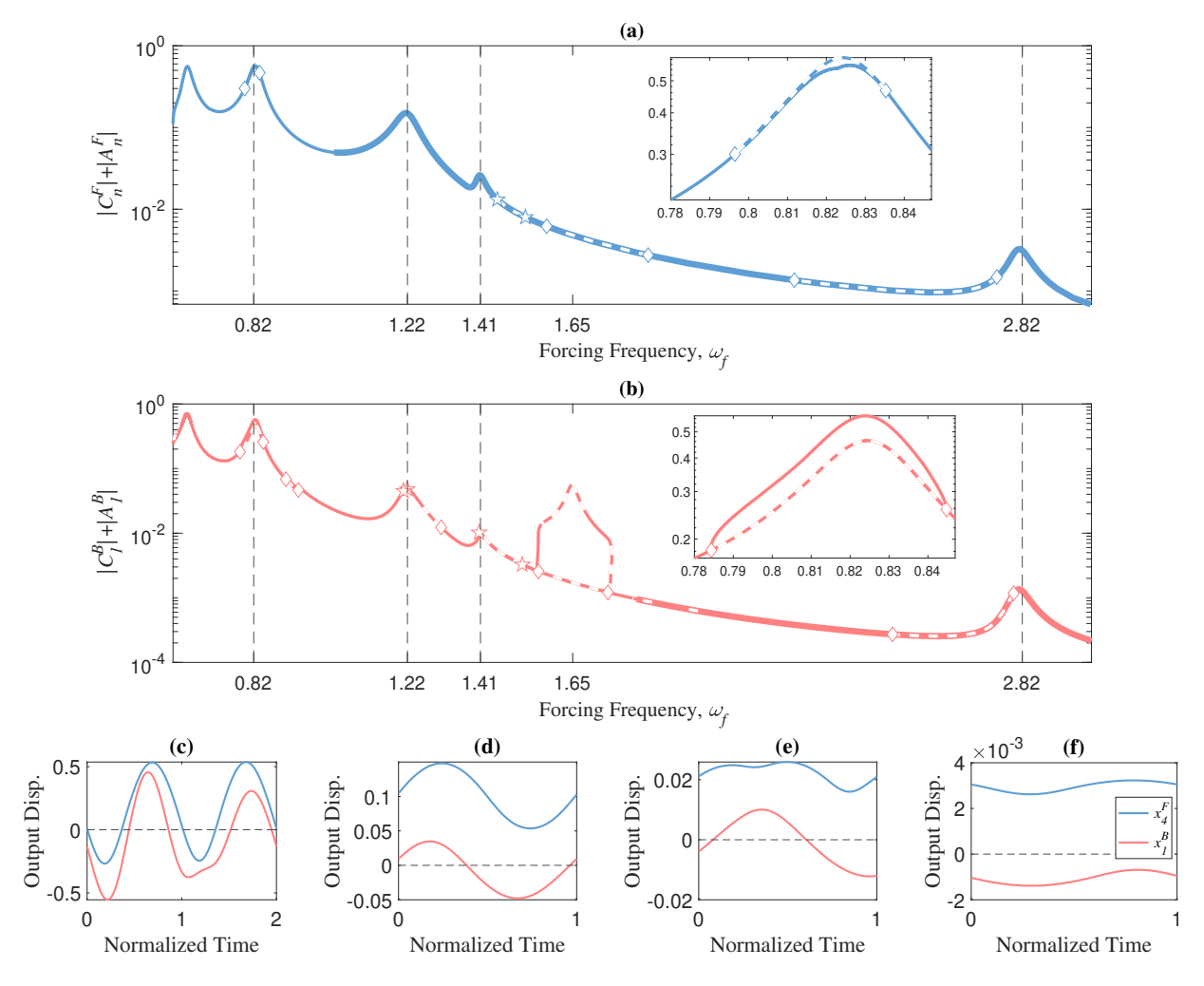


Figure 4.11: Frequency response of the system for n=2, $\mu=3$ and r=1 for (a) forward configuration and (b) backward configuration. Diamonds and pentagrams denote period-doubling and torus bifurcations, respectively. Time-domain response of the system for the forward and backward configurations at (c) $\omega_f=0.82$ (d) $\omega_f=1.22$, (e) $\omega_f=1.41$ and (f) $\omega_f=2.82$ indicated by vertical lines. In panel (e), $x_1^B(t)$ is computed using direct numerical integration.

4.4.2. Influence of damping

As the number of unit cells increases, vibrations are increasingly more suppressed as they propagate through the structure. Therefore, the output displacement in periodic structures with a large number of unit cells is significantly damped. This energy dissipation decreases the influence of nonlinearity, which is required for unilateral transmission to occur. Fig. 4.12(c) shows that the system with n=16 no longer exhibits unilateral transmission near peak frequencies.

To further clarify the role of damping in suppressing unilateral transmission, Fig. 4.13(a) shows the response of the system with n=16 at a lower damping ratio of $\zeta=0.01$; cf. Fig. 4.12(c). Unilateral transmission is restored in the system with lower damping at both peaks. At $\omega_f=1.41$, panel (b), only the forward configuration exhibits unilateral transmission, while at $\omega_f=2.82$, panel (c), the response is unilateral for both configurations. The response of the backward configuration is quasiperiodic at $\omega_f=1.41$. We note that the amplitude of the output displacements remains very small; vibrations are transmitted through 32 damped units to reach the last unit, in this case.

Another feature of the response of the long structure with low damping is instability of the response, specifically near the primary in-phase resonances (acoustic band); see the inset in Fig. 4.13. Period-doubling bifurcations appear to be the main mechanism for loss of stability in the acoustic band, while the instability at $\omega_f = 1.41$ is caused by a torus bifurcation. Investigating the detailed structure of these secondary bifurcations falls beyond the scope of the present work and warrants a separate analysis.

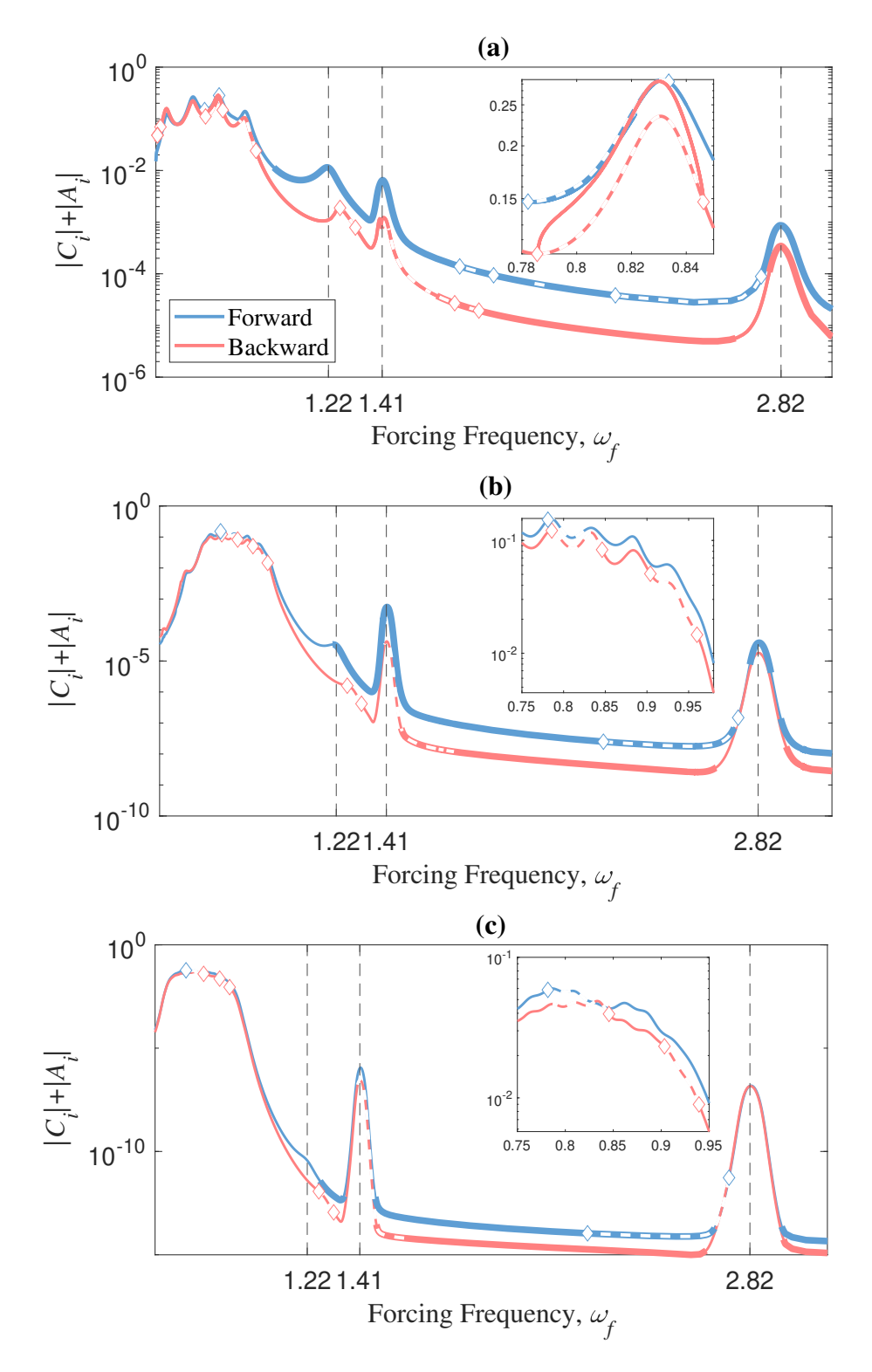


Figure 4.12: Frequency response curves of the forward and backward configurations for $\mu = 3$, r = 1, and $\zeta = 0.03$ for (a) n = 4, (b) n = 8, and (c) n = 16. Diamond markers denote period-doubling bifurcations. Subscript i in $|C_i| + |A_i|$ refers to either n or 1, corresponding to the forward and backward configurations, respectively.

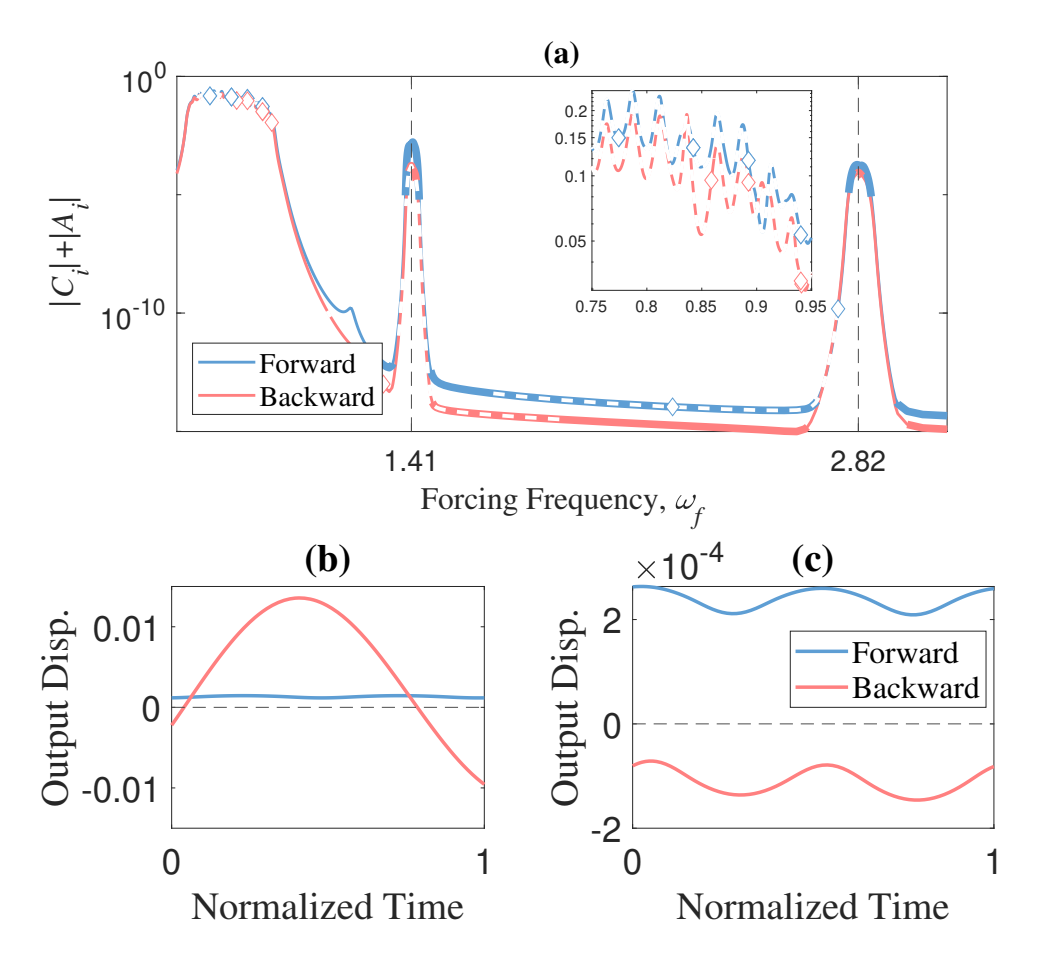


Figure 4.13: (a) Frequency response curves of the forward and backward configurations for n = 16, $\mu = 3$, r = 1, and $\zeta = 0.01$. Time-domain response of the system for the forward and backward configurations at (b) $\omega_f = 1.41$ and (c) $\omega_f = 2.82$. In panel (b), $x_1^B(t)$ is computed using direct numerical integration.

4.5. Conclusions

We investigated the phenomenon of unilateral transmission, where incoming harmonic waves attain a single sign (pure tension or compression) upon transmission through the system. We demonstrated this behavior in a system with bilinear elasticity, exhibiting different effective stiffness in compression and tension. We analyzed the steady-state response of a two-degree-of-freedom (2DoF) system with bilinear elasticity subject to external harmonic excitation using numerical continuation. We found that unilateral transmission can occur in a system with mirror symmetry (identical oscillators, coupled bilinearly), but this occurred away from resonant frequencies.

We demonstrated that breaking the mirror symmetry of the system allows unilateral transmission to occur near the resonances of the system. Specifically, both the stiffness ratio and the mass ratio of the system can be adjusted to enable near-resonance unilateral transmission. The introduction of asymmetry also resulted in nonreciprocal dynamics, which we explored in the context of unilateral transmission. We reported on response regimes that lead to nonreciprocal unilateral transmission: when unilateral transmission occurs in one direction but not the other. We also found nonreciprocal dynamics that is characterized by harmonic generation only in one direction.

Building on these findings, we extended our analysis to vibration transmission in a periodic structure that has the bilinear 2DoF system as its unit cell. We investigated the influence of the number of unit cells and energy dissipation on unilateral transmission. We demonstrated that stable nonreciprocal unilateral transmission can occur near the primary and internal resonances of the system, including a regime in which both the forward and backward configurations exhibit unilateral transmission (one in pure compression, the other in pure tension). We showed that as the number of unit cells increases from 2 to 16, energy dissipation can suppress unilateral transmission.

We hope that these findings on unilateral transmission open new avenues in the operation of vibration systems, providing insights for the design and optimization of such systems in engineering applications and devices.

Appendices

4A. Non-dimensional Equations of Motion

The governing equations for the system in Fig. 4.1 can be written as:

$$M_1 \bar{x}_1'' + k_c (\bar{x}_1 - \bar{x}_2) + k_1 \bar{x}_1 + c \bar{x}_1' = f_1 \cos \bar{\omega}_f t$$

$$M_2 \bar{x}_2'' + k_c (\bar{x}_2 - \bar{x}_1) + k_2 \bar{x}_2 + c \bar{x}_2' = f_2 \cos \bar{\omega}_f t$$
(4A.1)

where k_c is the coupling bilinear stiffness, k_1 and k_2 linear grounding stiffness for M_1 and M_2 , and c is the linear viscous damping connecting each mass to the ground. We divide the equations by k_1 and introduce the non-dimensional parameters $\tau = \omega_0 t$, $\omega_0^2 = k_1/M_1$, $\omega_f = \bar{\omega}_f/\omega_0$ to obtain

$$\frac{M_1 \omega_0^2}{k_1} \ddot{\bar{x}}_1 + \frac{k_c}{k_1} (\bar{x}_1 - \bar{x}_2) + \bar{x}_1 + 2\zeta \dot{\bar{x}}_1 = \frac{f_1}{k_1} \cos \omega_f \tau,
\frac{M_2 \omega_0^2}{k_1} \ddot{\bar{x}}_2 + \frac{k_c}{k_1} (\bar{x}_2 - \bar{x}_1) + \frac{k_2}{k_1} \bar{x}_2 + 2\zeta \dot{\bar{x}}_2 = \frac{f_2}{k_1} \cos \omega_f \tau.$$
(4A.2)

where $\dot{x} = dx/d\tau = (dx/dt)/\omega_0$, $\ddot{x} = d^2x/d\tau^2 = (d^2x/dt^2)/\omega_0^2$ and $\zeta = (c\omega_0)/(2k_1)$. We define the non-dimensional displacement and force as $x = \bar{x}/d$ and $F = f/(dk_1)$, where d is a characteristic displacement of the system. This results in

$$\ddot{x}_1 + K_c(x_1 - x_2) + x_1 + 2\zeta \dot{x}_1 = F_1 \cos \omega_f \tau$$

$$\mu \ddot{x}_2 + K_c(x_2 - x_1) + rx_2 + 2\zeta \dot{x}_2 = F_2 \cos \omega_f \tau$$
(4A.3)

where $\mu = M_2/M_1$, $K_c = k_c/k_1$, and $r = k_2/k_1$. Eq. (4A.3) is the non-dimensional form of Eq. (4A.1). Eq. (4A.3) is the same as Eq. (4.1) in the main text, where we have replaced τ with t for ease of reference.

4B. Amplitude independency of bilinear systems without offset

In bilinear stiffness systems without an offset, the transfer function remains unaffected by amplitude variations, preserving a linear relationship with the input. Fig. 4B.1 illustrates this observation by presenting the transfer function of the symmetric system under two distinct forcing amplitudes.

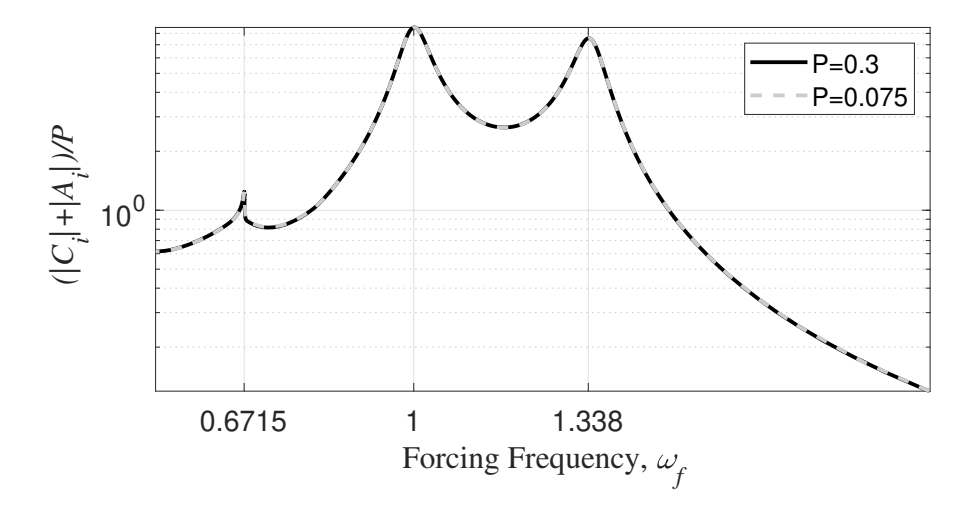


Figure 4B.1: Frequency response function of the symmetric 2DoF system for $r=\mu=1$, $\zeta=0.03,$ and $\beta=0.1,$ at two forcing amplitudes.

Chapter 5

Conclusions and Recommendations

5.1. Conclusions

This dissertation investigated three mechanisms of nonlinear nonreciprocal vibration transmission in periodic structures utilizing coupled oscillators as their unit cells. By systematically analyzing the roles of nonlinearity and asymmetry, we identified and characterized different regimes of nonreciprocal behavior: phase nonreciprocity, phase-preserved nonreciprocity, and nonreciprocal unilateral transmission. The findings provide new possibilities for the design and control of nonreciprocal wave propagation in mechanical systems.

We investigated nonreciprocal vibration transmission in a nonlinear periodic waveguide, where nonlinearity was introduced through cubic ground stiffness and asymmetry was incorporated via mass and stiffness ratios within the unit cells. We focused on the weakly nonlinear steady-state response under harmonic excitation, specifically in the frequency-preserving regime. Our analysis revealed scenarios where the system exhibits a nonreciprocal phase shift (phase nonreciprocity) without an accompanying difference in the transmitted energy. We conducted a parametric study on the influence of the forcing amplitude, damping, and asymmetry on the nonreciprocasl phase shift. We further demonstrated that reciprocity can be restored at specific parameter combinations despite the presence of asymmetry. This result highlights that breaking the mirror symmetry is a necessary but not sufficient condition for enabling nonreciprocal dynamics. These findings emphasize the critical role of asymmetry as a tunable design parameter, particularly in practical systems where perfect symmetry is often unattainable due to manufacturing imperfections or so-called mistuning.

In a system of coupled nonlinear oscillators, we identified phase-preserved nonreciprocity, a regime in which the transmitted amplitudes change upon interchanging the locations of the source and receiver, but the transmitted phases remain unchanged. These results highlight the overlooked role of phase in breaking reciprocity, as well as the interplay between nonlinearity, asymmetry, and phase effects in vibration transmission.

We investigated unilateral transmission, a phenomenon in which the transmitted waves remain exclusively in tension or compression. This effect was analyzed in a system with bilinear elasticity, where the effective stiffness is different in compression and tension. We examined the steady-state response of a bilinear system with two degrees of freedom (2DoF) in response to an external harmonic excitation. We found that unilateral transmission can occur in a

system with mirror symmetry, but only away from primary resonances. However, breaking the mirror symmetry in either elastic or inertial properties allows unilateral transmission to emerge near the resonances. Furthermore, asymmetry facilitates nonreciprocal unilateral transmission, where unilateral transmission occurs in only one direction. Additionally, we identified nonreciprocal regimes characterized by harmonic generation occurring in only one propagation direction.

Building on these findings, we investigated a bilinear periodic structures composed of the bilinear 2DoF system as it unit cell. We explored how the number of unit cells and energy dissipation influence unilateral transmission. We showed that stable nonreciprocal unilateral transmission can occur near both primary and internal resonances. We identified a regime in which both forward and backward waves exhibit unilateral transmission, with one transmission direction resulting in pure compression and the other direction in pure tension. We found that as the number of unit cells increases, energy dissipation can suppress unilateral transmission, underscoring the role of dissipation in practical implementations.

In summary, this dissertation presented a detailed study of nonreciprocity in nonlinear vibration systems, demonstrating how nonlinearity, asymmetry, and phase effects contribute to different forms of nonreciprocal behavior. These findings offer insights for the design and optimization of mechanical waveguides, coupled oscillators, and bilinear structures, with potential applications in vibration isolation, energy harvesting, and wave-based signal processing. We hope that this work will inspire further research into the control and exploitation of nonlinear nonreciprocity in engineering systems.

5.2. Future work

Throughout this study, the investigated phenomena were evaluated in structures subjected to harmonic excitation, with phase defined as the lag or lead of the response relative to the excitation. These findings cannot be easily generalized to the response of nonlinear systems under different types of loading because superposition does not hold in nonlinear systems. Future research could explore phase effects and unilateral transmission in response to other types of excitation such as impulse or step input, or more general periodic but non-sinusoidal excitations such as sawtooth or square waves. In this context, nonlinear modal analysis could provide a valuable framework, as it describes the system's intrinsic dynamics independent of the specific form of external forcing.

In Chapters 2 and 3 of this work, the phase of the response was defined based on the first harmonic, as it was observed to be the dominant component of the periodic response across the studied parameter ranges. While the full multiharmonic response was computed

in Chapter 3, the analysis centered on the first harmonic because it captures the primary contribution to the system's steady-state dynamics.

That said, future investigations could explore harmonic-by-harmonic assessments of nonreciprocity, offering a more detailed characterization of how nonreciprocal behavior may differ across higher-order frequency components. This would be particularly relevant in systems or parameter regimes where higher harmonics carry significant energy or where selective control of specific harmonics is of practical interest.

While this thesis has primarily employed numerical continuation methods to investigate the steady-state dynamics of nonlinear periodic systems, future research could benefit from the integration of classical analytical or semi-analytical techniques. Specifically, the application of perturbation methods such as the Method of Multiple Scales or the Lindstedt-Poincaré technique [111] could provide closed-form approximations that enhance physical understanding of key phenomena, including frequency shifts, bifurcation structures, and phase changes observed in the system responses.

Unilateral transmission was examined in systems that have a bilinear stiffness without an offset. The response of these systems, contrary to typical nonlinear systems, does not depend on the amplitude of motion. Introducing an offset to the bilinear coupling adds an amplitude-dependent transition regime, which warrants further investigation.

We examined the influence of the size of the periodic structure (the number of unit cells) on their nonreciprocal vibration transmission characteristics. The focus on finite systems was motivated by the fact that they better represent experiments on mechanical systems than a system with infinitely many unit cells. Exploring the limit of infinitely long systems is of theoretical value and is best done using a different methodology than the one used in this thesis.

Extending the analysis to two-dimensional structures (periodicity occurring in two dimensions) could uncover complex nonreciprocal phenomena not observable in one-dimensional systems, such as directionality of the transmission characteristics [144].

This work was conducted exclusively using computational methods. Conducting experimental studies to validate the observed nonreciprocal behaviors will be invaluable. This could involve designing physical prototypes of nonlinear periodic waveguides and coupled oscillator systems to observe nonreciprocal phase shifts and unilateral transmission under controlled conditions.

Considering the role of nonlinear damping mechanisms on nonreciprocal behavior could

provide a more comprehensive understanding of energy dissipation in these systems and its impact on performance. This is particularly relevant because the damping mechanism in periodic systems manufactured using additive manufacturing may not be adequately modeled using linear viscous dampers [145]. Also, the current model applies damping locally at each unit, causing the total damping to scale with the number of cells. Future work could explore alternative formulations where damping is normalized with system size, allowing the study of nonreciprocal behavior in large periodic structures without artificial scaling effects due to distributed damping.

The design and optimization of devices such as vibration isolators, energy harvesters, or mechanical diodes that leverage nonreciprocal properties could bridge the gap between theoretical research and practical applications.

References

- 1. Von Helmholtz, H. Theorie der Luftschwingungen in Röhren mit offenen Enden. Journal für die reine und angewandte Mathematik (1860).
- 2. Strutt, J. W. Some general theorems relating to vibrations. *Proceedings of the London Mathematical Society* 1, 357–368 (1871).
- 3. Achenbach, J. D. Reciprocity in Elastodynamics (Cambridge University Press, 2003).
- 4. Fahy, F. J. Some applications of the reciprocity principle in experimental vibroacoustics. *Acoustical Physics* **49**, 217–229 (2003).
- 5. Ten Wolde, T. Reciprocity measurements in acoustical and mechano-acoustical systems. Review of theory and applications. *Acta Acustica united with Acustica* **96**, 1–13 (2010).
- 6. Ewins, D. J. Modal testing: Theory, practice and application (John Wiley & Sons, 2009).
- 7. Van der Seijs, M. V., De Klerk, D. & Rixen, D. J. General framework for transfer path analysis: History, theory and classification of techniques. *Mechanical Systems and Signal Processing* **68**, 217–244 (2016).
- 8. Auld, B. A. General electromechanical reciprocity relations applied to the calculation of elastic wave scattering coefficients. *Wave Motion* 1, 3–10 (1979).
- 9. Anderson, M. J. & Liu, X. Use of reciprocity to characterize ultrasonic transducers in air above 100 kHz. *The Journal of the Acoustical Society of America* **103**, 446–453 (1998).
- 10. Knopoff, L. & Gangi, A. F. Seismic reciprocity. Geophysics 24, 681–691 (1959).
- 11. Liang, B., Yuan, B. & Cheng, J.-c. Acoustic Diode: Rectification of Acoustic Energy Flux in One-Dimensional Systems. *Physical Review Letters* **103**, 104301 (2009).
- 12. Darabi, A. et al. Broadband passive nonlinear acoustic diode. Physical Review B 99, 214305 (2019).
- 13. Cummer, S. A. Selecting the Direction of Sound Transmission. *Science* **343**, 495–496 (2014).
- Wang, C., Tawfick, S. & Vakakis, A. F. Irreversible energy transfer, localization and non-reciprocity in weakly coupled, nonlinear lattices with asymmetry. *Physica D: Non-linear Phenomena* 402, 132229 (2020).

- 15. Lu, L., Joannopoulos, J. D. & Soljačić, M. Topological photonics. *Nature Photonics* **8**, 821–829 (2014).
- 16. Zangeneh-Nejad, F. & Fleury, R. Doppler-Based Acoustic Gyrator. *Applied Sciences* 8 (2018).
- 17. Nassar, H. et al. Nonreciprocity in acoustic and elastic materials. Nature Reviews Materials 5, 667–685 (2020).
- 18. Hamoir, G., De La Torre Medina, J., Piraux, L. & Huynen, I. Self-Biased Nonreciprocal Microstrip Phase Shifter on Magnetic Nanowired Substrate Suitable for Gyrator Applications. *IEEE Transactions on Microwave Theory and Techniques* **60**, 2152–2157 (2012).
- 19. Palomba, M., Palombini, D., Colangeli, S., Ciccognani, W. & Limiti, E. Broadband Nonreciprocal Phase Shifter Design Technique. *IEEE Transactions on Microwave The*ory and Techniques **66**, 1964–1972 (2018).
- 20. Fleury, R., Sounas, D. L., Sieck, C. F., Haberman, M. R. & Alù, A. Sound isolation and giant linear nonreciprocity in a compact acoustic circulator. *Science* **343**, 516–519 (2014).
- 21. Trainiti, G. & Ruzzene, M. Non-reciprocal elastic wave propagation in spatiotemporal periodic structures. *New Journal of Physics* **18**, 083047 (2016).
- 22. Nassar, H., Chen, H., Norris, A. N., Haberman, M. R. & Huang, G. L. Non-reciprocal wave propagation in modulated elastic metamaterials. *Proceedings of the Royal Society A: Mathematical, Physical and Engineering Sciences* **473**, 20170188 (2017).
- 23. Nassar, H., Chen, H., Norris, A. N. & Huang, G. L. Non-reciprocal flexural wave propagation in a modulated metabeam. *Extreme Mechanics Letters* **15**, 97–102 (2017).
- 24. Wang, Y. et al. Observation of Nonreciprocal Wave Propagation in a Dynamic Phononic Lattice. Physical Review Letters 121, 194301 (2018).
- 25. Wallen, S. P. et al. Static and dynamic non-reciprocity in bi-linear structures in Proceedings of Meetings on Acoustics 34 (2018).
- 26. Grinberg, I., Vakakis, A. F. & Gendelman, O. V. Acoustic diode: Wave non-reciprocity in nonlinearly coupled waveguides. *Wave Motion* 83, 49–66. (2025) (2018).
- 27. Lu, Z. & Norris, A. N. Non-Reciprocal Wave Transmission in a Bilinear Spring-Mass System. *Journal of Vibration and Acoustics* **142** (2019).
- 28. Lu, Z. & Norris, A. N. Unilateral and nonreciprocal transmission through bilinear spring systems. *Extreme Mechanics Letters* **42**, 101087 (2021).

- 29. Nassar, H., Xu, X. C., Norris, A. N. & Huang, G. L. Modulated phononic crystals: Non-reciprocal wave propagation and Willis materials. *Journal of the Mechanics and Physics of Solids* **101**, 10–29 (2017).
- 30. Dickie, J. & Broughton, P. Geometric nonlinearity. *Journal of Structural Mechanics* 1, 249–266 (1972).
- 31. Ghuku, S. & Saha, K. N. A review on stress and deformation analysis of curved beams under large deflection. *International Journal of Engineering and Technologies* **11**, 13–39 (2017).
- 32. Mihai, L. A. & Goriely, A. How to characterize a nonlinear elastic material? A review on nonlinear constitutive parameters in isotropic finite elasticity. *Proceedings of the Royal Society A: Mathematical, Physical and Engineering Sciences* **473**, 20170607 (2017).
- 33. Goriely, A., Vandiver, R. & Destrade, M. Nonlinear euler buckling. *Proceedings of the royal society A: mathematical, physical and engineering sciences* **464,** 3003–3019 (2008).
- 34. Ma, Q. et al. A nonlinear mechanics model of bio-inspired hierarchical lattice materials consisting of horseshoe microstructures. *Journal of the Mechanics and Physics of Solids* **90**, 179–202 (2016).
- 35. Wriggers, P. & Laursen, T. A. Computational contact mechanics (Springer, 2006).
- 36. Byrtus, M. & Zeman, V. On modeling and vibration of gear drives influenced by nonlinear couplings. *Mechanism and Machine theory* **46**, 375–397 (2011).
- 37. Gaul, L. & Nitsche, R. The Role of Friction in Mechanical Joints. *Applied Mechanics Reviews* **54**, 93–106 (2001).
- 38. Lepri, S. & Casati, G. Asymmetric wave propagation in nonlinear systems. *Physical Review Letters* **106**, 164101 (2011).
- 39. Cui, J.-G., Yang, T. & Chen, L.-Q. Frequency-preserved non-reciprocal acoustic propagation in a granular chain. *Applied Physics Letters* **112**, 181904 (2018).
- 40. Nadkarni, N., Arrieta, A. F., Chong, C., Kochmann, D. M. & Daraio, C. Unidirectional transition waves in bistable lattices. *Physical review letters* **116**, 244501 (2016).
- 41. Boechler, N., Theocharis, G. & Daraio, C. Bifurcation-based acoustic switching and rectification. *Nature Materials* **10**, 665–668 (2011).
- 42. Wallen, S. P. *et al.* Static and dynamic non-reciprocity in bi-linear structures. *Proceedings of Meetings on Acoustics* **34**, 065002 (2018).

- 43. Lu, Z. & Norris, A. N. Non-Reciprocal Wave Transmission in a Bilinear Spring-Mass System. *Journal of Vibration and Acoustics* **142**, 021006 (2020).
- 44. Bernardo, M., Budd, C., Champneys, A. R. & Kowalczyk, P. *Piecewise-smooth dynamical systems: theory and applications* (Springer Science & Business Media, 2008).
- 45. Shaw, S. & Holmes, P. A periodically forced piecewise linear oscillator. *Journal of Sound and Vibration* **90**, 129–155 (1983).
- 46. Iwan, W. D. The Steady-State Response of a Two-Degree-of-Freedom Bilinear Hysteretic System. *Journal of Applied Mechanics* **32**, 151–156 (1965).
- 47. Thompson, J. M. T., Bokaian, A. R. & Ghaffari, R. Subharmonic Resonances and Chaotic Motions of a Bilinear Oscillator. *IMA Journal of Applied Mathematics* **31**, 207–234 (1983).
- 48. Wong, C., Zhang, W. & Lau, S. Periodic forced vibration of unsymmetrical piecewise-linear systems by incremental harmonic balance method. *Journal of Sound and Vibration* **149**, 91–105 (1991).
- 49. Ahmed, A. K. W. & Rakheja, S. An equivalent linearization technique for the frequency response analysis of asymmetric dampers. *Journal of Sound and Vibration* **153**, 537–542 (1992).
- 50. Narimani, A., Golnaraghi, M. E. & Jazar, G. N. Frequency response of a piecewise linear vibration isolator. *Journal of Vibration and control* **10**, 1775–1794 (2004).
- 51. Jiang, H., Chong, A. S., Ueda, Y. & Wiercigroch, M. Grazing-induced bifurcations in impact oscillators with elastic and rigid constraints. *International Journal of Mechanical Sciences* **127**, 204–214 (2017).
- 52. Shi, B., Yang, J. & Rudd, C. On vibration transmission in oscillating systems incorporating bilinear stiffness and damping elements. *International Journal of Mechanical Sciences* **150**, 458–470 (2019).
- 53. Fontanela, F. et al. Nonlinear vibration localisation in a symmetric system of two coupled beams. Nonlinear Dynamics 103, 3417–3428 (2021).
- 54. Yastrebov, V. A. Wave propagation through an elastically asymmetric architected material. *Comptes Rendus. Mécanique* **350**, 1–26 (2022).
- 55. Scalerandi, M., Agostini, V., Delsanto, P. P., Van Den Abeele, K. & Johnson, P. A. Local interaction simulation approach to modelling nonclassical, nonlinear elastic behavior in solids. *The Journal of the Acoustical Society of America* **113**, 3049–3059 (2003).

- 56. Chance, J., Tomlinson, G. R. & Worden, K. A simplified approach to the numerical and experimental modelling of the dynamics of a cracked beam in Proceedings-SPIE the International Society for Optical Engineering (1994).
- 57. Liu, Y., Páez Chávez, J., Pavlovskaia, E. & Wiercigroch, M. Analysis and control of the dynamical response of a higher order drifting oscillator. *Proceedings of the Royal Society A: Mathematical, Physical and Engineering Sciences* **474**, 20170500 (2018).
- 58. Saito, A., Epureanu, B. I., Castanier, M. P. & Pierre, C. Node Sampling for Nonlinear Vibration Analysis of Structures with Intermittent Contact. *AIAA Journal* **48**, 1903–1915 (2010).
- 59. Zucca, S. & Epureanu, B. I. Bi-linear reduced-order models of structures with friction intermittent contacts. *Nonlinear Dynamics* 77, 1055–1067 (2014).
- 60. Benveniste, Y. One-dimensional wave propagation in materials with different moduli in tension and compression. *International Journal of Engineering Science* **18**, 815–827 (1980).
- 61. Maslov, V. P. & Mosolov, P. P. General theory of the solutions of the equations of motion of an elastic medium of different moduli. *Journal of Applied Mathematics and Mechanics* **49**, 322–336 (1985).
- 62. Ostrovsky, L. A. Wave processes in media with strong acoustic nonlinearity. *The Journal of the Acoustical Society of America* **90**, 3332–3337 (1991).
- 63. Abeyaratne, R. & Knowles, J. K. Wave propagation in linear, bilinear and trilinear elastic bars. *Wave Motion* **15**, 77–92 (1992).
- 64. Gavrilov, S. N. & Herman, G. C. Wave propagation in a semi-infinite heteromodular elastic bar subjected to a harmonic loading. *Journal of Sound and Vibration* **331**, 4464–4480 (2012).
- 65. Nazarov, V. E., Radostin, A. V. & Kiyashko, S. B. Self-Similar Acoustic Waves in Homogeneous Media with Different-Modulus Nonlinearity and Relaxation. *Radiophysics and Quantum Electronics* **58**, 124–131 (2015).
- 66. Rudenko, O. V. Equation admitting linearization and describing waves in dissipative media with modular, quadratic, and quadratically cubic nonlinearities. *Doklady Mathematics* **94**, 703–707 (2016).
- Nazarov, V. E., Kiyashko, S. B. & Radostin, A. V. The Wave Processes in Micro-Inhomogeneous Media with Different-Modulus Nonlinearity and Relaxation. *Radio*physics and Quantum Electronics 59, 246–256 (2016).

- 68. Kuznetsova, M. S., Pasternak, E. & Dyskin, A. V. Analysis of wave propagation in a discrete chain of bilinear oscillators. *Nonlinear Processes in Geophysics* **24**, 455–460 (2017).
- 69. Lu, Z. & Norris, A. N. Passive nonreciprocity-induced directional wave scattering. Extreme Mechanics Letters 51, 101600 (2022).
- 70. Kogani, A., Zoka, H. & Yousefzadeh, B. On the Nonreciprocal Dynamics of Bilinearly Coupled Oscillators in 10th European Nonlinear Dynamics Conference, Lyon (2022).
- 71. Elachi, C. Waves in active and passive periodic structures: A review. *Proceedings of the IEEE* **64**, 1666–1698 (1976).
- 72. Bragg, W. H. & Bragg, W. L. The reflection of X-rays by crystals. *Proceedings of the Royal Society of London. Series A, Containing Papers of a Mathematical and Physical Character* 88, 428–438 (1913).
- 73. Wang, Y.-F., Wang, Y.-Z., Wu, B., Chen, W. & Wang, Y.-S. Tunable and Active Phononic Crystals and Metamaterials. *Applied Mechanics Reviews* **72** (2020).
- 74. Luo, B. *et al.* Non-reciprocal wave propagation in one-dimensional nonlinear periodic structures. *AIP Advances* 8, 015113 (2018).
- 75. Fang, L., Darabi, A., Mojahed, A., Vakakis, A. F. & Leamy, M. J. Broadband non-reciprocity with robust signal integrity in a triangle-shaped nonlinear 1D metamaterial. *Nonlinear Dynamics* **100**, 1–13 (2020).
- 76. Moore, K. J. *et al.* Nonreciprocity in the dynamics of coupled oscillators with nonlinearity, asymmetry, and scale hierarchy. *Physical Review E* **97**, 012219 (2018).
- 77. Brandenbourger, M., Locsin, X., Lerner, E. & Coulais, C. Non-reciprocal robotic metamaterials. *Nature Communications* **10**, 4608 (2019).
- 78. Wang, C., Vakakis, A. F. & Tawfick, S. Non-reciprocal frequency conversion in a two-dimensional waveguide incorporating a local nonlinear gate. *Communications in Nonlinear Science and Numerical Simulation* **118**, 107041 (2023).
- 79. Deng, B., Wang, P., He, Q., Tournat, V. & Bertoldi, K. Metamaterials with amplitude gaps for elastic solitons. *Nature Communications* **9**, 3410 (2018).
- 80. Vakakis, A. F., Gendelman, O. V., Bergman, L. A., Mojahed, A. & Gzal, M. Nonlinear targeted energy transfer: State of the art and new perspectives. *Nonlinear Dynamics* 108, 711–741 (2022).
- 81. Kamal, A. A parametric device as a nonreciprocal element. *Proceedings of the IRE* **48**, 1424–1430 (1960).

- 82. Yokoi, H., Mizumoto, T., Takano, T. & Shinjo, N. Demonstration of an optical isolator by use of a nonreciprocal phase shift. *Applied Optics* **38**, 7409–7413 (1999).
- 83. Yokoi, H. Calculation of nonreciprocal phase shift in magneto-optic waveguides with Ce:YIG layer. *Optical Materials* **31**, 189–192 (2008).
- 84. Tzuang, L. D., Fang, K., Nussenzveig, P., Fan, S. & Lipson, M. Non-reciprocal phase shift induced by an effective magnetic flux for light. *Nature Photonics* 8, 701–705 (2014).
- 85. Verba, R., Bankowski, E. N., Meitzler, T. J., Tiberkevich, V. & Slavin, A. Phase Nonreciprocity of Microwave-Frequency Surface Acoustic Waves in Hybrid Heterostructures with Magnetoelastic Coupling. *Advanced Electronic Materials* 7, 2100263 (2021).
- 86. Zangeneh-Nejad, F. & Fleury, R. Doppler-based acoustic gyrator. *Applied Sciences* 8, 1083 (2018).
- 87. Wang, T., Wu, L., Nobel, P. & Roychowdhury, J. Solving combinatorial optimisation problems using oscillator based Ising machines. *Natural Computing* **20**, 287–306 (2021).
- 88. Lu, Z. & Norris, A. N. Nonreciprocal and directional wave propagation in a twodimensional lattice with bilinear properties. *Nonlinear Dynamics* **106**, 2449–2463 (2021).
- 89. Yastrebov, V. A. Wave propagation through an elastically asymmetric architected material. *Comptes Rendus. Mécanique* **350**, 1–26 (2022).
- 90. Dang, W., Wang, Z., Chen, L. & Yang, T. A high-efficient nonlinear energy sink with a one-way energy converter. *Nonlinear Dynamics* **109**, 2247–2261 (2022).
- 91. Calvo, M. L. & Lakshminarayanan, V. Optical Waveguides: From Theory to Applied Technologies (CRC press, 2018).
- 92. Oliner, A. Waveguides for acoustic surface waves: A review. *Proceedings of the IEEE* **64,** 615–627 (1976).
- 93. Fronk, M. D., Fang, L., Packo, P. & Leamy, M. J. Elastic wave propagation in weakly nonlinear media and metamaterials: a review of recent developments. *Nonlinear Dynamics* **111**, 10709–10741 (2023).
- 94. Caloz, C. et al. Electromagnetic Nonreciprocity. Physical Review Applied 10, 047001 (2018).
- 95. Reiskarimian, N., Nagulu, A., Dinc, T. & Krishnaswamy, H. Nonreciprocal Electronic Devices: A Hypothesis Turned Into Reality. *IEEE Microwave Magazine* **20**, 94–111 (2019).

- 96. Sokolow, A. et al. Absorption of short duration pulses by small, scalable, tapered granular chains. Applied Physics Letters 87 (2005).
- 97. Wang, T. Achieving phase-based logic bit storage in mechanical metronomes. arXiv preprint arXiv:1710.01056 (2017).
- 98. Yousefzadeh, B. Computation of nonreciprocal dynamics in nonlinear materials. *Journal of Computational Dynamics* **9**, 451 (2022).
- 99. Giraldo, A. & Yousefzadeh, B. Restoring the reciprocity invariance in nonlinear systems with broken mirror symmetry. *Extreme Mechanics Letters* **61**, 102008 (2023).
- 100. Wu, G., Long, Y. & Ren, J. Asymmetric nonlinear system is not sufficient for a non-reciprocal wave diode. *Physical Review B* **97**, 205423 (2018).
- 101. Blanchard, A., Sapsis, T. P. & Vakakis, A. F. Non-reciprocity in nonlinear elastodynamics. *Journal of Sound and Vibration* **412**, 326–335 (2018).
- 102. Fang, L., Mojahed, A., Darabi, A., Vakakis, A. F. & Leamy, M. J. Passive Nonreciprocity in a System of Asymmetrical Rotational Oscillators. *Physical Review Applied* 15, 034005 (2021).
- 103. Mojahed, A., Bunyan, J., Tawfick, S. & Vakakis, A. F. Tunable Acoustic Nonreciprocity in Strongly Nonlinear Waveguides with Asymmetry. *Physical Review Applied* 12, 034033 (2019).
- 104. Fronk, M. D. *et al.* Acoustic non-reciprocity in lattices with nonlinearity, internal hierarchy, and asymmetry: Computational study. *Journal of vibration and acoustics* **141** (2019).
- 105. Guckenheimer, J. & Holmes, P. Nonlinear oscillations, dynamical systems, and bifurcations of vector fields (Springer Science & Business Media, 2013).
- 106. Olson, C. L. & Olsson, M. Dynamical symmetry breaking and chaos in Duffing's equation. *American Journal of Physics* **59**, 907–911 (1991).
- 107. Dankowicz, H. & Schilder, F. Recipes for Continuation (Society for Industrial and Applied Mathematics, 2013).
- 108. Von Groll, G. & Ewins, D. J. The harmonic balance method with arc-length continuation in rotor/stator contact problems. *Journal of Sound and Vibration* **241**, 223–233 (2001).
- 109. Detroux, T., Renson, L., Masset, L. & Kerschen, G. The harmonic balance method for bifurcation analysis of large-scale nonlinear mechanical systems. *Computer Methods in Applied Mechanics and Engineering* **296**, 18–38 (2015).

- 110. Krack, M. & Gross, J. Harmonic Balance for Nonlinear Vibration Problems (Springer International Publishing, 2019).
- 111. Nayfeh, A. H. & Mook, D. T. Nonlinear oscillations (John Wiley & Sons, 2024).
- 112. Ramakrishnan, V. & Frazier, M. J. Architected material with independently tunable mass, damping, and stiffness via multi-stability and kinematic amplification. *The Journal of the Acoustical Society of America* **153**, 1283–1292 (2023).
- 113. Liang, B., Guo, X., Tu, J., Zhang, D. & Cheng, J. An acoustic rectifier. *Nature Materials* **9**, 989–992 (2010).
- 114. Grinberg, I., Vakakis, A. F. & Gendelman, O. V. Acoustic diode: Wave non-reciprocity in nonlinearly coupled waveguides. *Wave Motion* 83, 49–66 (2018).
- 115. Fu, C., Wang, B., Zhao, T. & Chen, C. Q. High efficiency and broadband acoustic diodes. *Applied Physics Letters* **112**, 051902 (2018).
- 116. Tsakmakidis, K. L. *et al.* Breaking Lorentz reciprocity to overcome the time-bandwidth limit in physics and engineering. *Science* **356**, 1260–1264 (2017).
- 117. Wang, C., Tawfick, S. & Vakakis, A. F. Irreversible energy transfer, localization and non-reciprocity in weakly coupled, nonlinear lattices with asymmetry. *Physica D: Non-linear Phenomena* **402**, 132229 (2020).
- 118. Zangeneh-Nejad, F. & Fleury, R. Active times for acoustic metamaterials. *Reviews in Physics* 4, 100031 (2019).
- 119. Wu, J. & Yousefzadeh, B. Linear nonreciprocal dynamics of coupled modulated systems. The Journal of the Acoustical Society of America 157, 1356–1367 (2025).
- 120. Patil, G. U., Cui, S. & Matlack, K. H. Leveraging nonlinear wave mixing in rough contacts-based phononic diodes for tunable nonreciprocal waves. *Extreme Mechanics Letters* **55**, 101821 (2022).
- 121. Kogani, A. & Yousefzadeh, B. Nonreciprocal phase shifts in a nonlinear periodic waveguide. *Nonlinear Dynamics* **112**, 1–13 (2024).
- 122. Hussein, M. I., Leamy, M. J. & Ruzzene, M. Dynamics of phononic materials and structures: Historical origins, recent progress, and future outlook. *Applied Mechanics Reviews* **66**, 040802 (2014).
- 123. Phani, A. S. in *Dynamics of Lattice Materials* 53–92 (Wiley, 2017).
- 124. Yilmaz, C., Hulbert, G. M. & Kikuchi, N. Phononic band gaps induced by inertial amplification in periodic media. *Physical Review B—Condensed Matter and Materials Physics* **76**, 054309 (2007).

- 125. Swinteck, N. et al. Bulk elastic waves with unidirectional backscattering-immune topological states in a time-dependent superlattice. Journal of Applied Physics 118 (2015).
- 126. Nassar, H., Chen, H., Norris, A., Haberman, M. & Huang, G. Non-reciprocal wave propagation in modulated elastic metamaterials. *Proceedings of the Royal Society A:*Mathematical, Physical and Engineering Sciences 473, 20170188 (2017).
- 127. Hasan, M. A., Calderin, L., Lucas, P., Runge, K. & Deymier, P. A. Geometric phase invariance in spatiotemporal modulated elastic system. *Journal of Sound and Vibration* **459**, 114843 (2019).
- 128. Vakakis, A. F. & King, M. E. Nonlinear wave transmission in a monocoupled elastic periodic system. *The Journal of the Acoustical Society of America* **98**, 1534–1546 (1995).
- 129. Narisetti, R. K., Ruzzene, M. & Leamy, M. J. A Perturbation Approach for Analyzing Dispersion and Group Velocities in Two-Dimensional Nonlinear Periodic Lattices. *Journal of Vibration and Acoustics* 133, 061020 (2011).
- 130. Chen, Y., Nassar, H. & Huang, G. Discrete transformation elasticity: An approach to design lattice-based polar metamaterials. *International Journal of Engineering Science* 168, 103562 (2021).
- 131. Matlack, K. H., Serra-Garcia, M., Palermo, A., Huber, S. D. & Daraio, C. Designing perturbative metamaterials from discrete models. *Nature Materials* 17, 323–328 (2018).
- 132. Süsstrunk, R. & Huber, S. D. Classification of topological phonons in linear mechanical metamaterials. *Proceedings of the National Academy of Sciences* **113**, E4767–E4775 (2016).
- 133. Chen, H., Nassar, H. & Huang, G. A study of topological effects in 1D and 2D mechanical lattices. *Journal of the Mechanics and Physics of Solids* **117**, 22–36 (2018).
- 134. Patil, G. U. & Matlack, K. H. Review of exploiting nonlinearity in phononic materials to enable nonlinear wave responses. *Acta Mechanica* **233** (2022).
- 135. Doedel, E. J. in Numerical Continuation Methods for Dynamical Systems: Path following and boundary value problems 1–49 (Springer Netherlands, 2007).
- 136. Thompson, J. M. T. & Stewart, H. B. *Nonlinear dynamics and chaos* (John Wiley & Sons, 2002).
- 137. Yuan, J., Gastaldi, C., Denimal Goy, E. & Chouvion, B. Friction damping for turbomachinery: A comprehensive review of modelling, design strategies, and testing capabilities. *Progress in Aerospace Sciences* **147**, 101018 (2024).

- 138. Gendelman, O. V. & Vakakis, A. F. Exploiting the Use of Strong Nonlinearity in Dynamics and Acoustics (Springer, 2024).
- 139. Rajalingham, C. & Rakheja, S. Influence of suspension damper asymmetry on vehicle vibration response to ground excitation. *Journal of Sound and Vibration* **266**, 1117–1129 (2003).
- 140. Wagg, D. & Virgin, L. Exploiting nonlinear behavior in structural dynamics (Springer Science & Business Media, 2012).
- 141. Marino, L., Cicirello, A. & Hills, D. A. Displacement transmissibility of a Coulomb friction oscillator subject to joined base-wall motion. *Nonlinear Dynamics* **98**, 2595–2612 (2019).
- 142. Gaul, L. & Lenz, J. Nonlinear dynamics of structures assembled by bolted joints. *Acta Mechanica* **125**, 169–181 (1997).
- 143. Huang, Y., Krousgrill, C. & Bajaj, A. Dynamic behavior of offshore structures with bilinear stiffness. *Journal of Fluids and Structures* **3**, 405–422 (1989).
- 144. Langley, R. S. The response of two-dimensional periodic structures to point harmonic forcing. *Journal of sound and vibration* **197**, 447–469 (1996).
- 145. Fu, H., Huang, X. & Kaewunruen, S. Experimental investigations into nonlinear dynamic behaviours of triply periodical minimal surface structures. *Composite Structures* **323**, 117510 (2023).